

For Reference

NOT TO BE TAKEN FROM THIS ROOM

Ex LIBRIS
UNIVERSITATIS
ALBERTAEENSIS



THE UNIVERSITY OF ALBERTA

LABORATORY STUDIES OF THE CONVERSION OF NO^+ TO

$\text{H}^+(\text{H}_2\text{O})_n$ IN MOIST AIR

by



MARGARET ANN FRENCH

A THESIS

SUBMITTED TO THE FACULTY OF GRADUATE STUDIES AND RESEARCH

IN PARTIAL FULFILMENT OF THE REQUIREMENTS FOR THE DEGREE

OF

MASTER OF SCIENCE

DEPARTMENT OF CHEMISTRY

EDMONTON, ALBERTA

FALL 1971

THE UNIVERSITY OF ALBERTA

FACULTY OF GRADUATE STUDIES AND RESEARCH

The undersigned certify that they have read, and recommend to the Faculty of Graduate Studies and Research for acceptance, a thesis entitled

"LABORATORY STUDIES OF THE CONVERSION OF NO^+ TO $\text{H}^+(\text{H}_2\text{O})_n$ IN MOIST AIR"

submitted by MARGARET ANN FRENCH in partial fulfilment of the requirements for the degree of Master of Science.

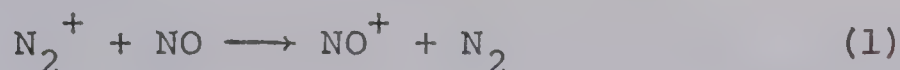
.....1st September 1971.....

Date

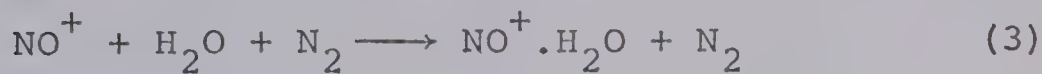
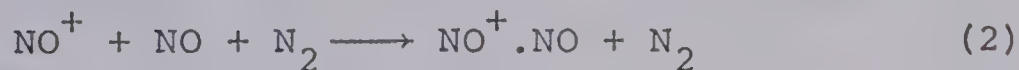
A B S T R A C T

The ion-molecule reactions in the system, nitric oxide and water in an atmosphere of nitrogen were investigated with a high-pressure pulsed electron beam mass spectrometer.

The primary ion, N_2^+ rapidly charge transferred to NO^+ :

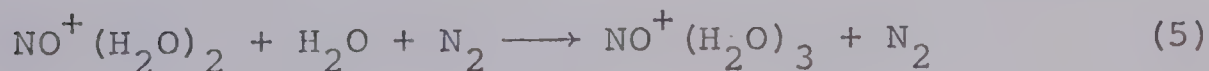
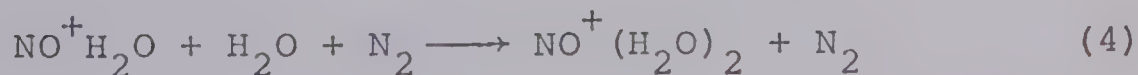


There were two reaction paths for the ion, NO^+ :

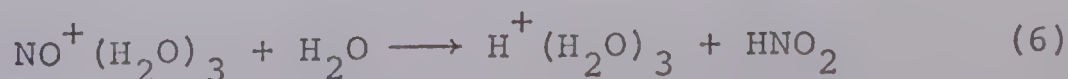


The concentrations of nitric oxide and water were chosen such that the hydration reaction (3) was predominant in most of the experiments.

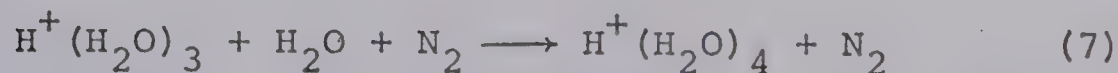
The monohydrate of NO^+ in turn reacted with water to form higher clusters.



$NO^+ (H_2O)_3$ was removed by a very fast second-order reaction (6) forming $H^+ (H_2O)_3$:



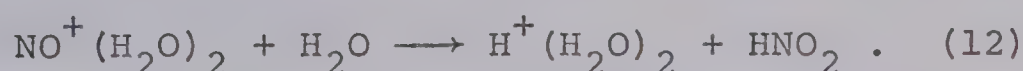
The cluster $\text{H}^+(\text{H}_2\text{O})_3$ reacted further with water:



Reaction (8) was only observed at high water concentrations.

The rate constants for reactions (2) to (7) were determined at 308°K.

Experiments performed at temperatures between 30°C and 130°C indicated that the reaction sequence changed as the temperature was increased. The tendency for the occurrence of cross-over reaction to the proton hydrate sequence at $\text{NO}^+(\text{H}_2\text{O})_2$ increased with temperature.



The activation energy for reaction (3) was calculated from the temperature dependence of the rate constant (k_3).

A C K N O W L E D G E M E N T S

I wish to express my appreciation to Dr. Paul Kebarle for his advice and encouragement throughout the course of this work.

The co-operation of Dr. Anthony Good in the initial stages of the work is acknowledged.

The author would like to thank the members of the mass spectrometry group for their assistance and valuable discussions during the course of this study.

The author wishes to thank Mrs. Mary Waters for her care in typing the manuscript.

The financial assistance provided by the University of Alberta is gratefully acknowledged.

T A B L E O F C O N T E N T S

	<u>Page</u>
Abstract	ii
Acknowledgements	iv
List of Tables	viii
List of Figures	x
 1. INTRODUCTION	
1.1 Development of the study of ion-molecule reactions	1
1.2 Cross-sectional measurements	3
1.3 Theoretical aspects of ion-molecule reactions	6
1.4 Classification of ion-molecule reactions.	8
(i) Simple charge transfer.	9
(ii) Charge transfer induced dissociation	9
(iii) Radical or atom abstraction	10
(iv) Ionic abstraction	10
(vi) Clustering reactions.	12
1.5 Previous studies at high pressures	13
1.6 The role of proton clusters $H^+(H_2O)_n$ and nitric oxide clusters $NO^+(H_2O)_n$ in the ionosphere.	17
 2. EXPERIMENTAL	
2.1 Design of the present instrument	23

	<u>Page</u>
2.2 The high pressure ion source	24
2.3 The electron gun	27
2.4 The vacuum chamber	28
2.5 The gas handling plant	29
2.6 Ion acceleration and gating	31
2.7 Pulsing circuits	31
2.8 Quadrupole mass analyser and detection system	34
2.9 Transmission of the analyser	40
2.10 Discrimination in detection by the electron multiplier	42
2.11 Purification of gases	44
2.12 Determination of component partial pressures in the ion source	45
2.13 Experimental procedure used to obtain data in a given run.	46
2.14 Experimental conditions	47.
3. RESULTS AND DISCUSSION	
3.1 Verification of sensitivity factors	49
3.2 Selection of concentration conditions	49
3.3 Pseudo-first-order rate constants, γ	65
3.4 Results at room temperature with a flow of NO, H ₂ O and N ₂	66

	<u>Page</u>
3.5 Rate constants obtained by graphical methods	68
(i) Decay of N_2^+	68
(ii) Decay of NO^+	69
(iii) Alternate determination of rate constant k_2 for reaction $NO^+ + NO + N_2 \longrightarrow NO^+ \cdot NO + N_2$	70
(iv) Reaction of $NO^+ \cdot H_2O$	79
(v) Reaction of $NO^+ (H_2O)_2$	83
(vi) Kinetics of the proton hydrate formation	88
3.6 Computer fitting of ion intensity curves .	93
3.7 Discussion of results obtained at room temperature	102
3.8 Reactions observed at higher temperature .	107
3.9 Conclusions	122
3.10 Suggestions for further experiments	124
BIBLIOGRAPHY	126

L I S T O F T A B L E S

<u>Table</u>	<u>Page</u>
3.1 Concentrations of reactants in experiments at 308°K	61
3.2 Rate constants for the decay of NO ⁺	78
3.3 Rate and equilibrium constants for the reaction	
$\text{NO}^+ \cdot \text{H}_2\text{O} + \text{H}_2\text{O} + \text{N}_2 \xrightleftharpoons[k_{-4}]{k_4} \text{NO}^+(\text{H}_2\text{O})_2 + \text{N}_2 \quad (4)$	84
3.4 Rate and equilibrium constants for the reaction	
$\text{NO}^+(\text{H}_2\text{O})_2 + \text{H}_2\text{O} + \text{N}_2 \xrightleftharpoons[k_{-5}]{k_5} \text{NO}^+(\text{H}_2\text{O})_3 + \text{N}_2 \quad (5)$	89
3.5 Rate constants for the reaction	
$\text{NO}^+(\text{H}_2\text{O})_3 + \text{H}_2\text{O} \xrightarrow{k_6} \text{H}^+(\text{H}_2\text{O})_3 + \text{HNO}_2 \quad (6)$	92
3.6 Equilibrium constants for hydrate clustering	
$\text{H}^+(\text{H}_2\text{O})_3 + \text{H}_2\text{O} + \text{N}_2 \xrightarrow{K_7} \text{H}^+(\text{H}_2\text{O})_5 + \text{N}_2 \quad (7)$	(7)
$\text{H}^+(\text{H}_2\text{O})_4 + \text{H}_2\text{O} + \text{N}_2 \xrightarrow{K_8} \text{H}^+(\text{H}_2\text{O})_5 + \text{N}_2 \quad (8)$	(8) 94
3.7 Comparison of calculated and computer fitted rate constants	99
3.8 Comparison of calculated and computer fitted rate constant for the reaction	
$\text{NO}^+ + \text{NO} + \text{N}_2 \xrightarrow{k_2} \text{NO}^+ \cdot \text{NO} + \text{N}_2 \quad (2)$	103
3.9 Determined rate constants for reactions (1) to (8)	104

	<u>Page</u>
3.10 Rate constants for reaction (3) at various temperatures	115
3.11 Rate constants for reaction (4) at various temperatures	119

L I S T O F F I G U R E S

<u>Figure</u>	<u>Page</u>
2.1 Apparatus showing ion source, electron gun, quadrupole mass analyser and vacuum housing	25
2.2 Gas handling plant	30
2.3 Ion acceleration and gating electrodes	32
2.4 Pulse generation circuit	33
2.5 Quadrupole rods. The hyperbolic cross-section is approximated by a circular cross-section	36
2.6 Stability diagram of the Mathieu parameters a and q	39
2.7 Sensitivity curve for medium mass range	43
3.1 Corrected total ionisation curve when $[N_2] = 5.6 \times 10^{16} \text{ molecule cc}^{-1}$, $[NO] =$ $3.5 \times 10^{15} \text{ molecule cc}^{-1}$, $[H_2O] = 1.7 \times 10^{14}$ molecule cc^{-1}	50
3.1a Normalised experimental data	50a
3.2 Normalised ion intensity curves $[N_2] =$ 7.8×10^{16} , $[NO] = 1.9 \times 10^{16}$, $[H_2O] =$ $1.2 \times 10^{14} \text{ molecule cc}^{-1}$	51
3.3 Normalised ion intensity curves $[N_2] =$ 8.2×10^{16} , $[NO] = 1.2 \times 10^{16}$, $[H_2O] =$ $1.0 \times 10^{14} \text{ molecule cc}^{-1}$	52

3.4	Normalised ion intensity curves $[N_2] = 5.2 \times 10^{16}$, $[NO] = 1.2 \times 10^{16}$, $[H_2O] = 0.7 \times 10^{14}$ molecule cc^{-1}	53
3.5	Normalised ion intensity curves $[N_2] = 3.7 \times 10^{16}$, $[NO] = 1.2 \times 10^{15}$, $[H_2O] = 2.1 \times 10^{14}$ molecule cc^{-1}	54
3.6	Normalised ion intensity curves $[N_2] = 6.7 \times 10^{16}$, $[NO] = 1.3 \times 10^{16}$, $[H_2O] = 1.2 \times 10^{14}$ molecule cc^{-1}	55
3.7	Normalised ion intensity curves $[N_2] = 8.4 \times 10^{16}$, $[NO] = 1.0 \times 10^{16}$, $[H_2O] = 1.0 \times 10^{14}$ molecule cc^{-1}	56
3.8	Normalised ion intensity curves $[N_2] = 5.9 \times 10^{16}$, $[NO] = 2.5 \times 10^{15}$, $[H_2O] = 1.4 \times 10^{14}$ molecule cc^{-1}	57
3.9	Normalised ion intensity curves $[N_2] = 6.0 \times 10^{16}$, $[NO] = 2.9 \times 10^{15}$, $[H_2O] = 1.3 \times 10^{14}$ molecule cc^{-1}	58
3.10	Normalised ion intensity curves $[N_2] = 6.2 \times 10^{16}$, $[NO] = 1.0 \times 10^{15}$, $[H_2O] = 1.4 \times 10^{14}$ molecule cc^{-1}	59
3.11	Normalised ion intensity curves $[N_2] = 5.5 \times 10^{16}$, $[NO] = 1.1 \times 10^{16}$, $[H_2O] = 2.0 \times 10^{15}$ molecule cc^{-1}	60

	<u>Page</u>
3.12 Calculation of γ_{obs} from exponential decay of NO^+	71
3.13 Determination of k_2 and k_3 from the slope and intercept	72
3.14 Normalised ion intensity curves observed at low water concentration	73
3.15 Normalised ion intensity curves observed at low water concentration	74
3.16 Normalised ion intensity curves observed at low water concentration	75
3.17 Logarithmic plots to calculate γ_{obs} . $\gamma_{\text{obs}} = \gamma_2$ under these conditions	77
3.18 Calculation of γ_4 by the graphical integration method	81
3.19 Determination of second or third-order dependence of k_4	82
3.20 Calculation of γ_5 by the graphical integration method	86
3.21 Determination of second or third order dependence of k_5	87
3.22 Calculation of γ_5 by the graphical integration method	90

	<u>Page</u>
3.23 Determination of second or third-order dependence of k_6	91
3.24 Analog Program simulating reactions (1) to (7)	97
3.25 Analog Program simulating reactions (1), (2) and (3')	101
3.26 Ions observed at different temperatures	109
3.27 Normalised ion intensity curves observed at 54°C	110
3.28 Normalised ion intensity curves observed at 63°C	111
3.29 Normalised ion intensity curves observed at 101°C	112
3.30 Normalised ion intensity curves observed at 127°C	113
3.31 Calculation of γ_3 from exponential decay of NO^+	114
3.32 Arrhenius plot to determine E_a for reaction (3)	117
3.33 Calculation of γ_4 by the graphical integration method	118

CHAPTER I

I N T R O D U C T I O N

This work describes a study of the measurements of ion molecule reaction rates with a pulsed electron beam mass spectrometer, operated in the torr range.

A mass spectrometer is an instrument which separates gaseous ions according to their mass to charge ratio (m/e). In a simple mass spectrometer, ions are formed in the ion source as a result of collisions between gaseous molecules and a beam of energetic electrons. A repeller electrode extracts the ions from the ion source and accelerates them towards the analysing region. Magnetic or electric fields or both, separate the ions according to their m/e ratio, the signal is multiplied and displayed as a mass spectrum.

1.1 Development of the study of ion-molecule reactions.

In the conventional analytical mass spectrometer, the ion source and mass analysis regions are kept at low pressures to reduce the probability of collisions between ions and gas molecules. Raising the ion source pressure increases the collision probability so that ion-molecule reactions begin to occur, which give rise to secondary ions and possibly neutral products. A secondary ion can in turn participate in an ion-molecule reaction and thus give rise to a whole series of reactions.

The first recorded observation of an ion-molecule

reaction was that by J. J. Thompson (1) in 1912. He detected ion currents in his parabola mass spectroscopy, which were not due to direct ionisation of any species known to be present in the apparatus. He observed such ions as those with m/e ratio 3 and 19 in the products from a discharge of hydrogen.

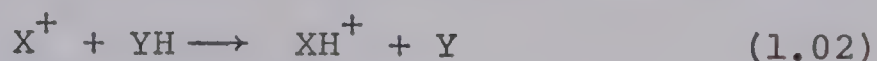
The ion of m/e ratio 3 was also observed by Dempster (2) in 1916, who showed that the ion was H_3^+ together with the fact that the intensity of the peak increased with an increase in hydrogen pressure. The presence of this ion was later explained (3,4) as originating from:



At this time most research in mass spectrometry was concentrated on measurements of isotopic abundance and later, on determinations of ionic heats of formation, ionisation potentials and vapour analysis. The occurrence of ion molecule reactions generally leads to errors in such applications. Therefore, prior to 1950, the occurrence of undesired ion-molecule reactions was minimised by the use of low pressure i.e. by the improvement in high vacuum techniques. It was not until this time that the importance of ion-molecule reactions in the primary initiation reactions of radiation chemistry was recognised.

Studies of ion-molecule reactions were initiated by such workers as Tal'rose and Lyubimova (5), Stevenson and

Schissler (6,7) and Gutbier (8). The two latter groups independently measured the reaction rates of the type:



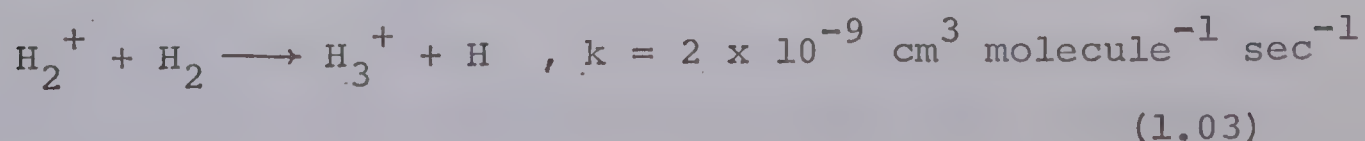
Renewed interest caused the field to expand rapidly. Spectrometers were especially designed to cope with the high pressures needed to observe ion-molecule reactions (9).

With the advent of rockets and earth orbiting satellites, it became feasible to examine the upper atmosphere using these vehicles to carry mass spectrometers (10,11). Direct ionospheric observations have increased the understanding of positive ion processes in the upper atmosphere. To eliminate the possibility of ion production by rocket exhaust contamination, laboratory experiments were designed to elucidate the mechanisms of positive ion formation (12,13,14).

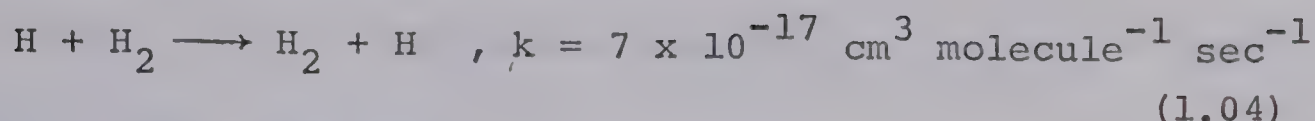
1.2 Cross-Sectional Measurements.

Reactions between ions and molecules are very fast compared to reactions between neutral species. Some typical second order reactions are shown in:

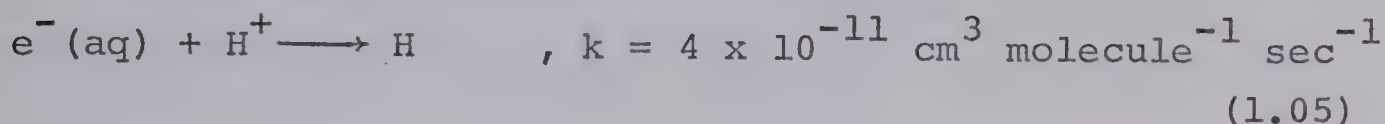
Ion-molecule reaction,



Atom and radical reactions,



Ions in aqueous solution,



A very large number of second order ion-molecule reaction rate constants determined experimentally were found to be 0.4 to $40 \times 10^{-10} \text{ cm}^3 \text{ molecule sec}$. It is assumed that the majority of ion molecule reactions, which are exothermic, have no energy of activation.

Early mass spectroscopists could not measure absolute rate constants with their instruments and so reaction kinetics were described by the cross-section of the reaction. The reaction cross-section may be conceived as the area of the target molecule presented to the approaching ion. If the ion approaches within the cross-section a reaction occurs (15).

If a beam of ions carrying a current, I passes through a gas target of small thickness, dx and density n molecules/ cm^3 , the small fraction of ions that react will be:

$$\frac{-dI}{I} = n q dx \quad (1.06)$$

where q is the cross section of the molecules. Therefore

for a target of thickness x :

$$-\ln I = n q x + C \quad (1.07)$$

where C is a constant.

The beam current, I remaining after the beam has travelled through the gas a distance x is given by:

$$I = I_0 e^{-nqx} \quad (1.08)$$

where $I = I_0$ at $x = 0$. Equation (1.08) is analogous to Beer's Law for the absorption of light passing through a medium. The factor nq is often defined as Q , the absorption coefficient at some standard density.

Equation (1.08) is only applicable when the ions are of identical energy and only one interaction is possible. Taking these conditions into account, the reaction cross-section can be measured by three different methods:

- (a) From the exponential decay of primary ions along the path, assuming that there is no scattering.
- (b) From the corresponding appearance of secondary ions along the path.
- (c) From measurements of the ratio of products to reactant flux along the path.

The reaction cross-section measured by any of the above methods would be the "microscopic cross-section".

Usually the incident ions have a Boltzmann distribution of energies, the result of such an experiment would be the "macroscopic" cross-section q' .

The thermal energy distribution can be used to give the values for the "thermal" rate constant, k . The following approximation can therefore be made:

$$k = q'v \quad (1.09)$$

where v is the mean relative velocity of ion and molecule, and k has units $\text{cm}^3 \text{ molecule}^{-1} \text{ sec}^{-1}$. For thermal ions, equation (1.08) can be rewritten:

$$I = I_0 e^{-nq'x} \quad (1.10)$$

Using equations (1.09 and (1.10):

$$I = I_0 e^{-nkx/v} \quad (1.11)$$

Thus:

$$I = I_0 e^{-nkt} \quad (1.12)$$

1.3 Theoretical Aspects of Ion-Molecule Reactions.

The first quantitative theory of ion-molecule interactions was developed by Langevin in 1903 (16,17). Stevenson (18) adapted the Langevin theory to ion-molecule reactions occurring in a mass spectrometer. The Langevin-Stevenson orbiting theory of ion-molecule reaction cross-sections considers that an ion approaching a molecule can induce an

appreciable polarisation in the molecule resulting in an attractive force between them. If the ion and molecule are a large distance from each other at their closest approach, the attractive forces are weak and the ion will be deviated from its original path. As the distance decreases, there is certain point where the attractive forces become so great that orbiting results. The theory assumes that an orbiting type of collision increases the time of interaction between the ion and the molecule and results in a reaction.

The theory leads to an expression for the reaction cross-section at a certain relative velocity of approach, v_o :

$$q = \frac{2\pi e}{v_o} \left(\frac{\alpha}{\mu}\right)^{\frac{1}{2}} \quad (1.13)$$

where α is the polarisability of the molecule and μ is the reduced mass of the ion and molecule.

Several groups have applied Langevin's theory to their data (19,20) with reasonable success. However, it is generally agreed that the theory is too simple. One cannot expect that the reaction cross-sections can be obtained by consideration of only two simple parameters, mass and polarisability, neglecting all other properties of the reacting species.

Recently several more detailed theories have been proposed which take into account the internal properties

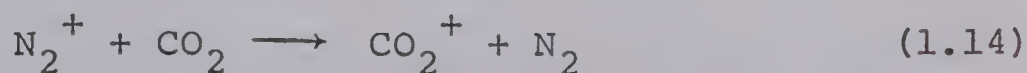
of the molecule also. A comprehensive review of these theories is given in reference (21).

1.4 Classification of Ion Molecule Reactions

Gas phase ion-molecule reactions can be classified according to the products formed.

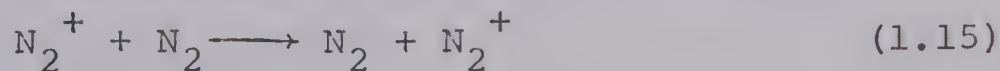
(i) Simple Charge Transfer.

During collision the ion abstracts an electron from the molecule and a new ion and molecule are formed:



The criterion for the occurrence of charge exchange at thermal energies is that the recombination energy of the ion must be greater than the ionisation potential of the neutral species, otherwise the reaction is endothermic.

When the ion and molecule are the same species, ΔH is zero and the reaction is termed Resonant Charge Transfer (22), for example:



Different species may occasionally give rise to resonant conditions, especially if the number of degrees of freedom of both the ion and molecule are small. The difference in energy, ΔH was observed to be -0.04 eV in reaction (1.16) of Xenon with ethylene (23):



(ii) Charge Transfer Induced Dissociation.

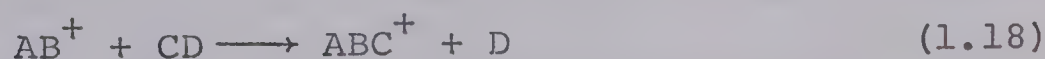
When the change in enthalpy, ΔH is large, the resultant ion possesses a large excess energy because of the large differences in ionisation potentials, and may dissociate (24) as in:



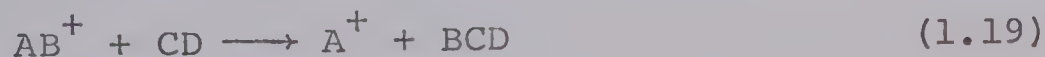
The large excitation energy of CH_4^+ , 1.55 eV is sufficient to break a C-H bond. Thus for dissociation to occur, the recombination energy must be greater than the appearance potential of the fragmentation.

(iii) Radical or Atom Abstraction.

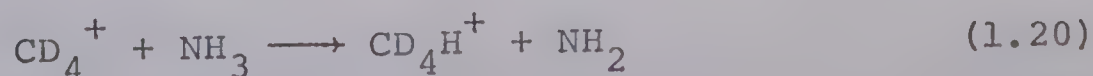
Many ion-molecule reactions involve abstraction by the ion of a neutral fragment from the molecule as in:



Conversely, the neutral molecule may abstract a neutral fragment from the ion:



These types of reactions frequently include the transfer of a hydrogen atom (25):

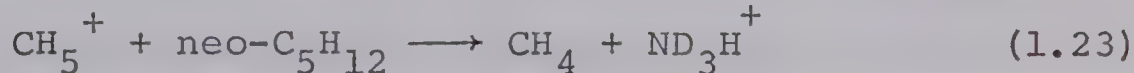


(iv) Ionic Abstraction.

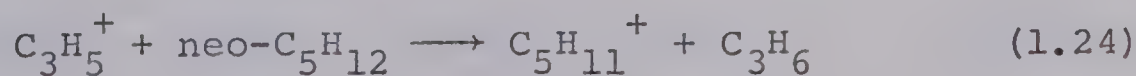
This type of reaction is similar to section (iii) above but involves the transfer of a charged fragment. There are two types of reactions, which are shown in the generalised form:



An example of (1.21) is proton donation (1.23) and often occurs when there are no electron vacancies in the valence shell (26). The cross-section for proton donation processes are large, about 100 \AA^2 :



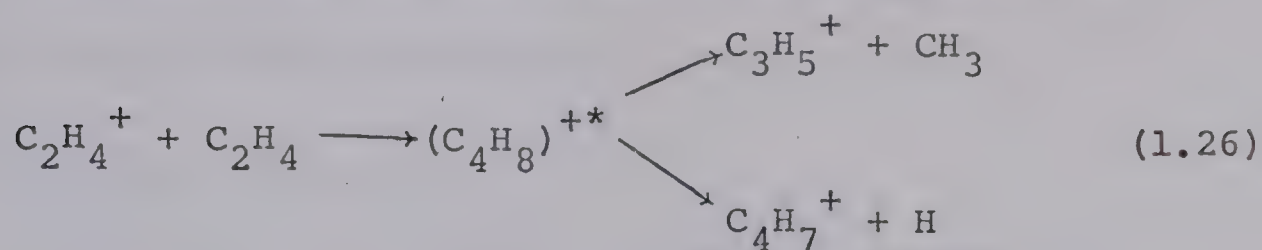
Ions in which there are two vacancies in the valence orbital give rise to hydride ion abstraction from saturated molecules (25,27). This type of reaction has a lower cross-section than the proton transfer:

(v) Condensation Reactions.

The largest group of reactions involving organic ions and molecules is the condensation reaction. The general reaction is given by:

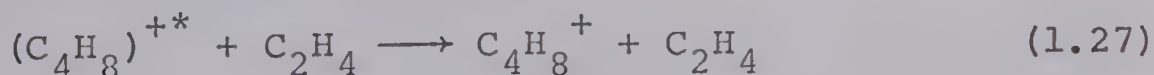


An example is the condensation of ethylene:

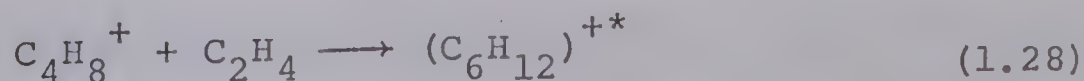


Reaction (1.26) was observed at a low pressure i.e. 10 m torr. If the pressure were increased, the reaction path should change. The intermediate complex in a condensation reaction has a large excitation energy, gained from the formation of bonds during the attachment. The excitation energy can be distributed amongst its vibrational and rotational modes, and may be transformed into translational kinetic energy by colliding with other gas molecules. As the pressure is increased the collision probability increases also. Thus the complex becomes thermalised by collisions with other molecules.

At high pressures the product of reaction (1.26) changes and $(\text{C}_4\text{H}_8)^{+*}$ is stabilised as in:



Also under these conditions the concentration of the secondary ion becomes large enough to observe consecutive reactions. The product of reaction (1.28) can react further:



It now becomes possible to observe reactions with low reaction rates at high pressures.

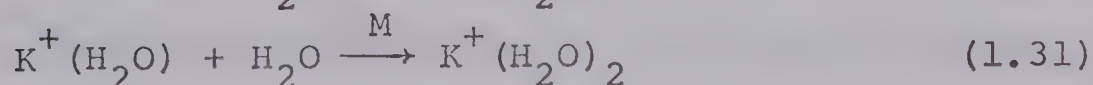
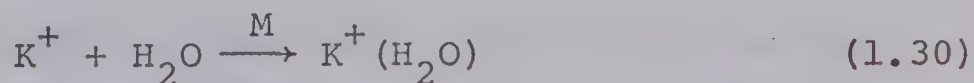
(vi) Clustering Reactions.

Clustering reactions are a class of condensation reactions of the type:



where M signifies a third body. A clustering reaction may be distinguished from ionic polymerisation (as in equations (1.27) and (1.28)) by assuming that for the case of ion clusters no stable neutral species of the same formula exists. Some examples of ion clustering reactions are given in (1.30) to (1.34).

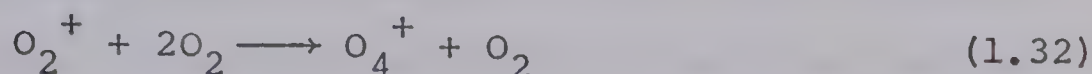
The excess energy due to the exothermicity of the formation of the complex must be removed by collisions with third bodies. For this reason the overall reaction rate is slow and to observe such reactions the experiment must be carried out in the torr range



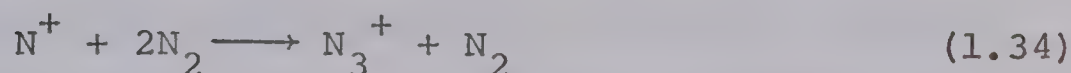
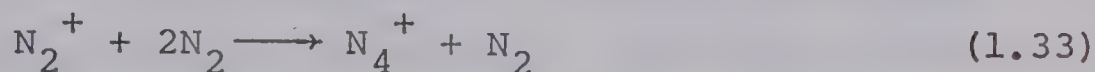
The bond formed by the clustering reactions (1.30) and (1.31) is mainly ionic. Only ion-dipole forces are involved in the water clustering reactions of K^+ (28), but the covalency contribution to the bond was found to increase

with the series K^+ to Li^+ . Water clustering reactions are of interest because their behaviour may be compared to ion solvation in an aqueous solution.

The three body attachment of oxygen in reaction (1.32) exemplifies a bond involving partially ionic and partially covalent character (29):



Extensive studies have been made of ion-molecule reactions in pure nitrogen (30,31,32). The major reactions involving the two primary ions N_2^+ and N^+ are:



1.5 Previous Studies at High Pressures.

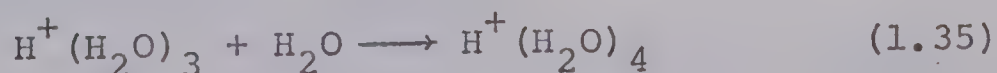
To observe ion-molecule reactions at high pressures, several modifications must be made to a conventional mass spectrometer. Thus while the ion source pressure must be high, the pressure outside the ion source should be low (less than 10^{-4} torr) if collisions of the ions with molecules in the acceleration and mass analysis system are to be avoided. Such collisions may lead to undesired ion-molecule reactions and scattering of the ion beam.

Field and Franklin modified their mass spectrometer

to decrease the rate of escape of gas from the ion source. The electron entrance aperture and the ion exit slit were made small. A pressure gradient could be maintained across the slit by fast pumping of the vacuum housing outside the ion source. Field et al. observed high order reactions in methane (33) and ethylene (34) at pressures of 0.3 torr. Further improvements made pressures up to 2 torr possible (35,36) and the ions produced in methane could be compared to the proposed reactions in the radiolysis of methane. In most experiments with ion-molecule reactions a repeller electrode was used to extract the ions from the source. As a result the ions observed did not have thermal energies.

Kebarle and Godbole (37) built a mass spectrometer with a field free ion source in order to simulate conventional gas radiolysis. Data on the ionic polymerisation of ethylene was extended to a pressure of 40 torr (38,39). Since the reactions were carried out at thermal energies, the results could be applied to the radiolysis of ethylene.

Water clustering reactions (40), involving ion-dipole interactions, of the type shown in equation (1.33), were also studied with this instrument:



Since the ion source was field free, the removal of ions depended solely on diffusion and mass flow and the reaction times were uncertain.

A low pressure ion-molecule reaction technique has been developed by Tal'rose (41,42) which can be used to follow the time dependence of a reaction. A pulse switches on the electron beam for a short time and the ions are produced. After this there is a delay, t_d , during which the ion source is field-free and the ions can react under thermal conditions. After the delay a pulse is applied to the repeller electrode, expelling the ions from the ion source.

By measuring the primary ion intensity, I_p , and the secondary ion intensity, I_s , as a function of t_d , the rate constant k can be calculated if the concentration, n , of the gas is known.

Fite et al. (43) and Sayers and Smith (44) used this technique to measure the first value of the rate constants of aeronomic reactions.

Fite et al. observed the attachment of N_2 to N_2^+ and obtained a value for the rate constant of the reaction:



Sayers and Smith obtained a rate constant for reaction (1.37) which was temperature dependent:



Ferguson, Fehsenfeld and Schmeltekopf (45) developed the flowing afterglow technique to study ion-molecule

reactions at thermal energies in a flow system. Typically the carrier gas is helium. Helium ions are produced by a microwave discharge or electrons from a filament and carried by a fast gas flow. The pressure in the flow tube is about 0.5 torr. Gas inlets can be placed downstream and reactants injected. The helium ions and excited helium atoms ionise the reactant gas molecules. Another gas can be injected further downstream and the reaction between the ions of the first gas and the molecules of the second gas can be observed by a mass spectrometer which samples the flowing gas some distance downstream of the reactant inlets. The reaction times may be calculated from the flow rate and path length. Since the reactant gas is injected after the discharge, most of the molecules will be in the ground state.

Ferguson further elaborated the technique so that reactant gases could be excited by a second gas discharge, just before they entered the stream. This enabled unstable species, such as atoms, to be added to the reaction selectively. Many ion-atom interchange reactions of aeronomic interest were studied which have never been successfully investigated before. An example of a reaction investigated is given in equation (1.39) where the change of the rate of reaction with the vibrational temperature of N_2 was studied (46):



1.6 The Role of Proton Clusters $H^+(H_2O)_n$ and Nitric Oxide Clusters $NO^+(H_2O)_n$ in the Ionosphere.

The ionosphere extends from about 50 km above the earth's surface into outer space. The ionosphere contains relatively large concentrations of free electrons and ions produced by the effect of the sun's ultraviolet radiation upon the molecules in the atmosphere.

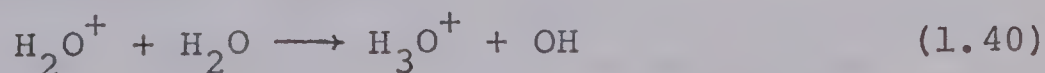
Since Marconi's discovery that radio waves could be propagated over long distances by reflection from an electrically conducting layer in the upper atmosphere, scientists have measured electron densities as a function of altitude by the same principle.

Two distinct regions of electron densities were found by E. V. Appleton (47) which he called the E and F regions. Subsequently a lower region, the D region, was discovered between 50 and 85 km. The pressure in this region varies from 0.01 to several torr and the temperature drops from 270° at 50 km to 200° at 85 km.

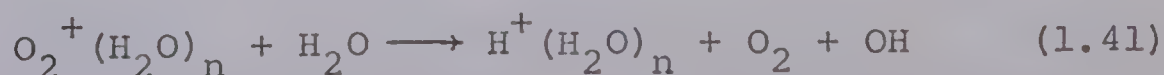
Prior to 1960 the only information available regarding the ionosphere was the variation of electron density with distance above the earth and that the source of ions in the D region was probably the ionisation of nitric oxide by Lyman- α radiation. It was also believed that NO^+ , O_2^+ and small amounts of N_2^+ were the only positive ions in this region.

Rocket-borne mass spectrometers fired into the D and E region produced totally unexpected results. Narcisi (10,48) found that NO^+ , O_2^+ and N_2^+ accounted for only 15% of the positive ions in the D region while 35% was due to the cluster ions $\text{H}^+(\text{H}_2\text{O})_2$ and H_3O^+ . The remaining 50% of ions had mass greater than 45^+ . A small amount of mass 48^+ was observed in later flights which has since been attributed to $\text{NO}^+\cdot\text{H}_2\text{O}$ (49,50). The major ions in the range 64 to 82.5 km were therefore H_3O^+ , NO^+ and $\text{H}^+(\text{H}_2\text{O})_2$. A sharp transition in ion composition occurred at 82.5 km where the H_3O^+ and $\text{H}^+(\text{H}_2\text{O})_2$ abundance decreased abruptly. Since contamination by the rocket could not be completely excluded, several groups of workers set out to find a reaction mechanism that could produce proton hydrate clusters in the laboratory.

Previous experiments in this laboratory have shown that N_2^+ and O_2^+ are important precursors in the mechanisms producing proton hydrates, $\text{H}^+(\text{H}_2\text{O})_n$ (30,51). In moist oxygen O_2^+ and O_4^+ cannot charge transfer to H_2O to start the proton hydration:



However, it was found that the O_2^+ ion was hydrated and at a certain point crossed over to the proton hydrate:



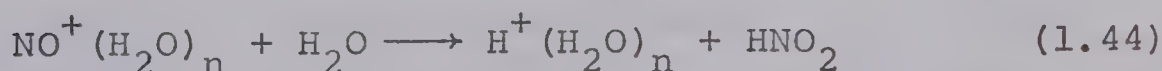
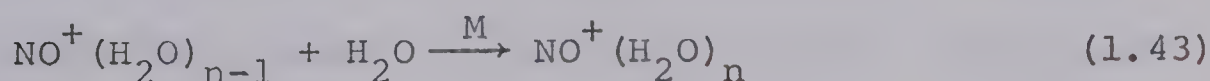
n was found to be 2 in the case of O_2 .

In moist nitrogen N_2^+ clustered with a molecule of N_2 to give N_4^+ which could then charge exchange with water.



Reaction (1.40) would then initiate the proton hydration sequence. No hydrates of N_2^+ or N_4^+ were observed.

Ferguson and Fehsenfeld (52) independently proposed substantially the same mechanism for the production of proton hydrates O_2^+ . At the same time they suggested that the hydration of NO^+ may also occur in the ionosphere and at a certain point cross over to the proton hydrate sequence by the mechanism:

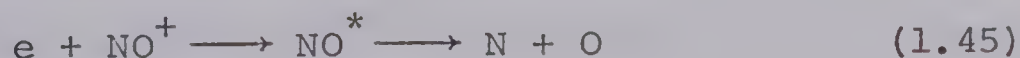


The ions $NO^+(H_2O)_n$ where $n = 1, 2$ and 3 had already been observed by Shahin in the laboratory (53) in 1965, however no rate constant measurements had been performed. It seemed of considerable interest to measure the rates of reactions (1.43) and (1.44) in order to establish whether these reactions can explain the ionospheric observations.

The presence of $H^+(H_2O)_n$ clusters in the ionosphere is of considerable importance for the following reasons.

Rocket-borne probes measuring the electron number density in the ionosphere (55) have shown that there is a region of very high gradient in the electron density between 80 and 90 km forming a ledge in the profile. This abrupt increase in electron density has been explained by Reid (56) who has performed model calculations correlating laboratory measured rate constants and recombination coefficients with the observed ionospheric ion and electron populations.

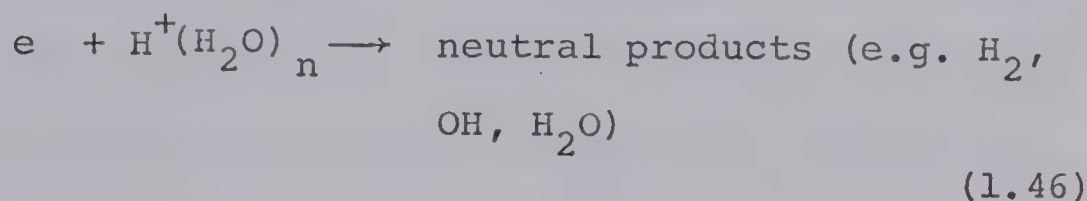
Reid noticed that the increase in electron density coincided with the abrupt disappearance of proton hydrates above 85 km observed by Narcisi in his earlier rocket probes. Reid calculated that the abrupt increase in electron density was due to a sudden decrease in the recombination coefficient, α_d . α_d is the second order dissociative electron attachment rate constant. At 90 km, above the ledge, the calculated value of α_d was in the range known for NO^+ (57), $1 \times 10^{-6} \text{ cm}^3 \text{ sec}^{-1}$



The neutral molecule NO dissociates because of the excess energy. The small value of the recombination coefficient can be explained by the strong N-O bond and that few degrees of freedom are available among which to distribute the excess energy. The reverse reaction is therefore quite

significant.

Below the ledge the α_d values are much larger, of the order of $5 \times 10^{-5} \text{ cm}^3 \text{ sec}^{-1}$ in the range of recombination coefficients measured for H_3O^+ by Biondi (58). Reid concluded that the large recombination coefficients were most probably due to the dissociative electron attachment of the proton hydrates:

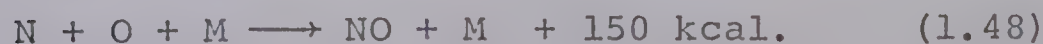


where $n = 1$ or 2 .

The recombination coefficient for reaction (1.46) is much larger than for reaction (1.45) because the bonds in the cluster $\text{H}^+(\text{H}_2\text{O})_n$ are much weaker and there are many more internal degrees of freedom among which to distribute the excess energy of the neutral molecule. Reaction (1.46) is therefore more favourable than (1.45).

Reid inferred that the sudden change in the rate of recombination of water clusters might be due to a sudden change in temperature.

Nitric oxide is formed in the ionosphere by two and three body neutral reactions (59), such as:



The nitric oxide may give rise to further nitrogen oxides or may be ionised by Lyman- α radiation. NO^+ is also produced by many simple ion-molecule reactions (60,12) such as:



The role of NO^+ and $\text{H}^+(\text{H}_2\text{O})_n$ hydrates in the ionosphere are very important, thus the present work was initiated in order to elucidate the reaction mechanism of NO and H_2O and measure the reaction rate constants. Before the completion of the present study other research groups had published partial elucidations of the mechanisms leading from NO^+ to $\text{H}^+(\text{H}_2\text{O})_n$. This work will be considered in the discussion in connection with the present results.

CHAPTER IIE X P E R I M E N T A L2.1 Design of the Present Instrument.

The apparatus was designed to produce the experimental conditions necessary for the observation of ion-molecule reactions in the absence of electric fields, at gas pressures in the torr range and at different reaction temperatures.

While a high ion source pressure is required for the present experiments the mass analyser must be operated at a pressure of less than 10^{-4} torr in order to avoid collisions during flight to and in the analyser. Thus an ion source with narrow electron entrance and ion exit slits and a large capacity pumping system are necessary to maintain the required pressure differential.

A high energy beam of electrons was chosen as a source of ionising radiation since radioactive particle sources gradually spread in the vacuum and contaminate the apparatus. A high energy electron beam has a reasonable penetrating power and may be conveniently pulsed by electrostatic means.

A quadrupole mass spectrometer was chosen as the mass analyser since it is compact and easy to mount in a vacuum chamber. The quadrupole has a high sensitivity compared to that of a magnetic mass spectrometer and can withstand temperatures up to 400°C.

The reaction times could be defined quite accurately by pulsing an ion gate, which then allowed ions to pass

through the quadrupole for analysis.

Only a general outline of the experimental configuration will be given here. Complete technical details and design rationale have been published previously (61,62,30,51).

A diagram of the instrument is shown in Figure (2.1).

2.2 The High Pressure Ion Source.

The apparatus contained two ion sources, one was attached to the quadrupole assembly and could be used for analysing gases conventionally, i.e. at pressures less than 10^{-4} torr. The other ion source was designed to withstand a pressure of several torr.

The high pressure ion source was made by boring a narrow channel along the axis of a cylindrical piece of stainless steel to define the reaction chamber. On one side of the cylindrical cavity the electron entrance slit was mounted on a cone. The electron entrance slit was defined by two parallel edges of a stainless steel razor blade. The size of the slit was 1.70 mm x 0.04 mm.

Outside the ion source in front of the electron entrance slit an electron beam focussing plate was mounted. A 5 mm diameter hole was drilled through the plate which was axial with the entrance cone. The plate was coated with a mixture of phosphor, sodium silicate and sodium chloride. The phosphor glowed where the electron beam impinged upon the plate thus providing a means of focussing

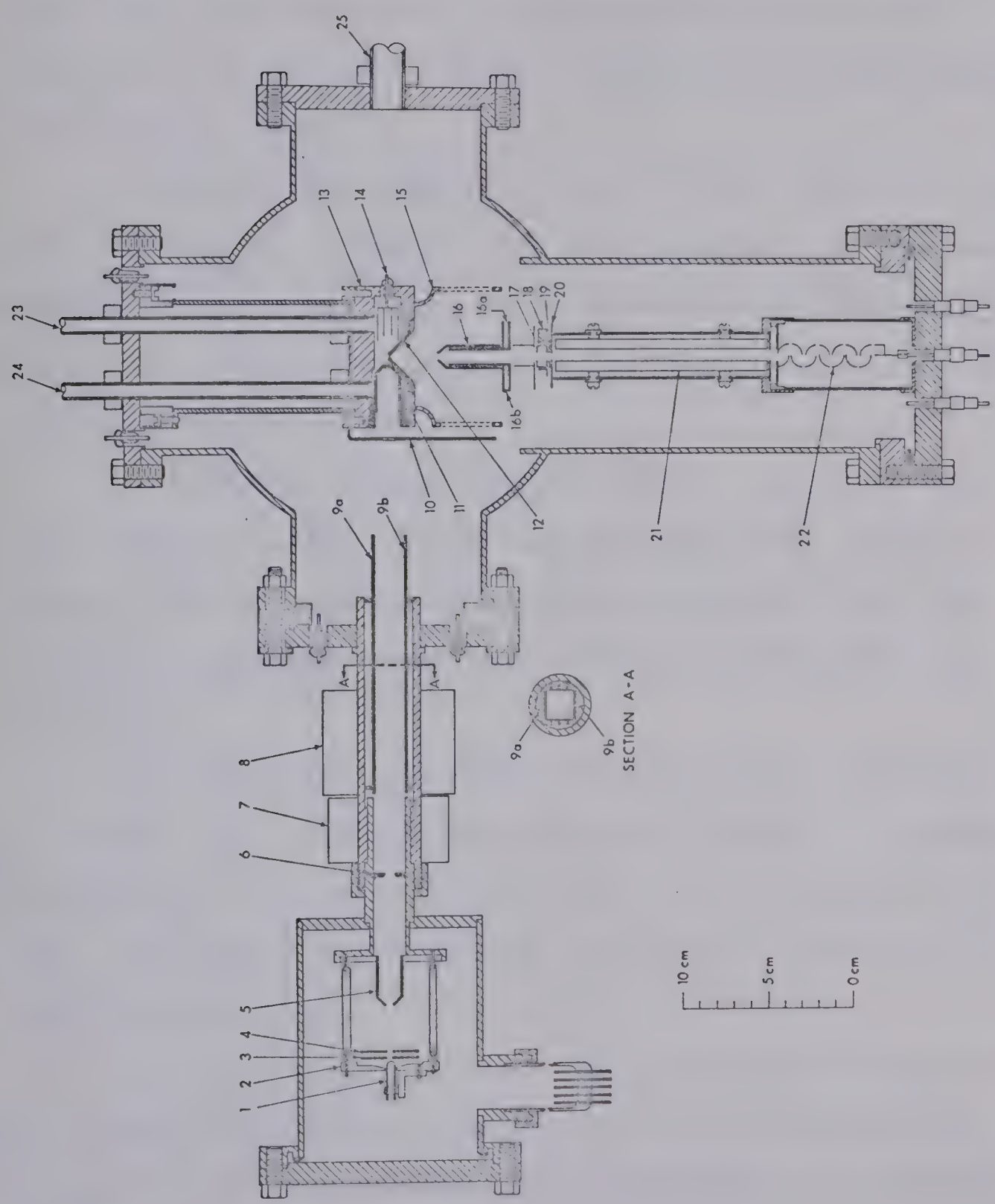


FIGURE 2.1. Apparatus Showing Ion Source, Electron Gun, Quadrupole Mass Analyser and Vacuum Housing.

the beam. The purpose of the sodium chloride was to make the phosphor coating conductive and so prevent surface charging. The plate extended in front of the electrostatic shield [15] to prevent spurious ionisation by stray electrons from the beam.

A Faraday cup electron trap [14] was mounted at the opposite reaction chamber. The trap consisted of two concentric tantalum cylinders which prevented any secondary electrons, produced by impact of the primary electrons on the trap, from escaping.

Gas flowed through the ion source by way of two glass tubes [23,24]. If no flow was required, a static system could be maintained by closing the exit tube and gas would diffuse through the electron entrance and ion exit slits.

Ions left the ion source through a small slit mounted on a cone [12]. The ion exit hole was 0.12 mm in diameter. The plane of the electron beam was 0.67 mm over the ion exit leak. The distance between the electron slit and the ion exit leak was 5 mm.

An electrostatic shield [15] was mounted below the ion source to provide a boundary for the electric field between the ion source and the ion acceleration electrodes. The shield consisted of a thin wall cylinder slotted longitudinally to maintain pumping speed but without deforming the electric field.

Since the ion source contained elastomer (Viton A) gaskets it could be heated only to a maximum allowable temperature of 150°C . There were six heaters, which consisted of nichrome wire wound around ceramic rods. Two iron-constantan thermocouples were inserted into the ion source. One was positioned near the heaters to allow automatic control. The other was inserted into a well close to the reaction chamber so that the temperature of the gas could be measured. This assumed that the gas attained the temperature of the walls of the chamber.

The ion source was mounted on the vacuum chamber port flange by a cylindrical steel support which was insulated by a disc of Araldite epoxy resin, capable of withstanding a temperature of about 100°C . The Araldite disc was bolted directly to the flange which remained at room temperature. The thermo-electric e.m.f. of the thermocouple that monitored the gas temperature was measured by a potentiometer, which was accurate to $\pm 0.5^{\circ}\text{C}$. The whole ion source was maintained at a constant +7 volts.

2.3 The Electron Gun.

The electron gun is shown in Figure (2.1). The thoriated-iridium filament [1] emitted electrons which were accelerated slightly by the field between the filament support plate [2] and the extraction electrode [3]. The

electrons were then accelerated and collimated slightly by the focus electrode [4] and finally accelerated to the grounded cone [5]. The filament support plate and the centre of the filament were maintained at -4000 volts. The extractor potential was -3990 volts. The potential on the focus electrode could be varied from -3500 to -3900 volts. After passing through the grounded cone, the electron beam was first collimated by electrode [6] to avoid any stray electrons hitting the deflection plates and then focussed magnetically by a solenoid coil [7] mounted outside the envelope. The size of the spot on the phosphorescent screen was adjusted to be between 1 and 2 mm diameter. The vertical and horizontal position of the beam was controlled by a television tube yoke, also mounted outside the vacuum envelope.

The electron beam was pulsed by applying a voltage to one deflection plate [9a] and maintaining the other one [9b] at ground. Three guard rings were required to give a uniform field between the two deflection plates. The pulse generator output and a total resistance of 10^4 ohms could be varied from 0 to 40 volts, which was sufficient to deflect a 2 mm spot from the 5 mm hole completely.

2.4 The Vacuum Chamber.

The main vacuum chamber consisted of an 8 inch diameter stainless steel tube of 12 inch length which was

pumped by a 1500 l/sec oil diffusion pump. At the top of the pumping lead four 4 inch pipes were welded into the 8 inch lead, mutually perpendicular, to provide mounting flanges. The unused flange in Figure (2.1) carried an ion gauge [25]. A second high capacity diffusion pump was mounted on the flange that held the quadrupole assembly so that it was differentially pumped.

2.5 The Gas Handling Plant.

The gas handling plant was constructed of stainless steel and glass Figure (2.2). The main manifold was surrounded by an oven which could be heated to 150°C to reduce impurities. The pressure in the ion source and inlet system was monitored by an Atlas MCT manometer which could read pressures up to 20 torr.

Two mercury diffusion pumps evacuated the gas handling plant. During a flow experiment the calibrated 4 litre bulb was kept open to provide ballast volume. The flow of dry nitrogen into the gas handling plant was controlled by a Granville-Phillips variable leak. Nitric oxide was leaked into the stream of nitrogen through a very narrow conductance valve. Water was stored in a bulb surrounded by a thermostatically controlled water bath. The vapour pressure of the water in the bulb was determined by the temperature of the bath which in turn determined the

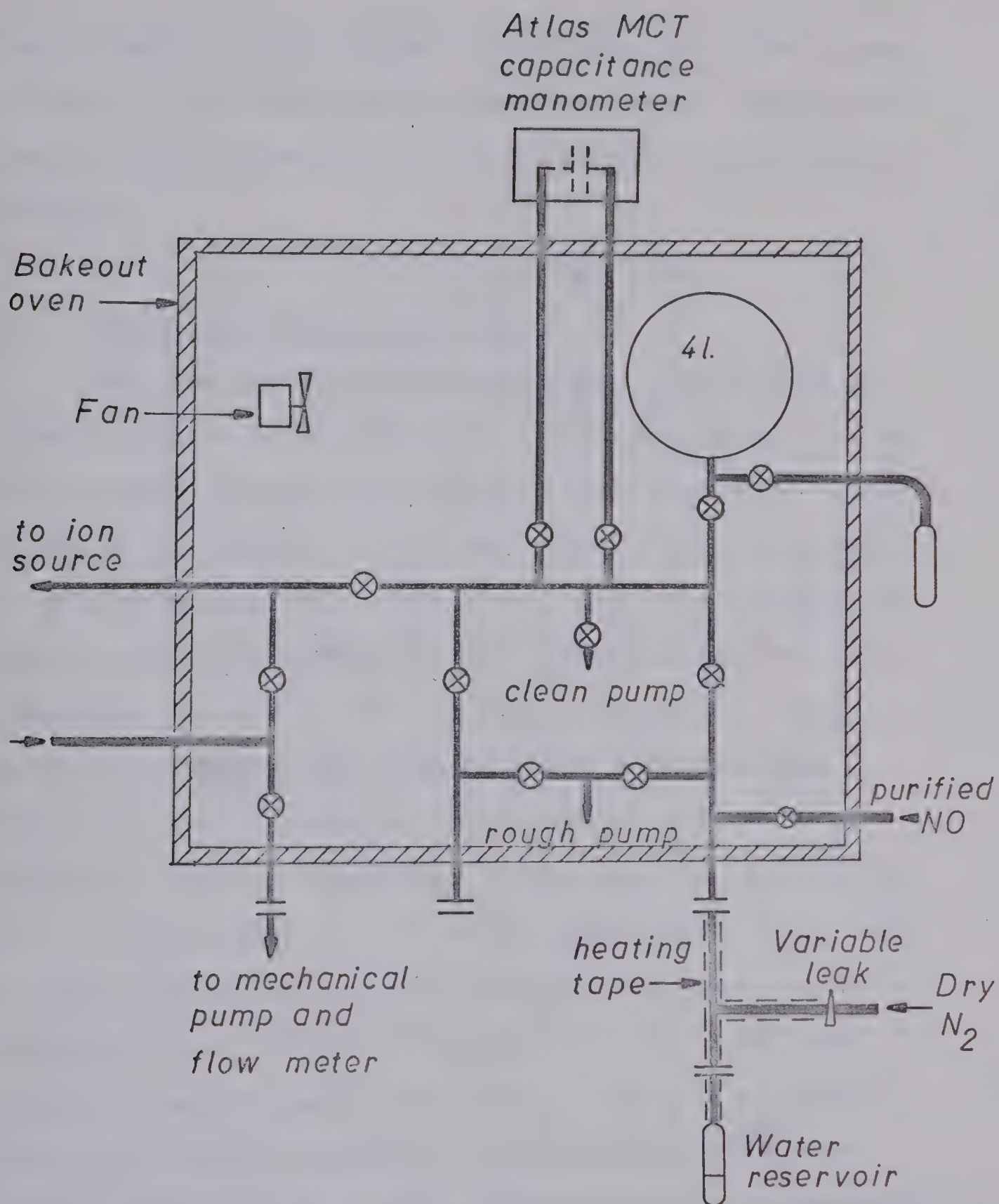


FIGURE 2.2 Gas Handling Plant

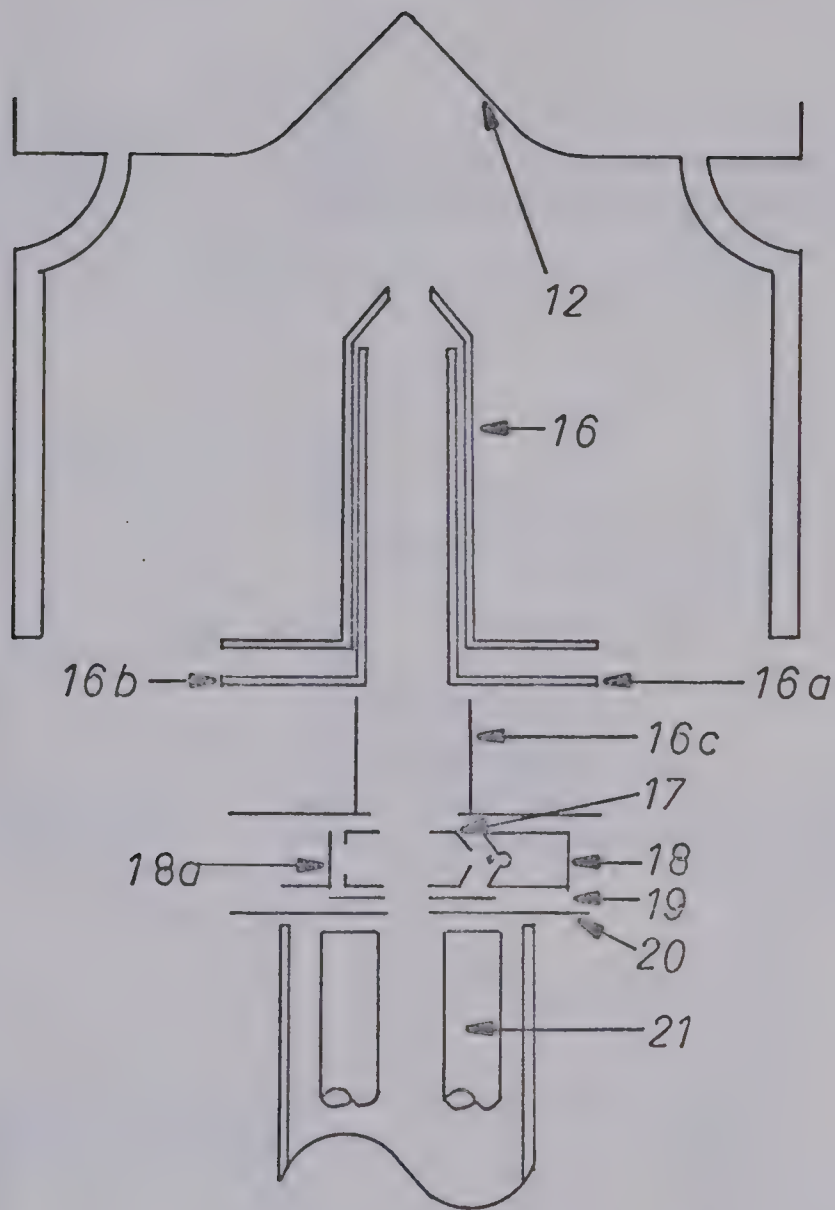
flow of water vapour through a capillary into the stream of gases. The copper tubing where the water vapour was bled into the stream of gases was heated to prevent condensation.

2.6 Ion Acceleration and Gating

The ion acceleration electrodes [16] to [18] are shown in Figure (2.1) and in detail in figure (2.3). As ions diffused through the ion exit slit they were accelerated to the quadrupole entrance cone [16] by a potential of $-67\frac{1}{2}$ volts applied to the cone. The cone was mounted upon the existing quadrupole mass spectrometer ion source equipment, electrodes [17] to [20]. Inside the cone, two half cylinders were mounted [16a] and [16b] and insulated from the cone at the base by a Teflon disc. Electrode [16b] was connected to the cone and was therefore at a potential of $-67\frac{1}{2}$ volts also. Electrodes [16c] to [20] were kept at ground potential. Between pulses electrode [16a] was also at ground, so that ions were deflected and discharged on [16a] or [16c]. A pulse of $-67\frac{1}{2}$ volts would be applied to [16a] so that the cone would be field free and ions could pass into the quadrupole and be analysed.

2.7 Pulsing Circuits.

The pulsing circuits are shown in Figure (2.4).



Scale 1:1

FIGURE 2.3 Ion Acceleration and Gating Electrodes

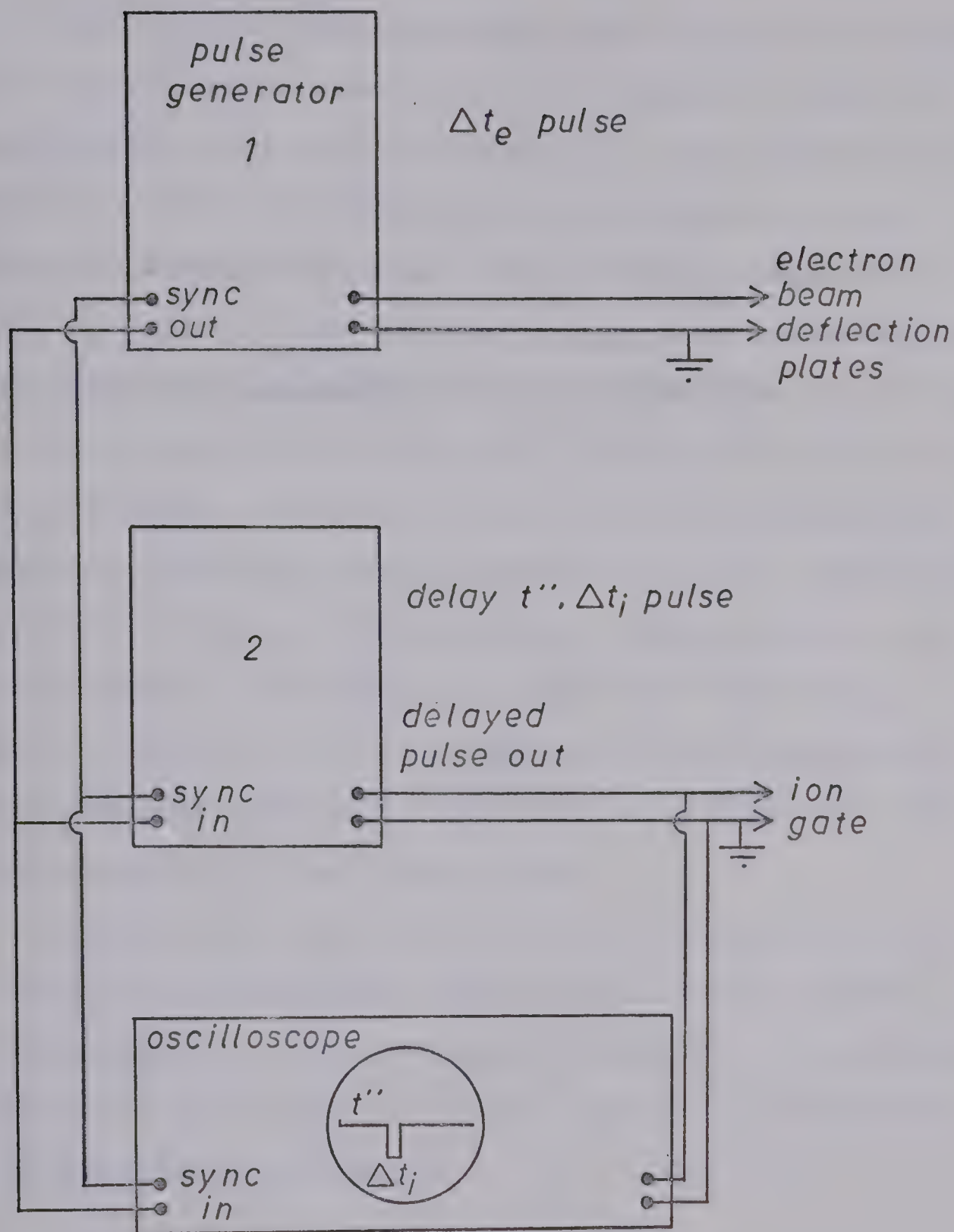


FIGURE 2.4 Pulse Generation Circuit.

The electron beam deflection plate voltage was pulsed by a General Radio pulse generator. A pulse of width Δt_e was applied to the deflection plates. The synchronisation signal was fed into a Datapulse pulse generator which triggered the oscilloscope. After a delay time t'' , a pulse of width Δt_i was applied to the plate inside the cone. This delay time consisted of the reaction time, t_r in the ion source plus the flight time t_f from the ion source to the quadrupole. The vernier scale on the Datapulse generator was not sufficiently accurate and so an oscilloscope was used to measure the delay time. Since only one ion was monitored at one time the flight time for each ion could be preset on the oscilloscope and the reaction time set at regular intervals, otherwise the flight time must be subtracted from each delay time.

In order to pulse the ion signal, an ion gate must be used or the mass spectrometer itself must be pulsed. The technique of using an ion gate results in a reasonably square wave ion signal and allows the mass spectrometer to be operated continuously.

2.8 Quadrupole Mass Analyser and Detection System.

The quadrupole mass spectrometer was an Electron Associates Inc. Quadrupole Residual Gas Analyser, Model 200. Three mass ranges were provided, Low (m/e 1-50), Medium (10 to 150) and High (10 to 500). The quadrupole

probe was powered by an R.F./D.C. Generator. Ions were detected with a secondary electron multiplier (SEM). The signal from the electron multiplier was fed into a Keithley picoammeter and then into a high speed oscillographic recorder. Since the amplifier had a slow response time, the signal indicated on the chart recorder was the integrated signal from many successive pulses.

The Quadrupole Mass Spectrometer was developed by Paul and co-workers (63,64,65). The quadrupole assembly consists of four parallel stainless steel rods, 12.5 cm long. The cross section of the rods should theoretically be hyperbolic, but a circular shape is an adequate approximation (Figure (2.5)). Opposite rods are connected electrically. A D.C. voltage U and a superimposed R.F. voltage $V_0 \cos(\omega t)$ are applied to the rods so that the positive pair of electrodes has a potential of $+(U + V_0 \cos(\omega t))$ and the negative pair a potential of $-(U + V_0 \cos(\omega t))$. An electrostatic field is therefore generated in the region between the rods. The electrodes are separated by a distance of $2r_0$ and the potential V at any point is given by:

$$V = \frac{(x^2 - y^2)}{r_0^2} (U + V_0 \cos(\omega t)) \quad (2.01)$$

where x is the direction of the positive rods and y the direction of the negative rods. z is the longitudinal axis.

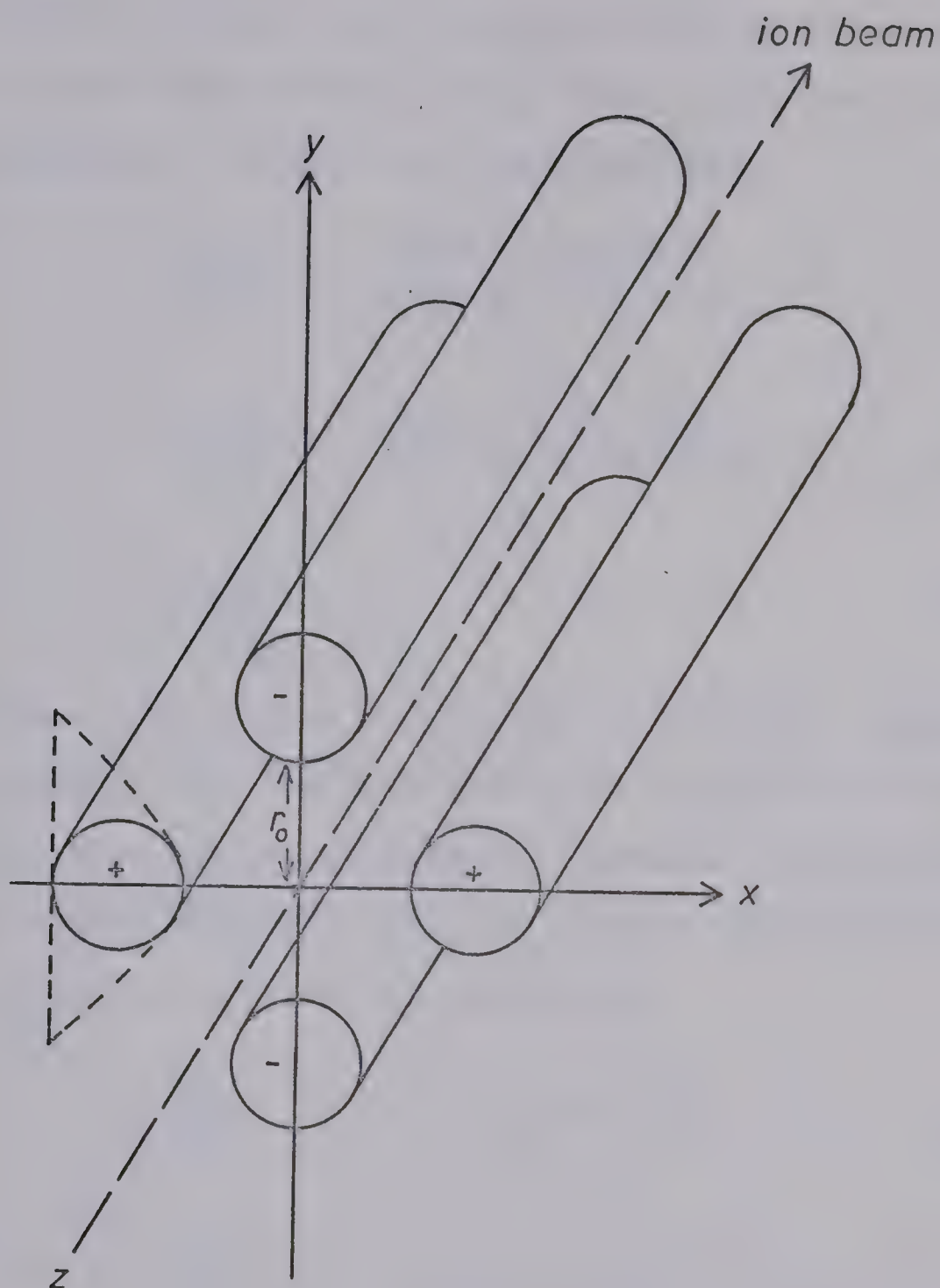


FIGURE 2.5 Quadrupole Rods. The Hyperbolic Cross-section is Approximated by a Circular Cross-section.

Singly charged ions are accelerated by the electrostatic field into the R.F./D.C. field along the z axis.

The equations of motion are described by:

$$m \frac{d^2 x}{dt^2} + \frac{2e(U + V_o \cos(\omega t))}{r_o^2} = 0 \quad (2.02)$$

$$m \frac{d^2 y}{dt^2} - \frac{2e(U + V_o \cos(\omega t))}{r_o^2} = 0 \quad (2.03)$$

$$m \frac{d^2 z}{dt^2} = 0 \quad (2.04)$$

Equation (2.04) may be integrated to give $\frac{dz}{dt} = \text{constant}$, which implies that the ions travel at a constant forward velocity through the quadrupole assembly. Equations (2.02) and (2.03) are solved by using a Mathieu function. The resulting equations of motion are:

$$\frac{d^2 x}{d\phi^2} + (a + 2q \cos(2\phi))x = 0 \quad (2.05)$$

$$\frac{d^2 y}{d\phi^2} - (a + 2q \cos(2\phi))y = 0 \quad (2.06)$$

The three dimensionless parameters are:

$$\phi = \frac{\omega t}{2} \quad (2.07)$$

$$a = \frac{8eU}{mr_o^2 \omega^2} \quad (2.08)$$

$$q = \frac{4eV_o}{mr_o^2 \omega^2} \quad (2.09)$$

The trajectory of an ion entering the quadrupole assembly is determined by the parameters ϕ , a and q . There is a region of stable oscillations where the amplitude remains less than $2r_o$. This region is shown in the stability diagram in Figure (2.6). Ions which have parameters outside the stability region follow a trajectory of increasing amplitude and strike the rods. Therefore only ions which possess the parameters which lie in the stability region pass through the quadrupole assembly and are detected. The range of different masses observed at one time is determined by the ratio a/q . If a/q is small (dashed line in Figure (2.6)) many ions of similar mass (m_1, m_2, m_3) will be detected and the resolution is low. If a/q is large (solid line), the range of masses observed becomes very small until the ideal situation occurs where only one ion is observed. The resolution increases with the a/q ratio and should theoretically become infinite when $a/q = 0.336$. The quadrupole is operated as a mass spectrometer with a/q just smaller than 0.336.

Masses can be scanned in two ways, ω can be kept constant while U and V_o are varied such that the ratio U/V_o is constant or U and V_o can be kept constant while

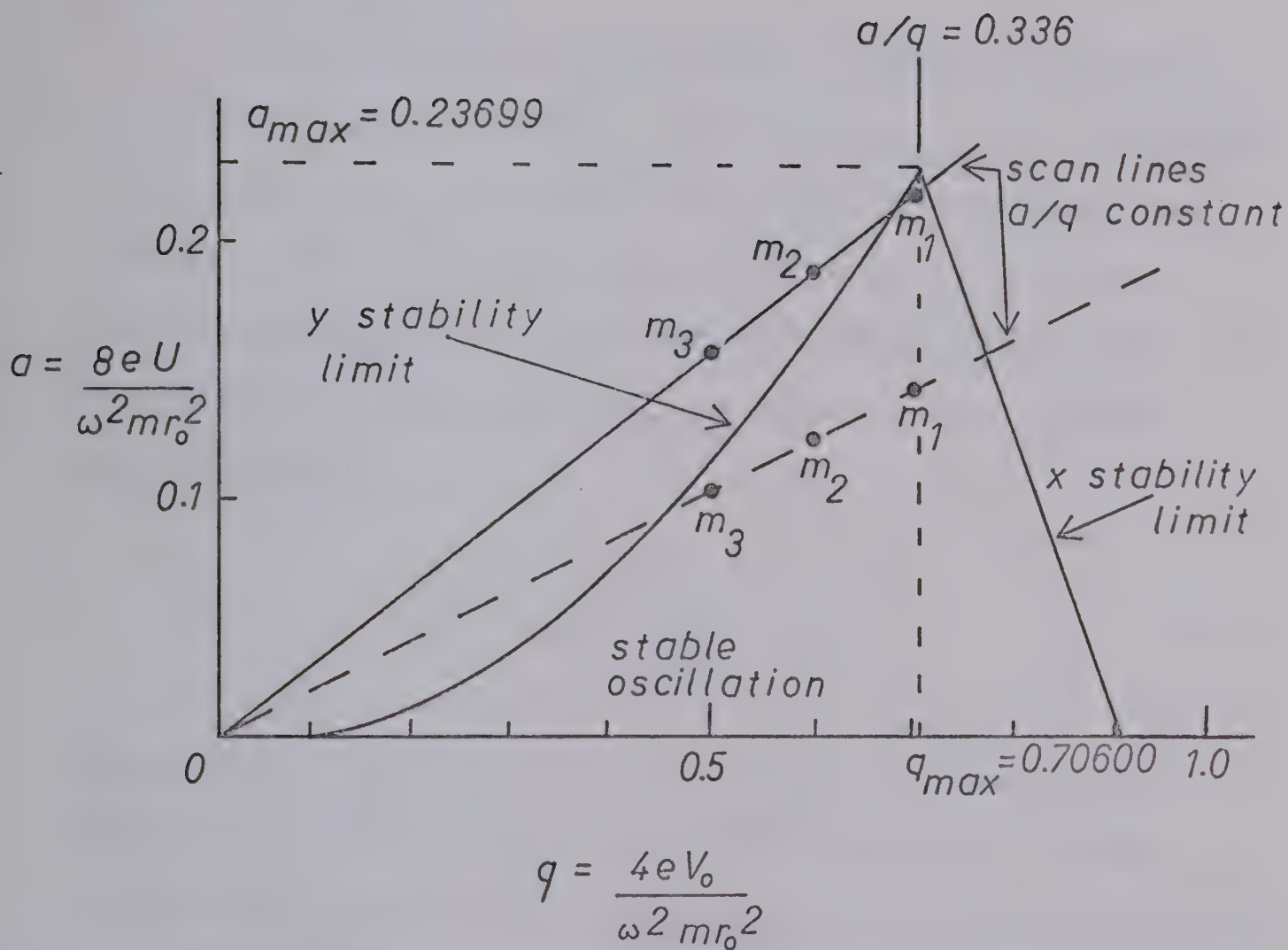


FIGURE 2.6 Stability Diagram of the Mathieu Parameters a and q .

ω is varied. The former method is used by the mass spectrometer in this case.

2.9 Transmission of the Analyser.

The quadrupole mass spectrometer requires no ion defining apertures as a result the transmission of the quadrupole is large.

The transmission of an ion is dependent upon the U/V_0 ratio ($U/V_0 = a/2q$). Von Zahn et al. (66) assumed that q was kept constant at the apex of the stability diagram and that any deviations from $a/q = \text{constant}$, were dependent on a . Von Zahn developed an equation for the observed intensities of two ions I_1 and I_2 after mass analysis:

$$\frac{I_1}{I_2} = \frac{I_1^\circ (a_{\max} - a_1)}{I_2^\circ (a_{\max} - a_2)} \quad (2.10)$$

where $a_{\max} = 0.23699$ and I_1° and I_2° are the original intensities of the two ions before analysis. If the ratio U/V_0 remains constant as U and V_0 are changed then a/q will remain constant also and the transmission for all ions will be constant. It was found that the ratio U/V_0 did not remain constant as U and V_0 were changed (62). The instrument therefore had to be calibrated for each mass range.

The quadrupole transmission was calibrated by a

technique described by Brunée et al. (67). The instrument was modified to permit collection of the total ionisation. When the D.C. voltage is switched off, $a/q = 0$ and there is no discrimination of ions. A small R.F. voltage is required to focus the ions and all ions of mass greater than that corresponding to the small value of V_0 are collected.

The transmission factors were measured in the following manner. The ion source exit leak was replaced by a large leak, about 1 mm in diameter. A repeller was spot welded to the electron trap so that the ion source could be operated as a conventional low pressure ion source but with electron energy of 4000 eV instead of 70 eV. The large leak was necessary because a large signal was required since the measurement was made with the SEM turned off. The gases used to calibrate the mass spectrometer were chosen so that electron impact produced ions of one mass or ions spread over a narrow mass range.

First, the intensity of the ions were measured with both U and V_0 switched on. The D.C. voltage U was then switched off and the total ionisation focussed and then measured. Both measurements were taken without the SEM.

The intensity of the major ion was corrected for fragmentation from API tables for 70 eV electrons.

Kebarle and Godbole (68) showed that the fragmentation

pattern remained essentially the same as the electron voltage was increased.

The medium mass range was the only one used in this work, the transmission curve is shown in Figure (2.7).

2.10 Discrimination in Detection by the Electron Multiplier.

The ion current in the present apparatus was detected by a 14 stage, copper-beryllium secondary electron multiplier (SEM). The electron multiplier does not detect ions of different masses with equal efficiency. The number of ions ejected from the first dynode by the collision of an ion, depends on the ionic mass and chemical structure. The total amplification is therefore proportional to the number of electrons ejected from the first dynode. Beynon reported (69) that the secondary electron current is proportional to the velocity of the ion. Positive ions of different masses are accelerated towards the first dynode by its negative potential. All the ions will have the same energy when the first dynode is reached and their velocities will be proportional to $(\text{mass})^{-1/2}$. The relative electron currents for two ions of masses m_1 and m_2 will be related by:

$$\frac{i_1}{i_2} = \left(\frac{m_1}{m_2} \right)^{1/2} \quad (2.11)$$

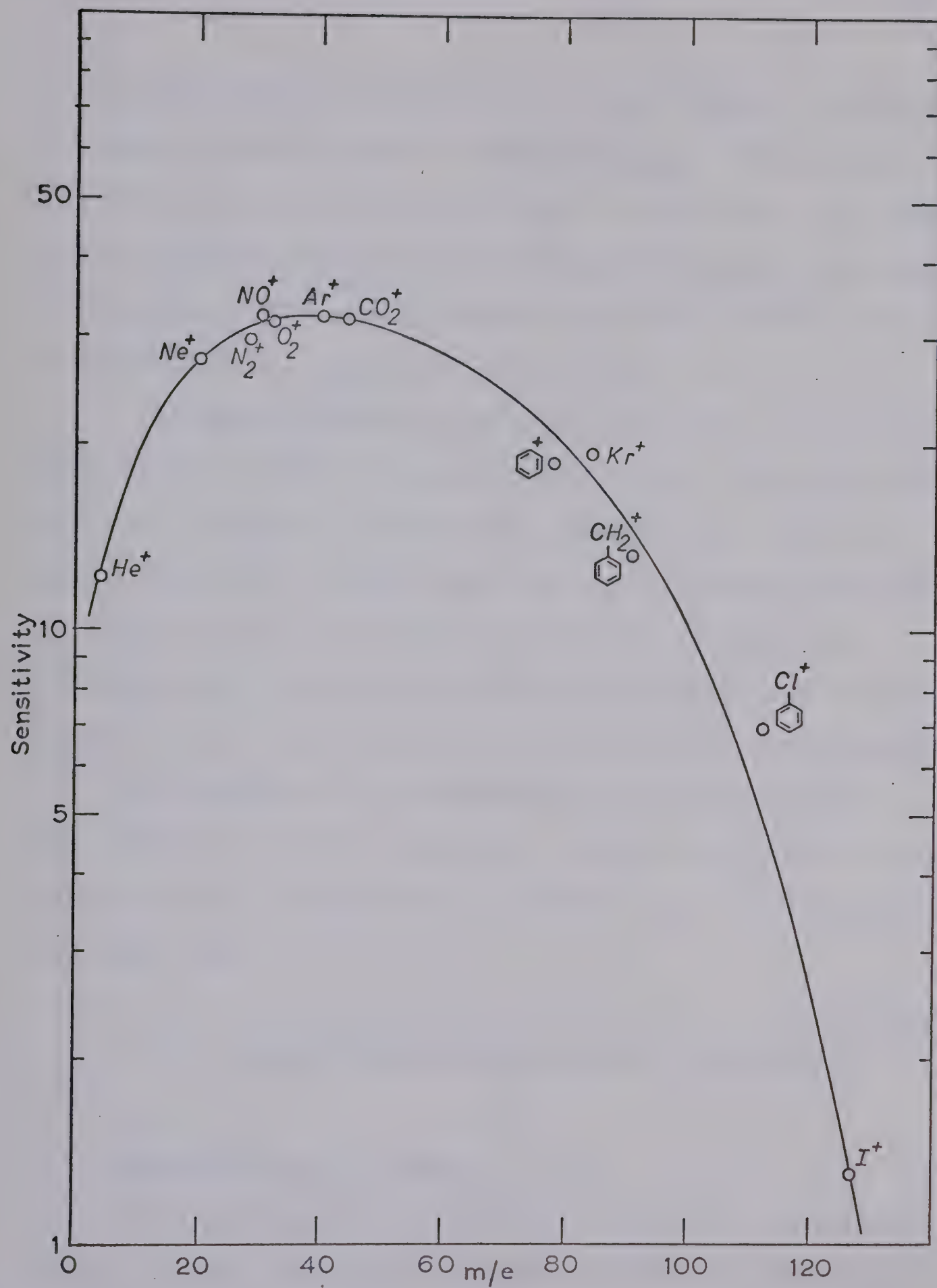


FIGURE 2.7 Sensitivity curve for medium mass range

The chemical composition is also thought to affect the amplification factor. Stanton et al. (70) found that multi-atomic ions break apart on collision with the first dynode and behave as a group of particles with the same energy. The amplification factor was found to increase with the complexity of the ion.

The amplification factors of the ions to be studied were measured with the present instrument. The ion signal was first measured with the SEM switched on. The ion signal was then recorded with the first dynode connected directly to the chart recorder, so that it acted as a Faraday cup. The amplification or SEM factor was calculated from the ratio of the first and second ion signals.

The measured ion intensities were corrected for discrimination by the quadrupole analyser and the electron multiplier by multiplying by a factor F_i , calculated for each ion i by:

$$F_i = \frac{1}{\text{Quad. Sensitivity factor} \times \text{SEM factor}} \quad (2.12)$$

2.11 Purification of Gases.

High purity nitrogen (Matheson Co. Inc. containing 2 ppm O_2 , and 7 ppm H_2O) was passed through a molecular sieve (Type 3A) to remove water. Nitric oxide (Matheson Co. Inc. Research grade) contained about 3% nitrogen

dioxide which together with water was removed by passing through a trap which was cooled to -78° by a slush bath of acetone and dry ice.

2.12 Determination of Component Partial Pressures in the Ion Source.

The total pressure in the ion source was monitored by the MCT manometer. The intensities of N^{+} , H_2O^{+} , N_2^{+} and NO^{+} were measured with the auxiliary low pressure ion source. The ionisation cross-sections of H_2O^{+} , N_2^{+} and NO^{+} are almost identical (71) and so can be neglected. The measured intensity of each ion was multiplied by the respective sensitivity factor, F_i and the total ion intensity $\sum I$ calculated. The partial pressure of NO was found from the ratio:

$$\frac{P_{NO}}{P_{tot}} = \frac{I_{NO^{+}}}{\sum I} \quad (2.13)$$

The spectrum was remeasured at the end of the experiment to establish that the partial pressures of the reactants had not changed.

The water pressure could not be measured in the same manner as the intensity of H_2O^{+} was so small. Instead, the partial pressure was found by the weight loss of water in the bulb over a known period of time. If x gms of water are lost per minute. Then the water flow rate through the system is given by:

$$\text{Flow rate of water (cc/min)} = 22400 \times \frac{T_f}{273} \times \frac{760}{700} \times \frac{x}{18} \quad (2.14)$$

where T_f is the temperature of the flowmeter in °K.

The total rate of flow of the gases was determined by means of a bubble flow-meter attached to the exhaust of the backing pump. Assuming that all of the gases flow at the same rate the partial pressure of water can be calculated from:

$$\frac{P_{H_2O}}{P_{total}} = \frac{\text{Flow rate of water (cc/min)}}{\text{Total flow rate (cc/min)}} \quad (2.15)$$

The gases were allowed to flow for several hours in order to observe a measurable weight loss of water.

2.13 Experimental Procedure Used to Obtain Data in a Given Run.

The flowing gases were allowed to equilibrate for several hours before any measurements were taken. The spectrum using the quadrupole filament (70 eV) was first measured and then switched off and the quadrupole assembly kept at ground potential. Ions from ion-molecule reactions in the high pressure ion source could then be observed.

A spectrum was recorded with the electron beam

entering the ion source continuously and was used to identify the ions present. The electron beam was then pulsed and the spectrum recorded with the ion gate open continuously. The mass spectrometer was adjusted so that only one mass was observed and the ion gate switched to the pulsed mode. The delay curve was measured for each ion observed in the previous spectrum by recording the ion intensity at increasing delay times. The ion intensities were measured at certain times between 0 and 1000 μsec .

Each time the ion intensity was measured the chart recorder was moved forward and stopped so that the delay curves appeared as step functions on the chart paper.

The measured intensities of each ion were then multiplied by the sensitivity factor F_i and then normalised so that the intensity of an ion at any time was expressed as a fraction of the total ion intensity at that time. The normalisation procedure was necessary as the total ion current varied with time.

2.14 Experimental Conditions.

The electron beam was pulsed on every 2 msec for a period of 10 μsec . A current of 4.5 amps was passed through the filament and the current observed on the electron trap was approximately 1 μamp .

Most of the experiments were carried out at approximately room temperature. The heating effect of the electron

beam raised the actual temperature in the ion source to $35 \pm 0.5^\circ\text{C}$. Several experiments were conducted at various temperatures between 35°C and 130°C .

The total pressure in the ion source was varied between 1.5 and 3.5 torr. Most experiments were performed at a total pressure of 2.0 torr. The pressure of nitric oxide was varied between 0.03 and 0.70 torr. The actual pressure of nitric oxide in the D region of the ionosphere is of the order of 10^{-7} torr. The water vapour pressure was maintained in the millitorr range.

In the ionosphere N_2 and O_2 are involved as third bodies in ion-molecule reactions. Since the kinetics of the reactions of N_2 and O_2 in water were also well known, they were chosen as a diluent in the flow system. Both O_2^+ and N_2^+ are capable of charge exchanging with NO. The charge exchange with O_2^+ would be more efficient but the reaction of NO with O_2 would produce undesired NO_2 and complicate the kinetics. Nitrogen was therefore chosen as a diluent.

CHAPTER 3

R E S U L T S A N D D I S C U S S I O N

3.1 Verification of Sensitivity Factors.

An experiment was conducted at a pressure of 1.7 torr N_2 , 0.1 torr NO and 5 mtorr water vapour. Figure (3.1) shows the total ion intensity $\sum_{m=1}^n I_m F_m$ as a function of time where $n = 10$, I_m is the detected ion intensity and F_m is the mass dependent sensitivity correction factor (see section 2.9). Errors in the determination of measured sensitivity or SEM factors of an ion may be detected by obvious discontinuities in the normal smooth decay of the total ionisation at times when the contribution by that ion to the total intensity is significant. In Figure (3.1) the large initial peak is characteristic of this instrument and is thought to be due to stray electrons from the beam colliding with molecules outside the ion source. Otherwise the decay is smooth and no discontinuities appear. Figure (3.1) suggests that the measured sensitivity factors are correct.

3.2 Selection of Concentration Conditions

The variation of ion intensities with time are shown in Figures (3.2) to 3.11), (dashed lines) for total pressures varying from 1.5 to 3.5 torr. The concentrations of reactants during the experiment are shown in Table 3.1.

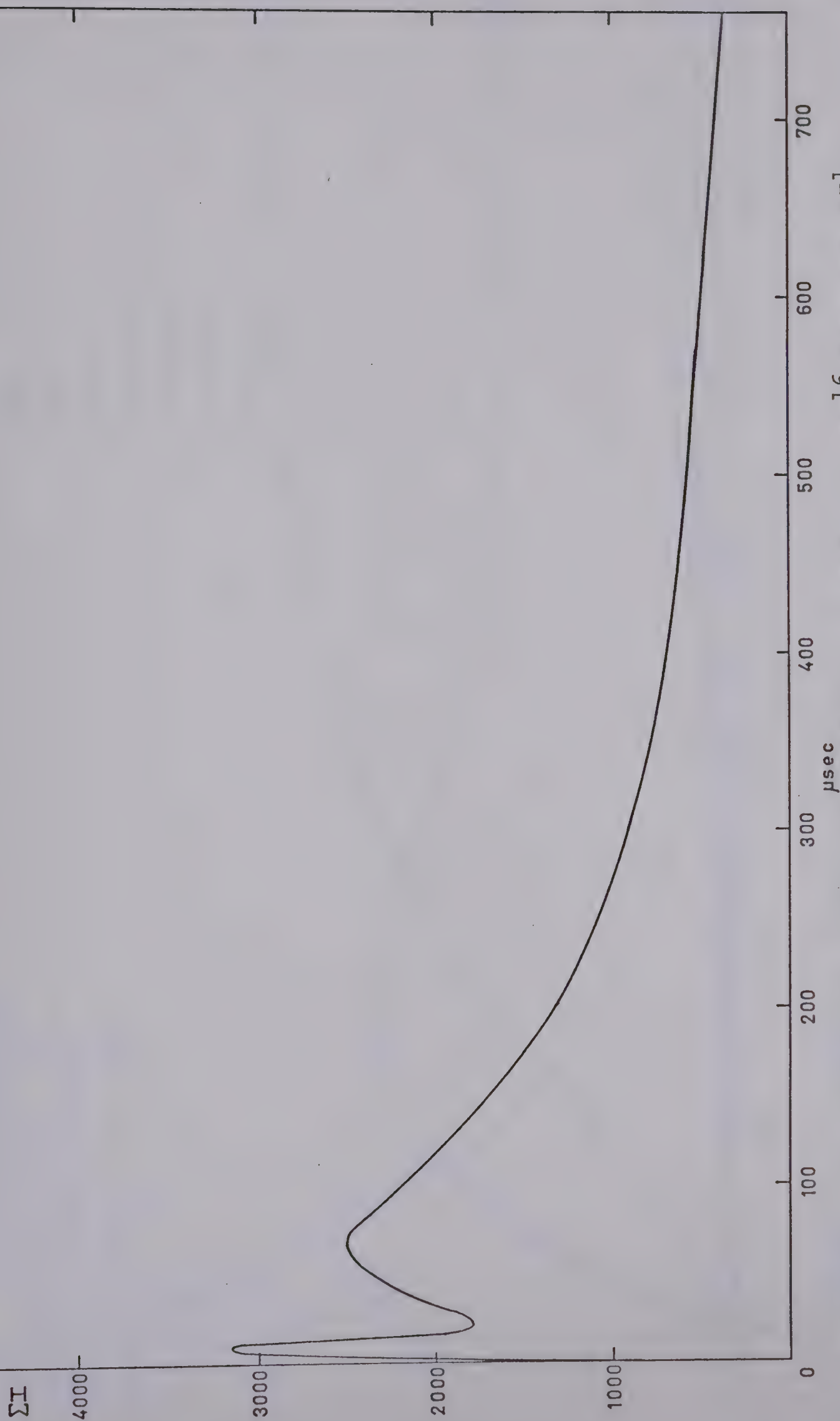


FIGURE 3.1 Corrected total ionisation curve when $[\text{N}_2] = 5.6 \times 10^{16}$ molecule cc^{-1} ,
 $[\text{NO}] = 3.5 \times 10^{15}$ molecule cc^{-1} , $[\text{H}_2\text{O}] = 1.7 \times 10^{14}$ molecule cc^{-1} .

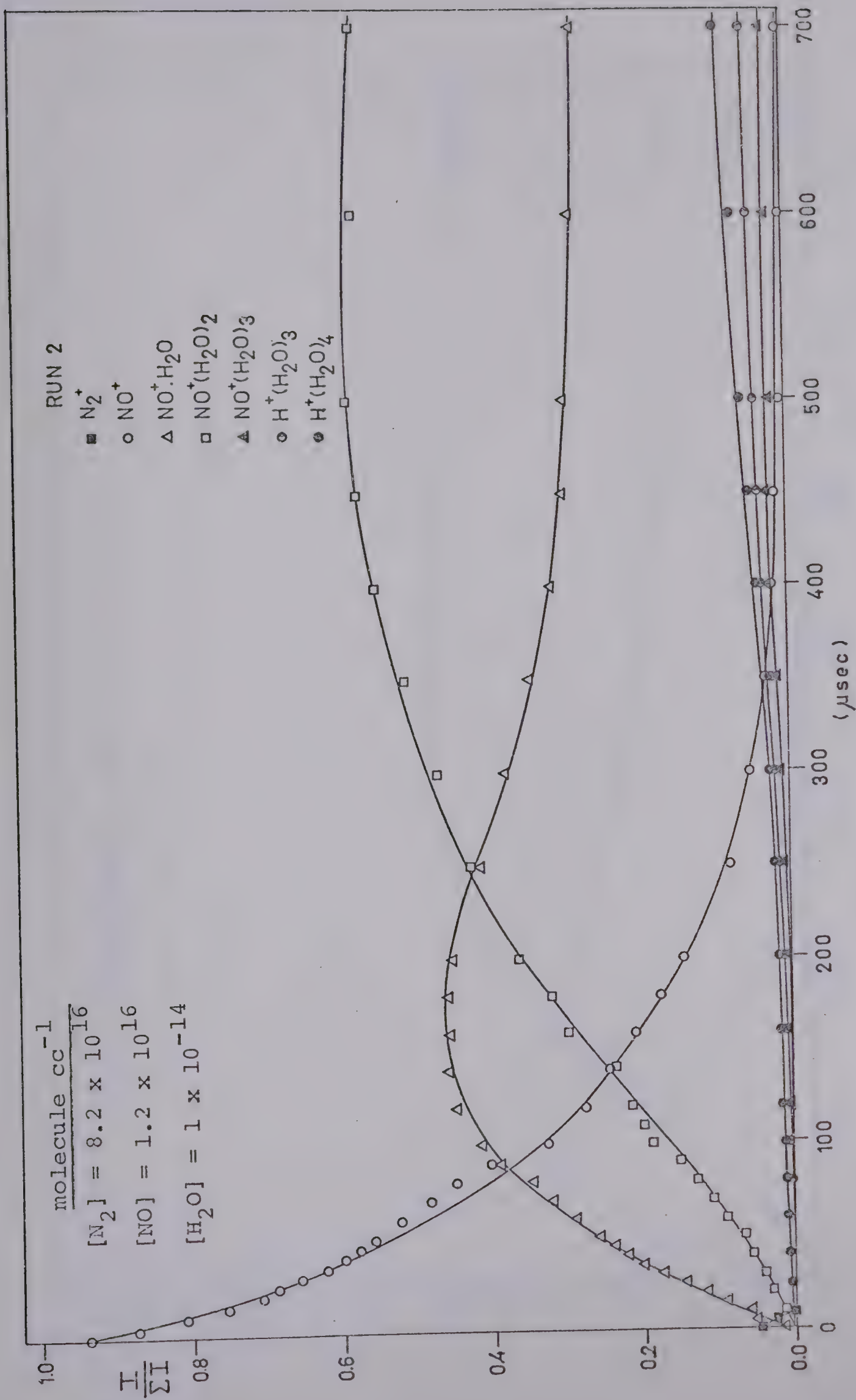


FIGURE 3.1a Normalised experimental data.

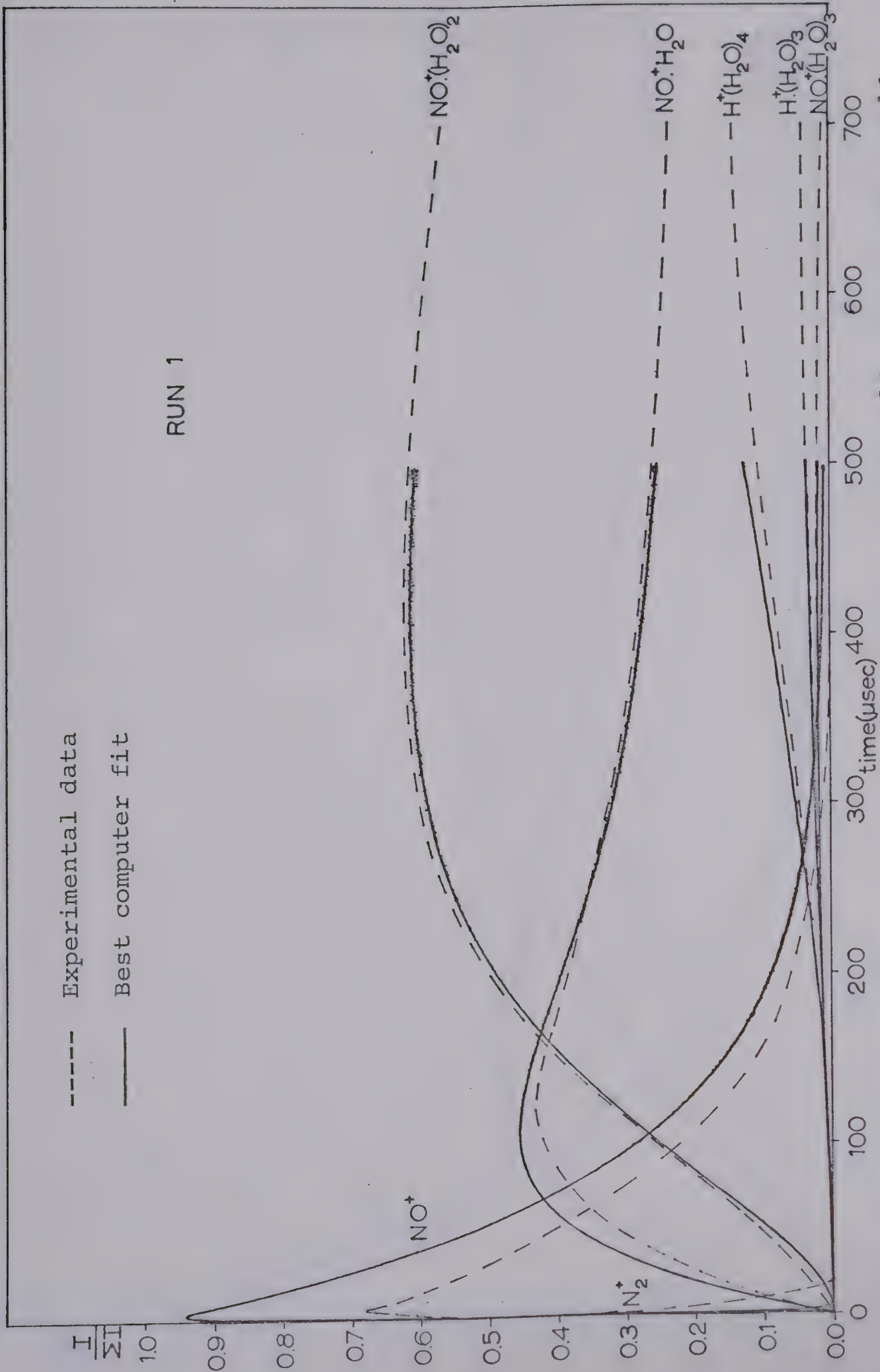


FIGURE 3.2 Normalised ion intensity curves $[\text{N}_2] = 7.8 \times 10^{16}$, $[\text{NO}] = 1.9 \times 10^{16}$, $[\text{H}_2\text{O}] = 1.2 \times 10^{14}$ molecule cc^{-1} .

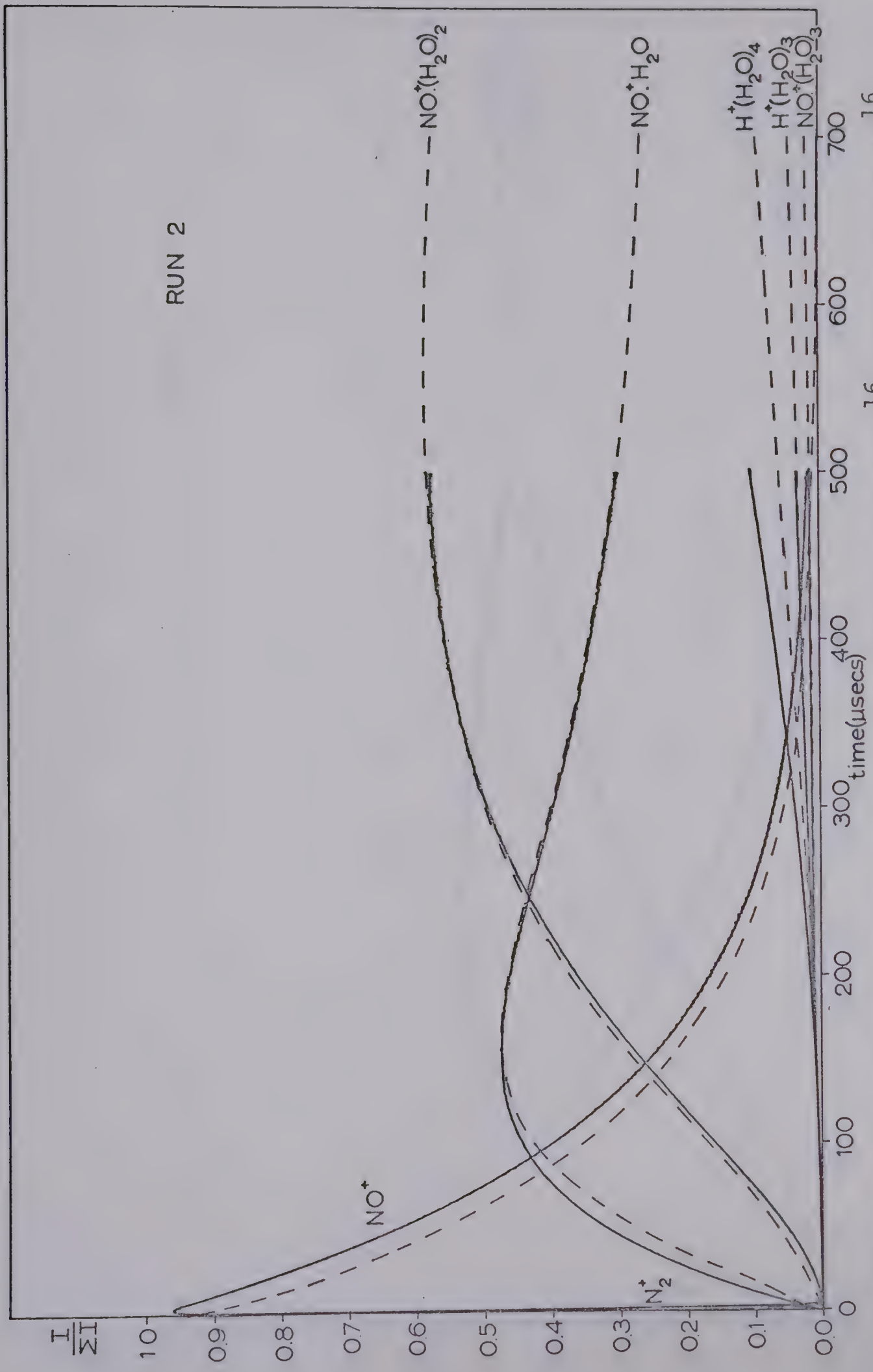


FIGURE 3.3 Normalised ion intensity curves $[\text{N}_2] = 8.2 \times 10^{16}$, $[\text{NO}] = 1.2 \times 10^{16}$, $[\text{H}_2\text{O}] = 1.0 \times 10^{14}$ molecule cc^{-1} .

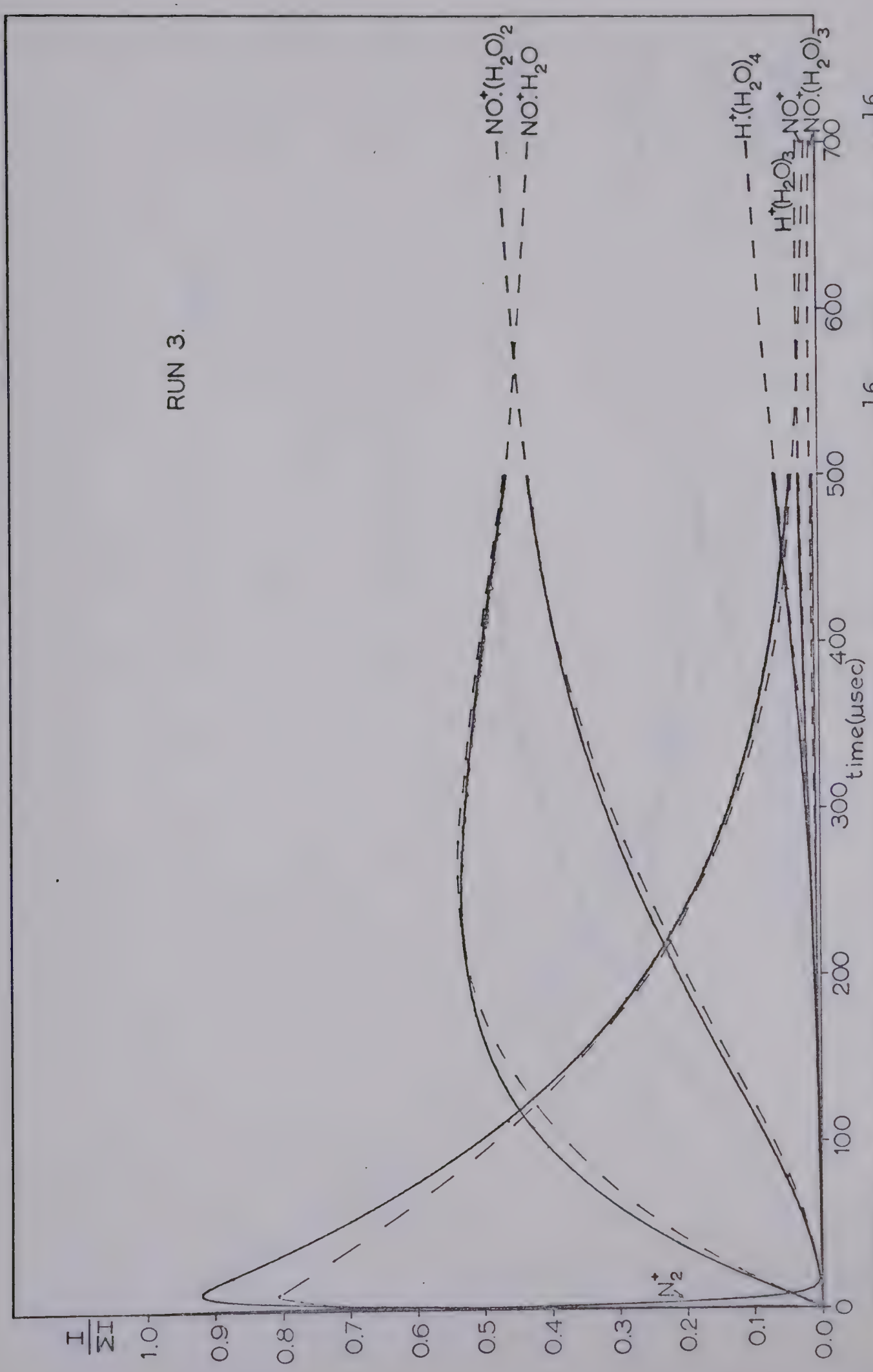


FIGURE 3.4 Normalised ion intensity curves $[N_2] = 5.2 \times 10^{16}$, $[NO] = 1.2 \times 10^{16}$, $[H_2O] = 6.7 \times 10^{13}$ molecule cc^{-1} .

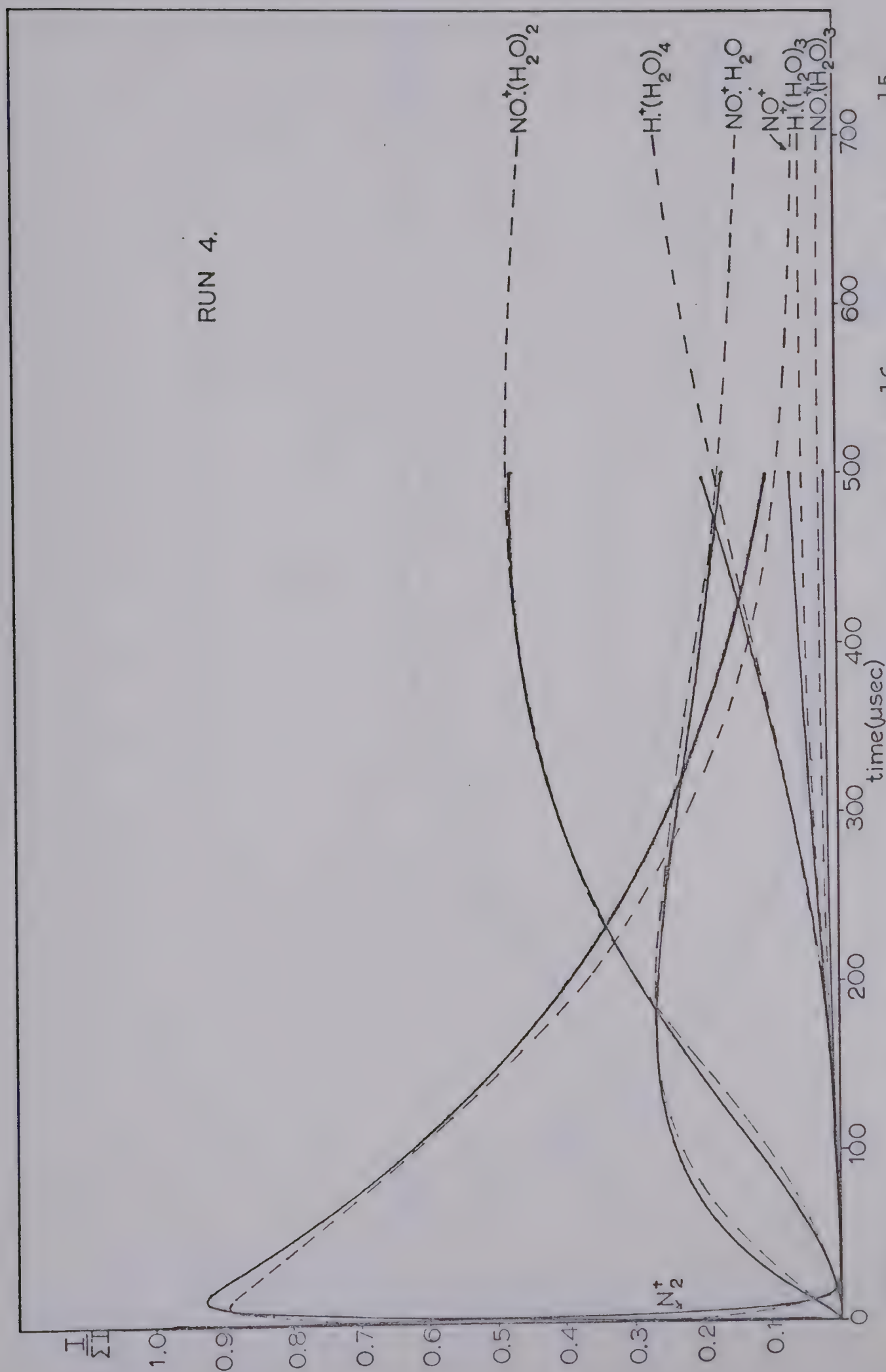


FIGURE 3.5 Normalised ion intensity curves $[N_2] = 3.7 \times 10^{16}$, $[NO] = 1.2 \times 10^{15}$, $[H_2O] = 2.1 \times 10^{14}$ molecule cc^{-1} .

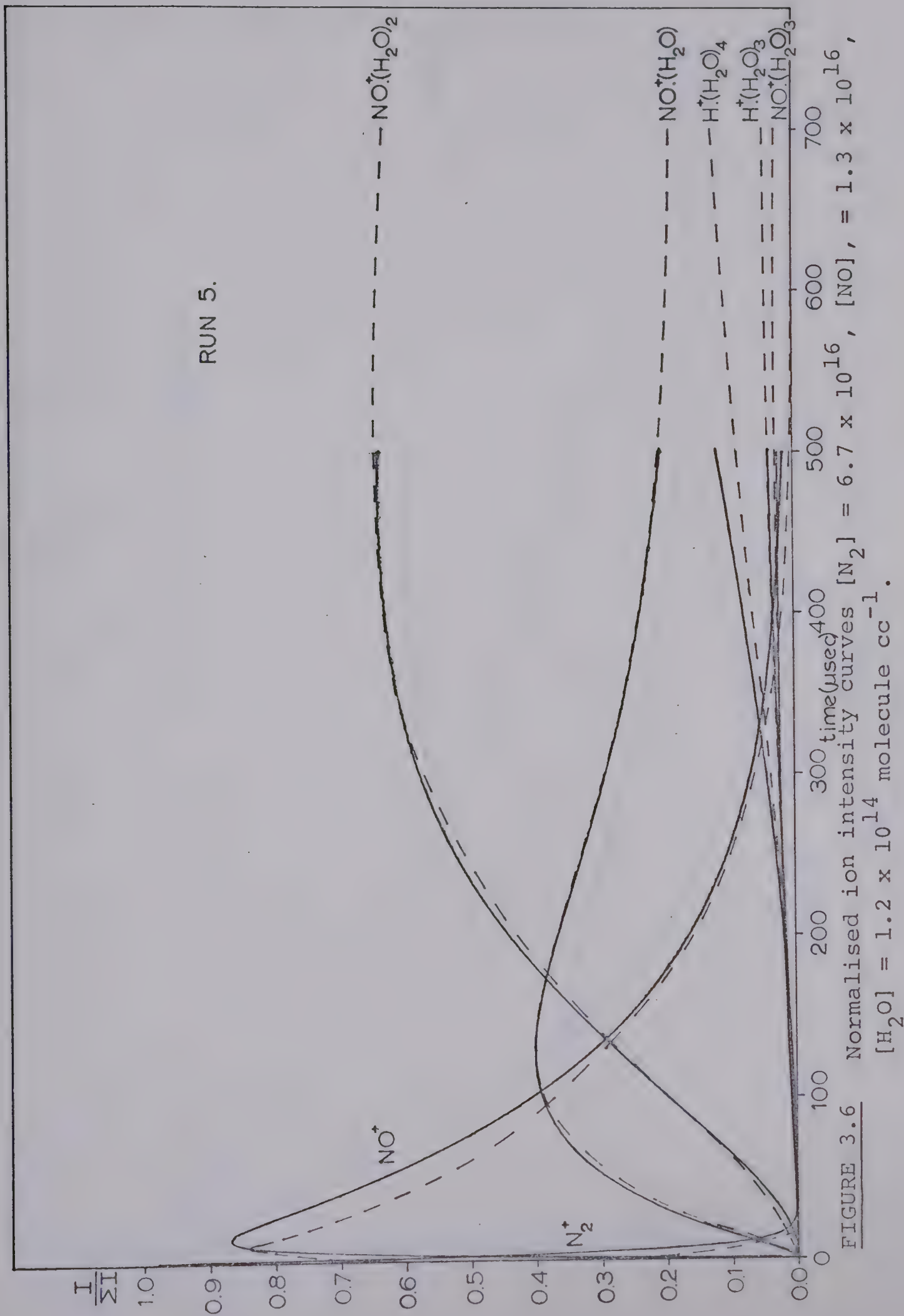


FIGURE 3.6 Normalised ion intensity curves $[\text{N}_2] = 6.7 \times 10^{16}$, $[\text{NO}] = 1.3 \times 10^{16}$, $[\text{H}_2\text{O}] = 1.2 \times 10^{14}$ molecule cc^{-1} .

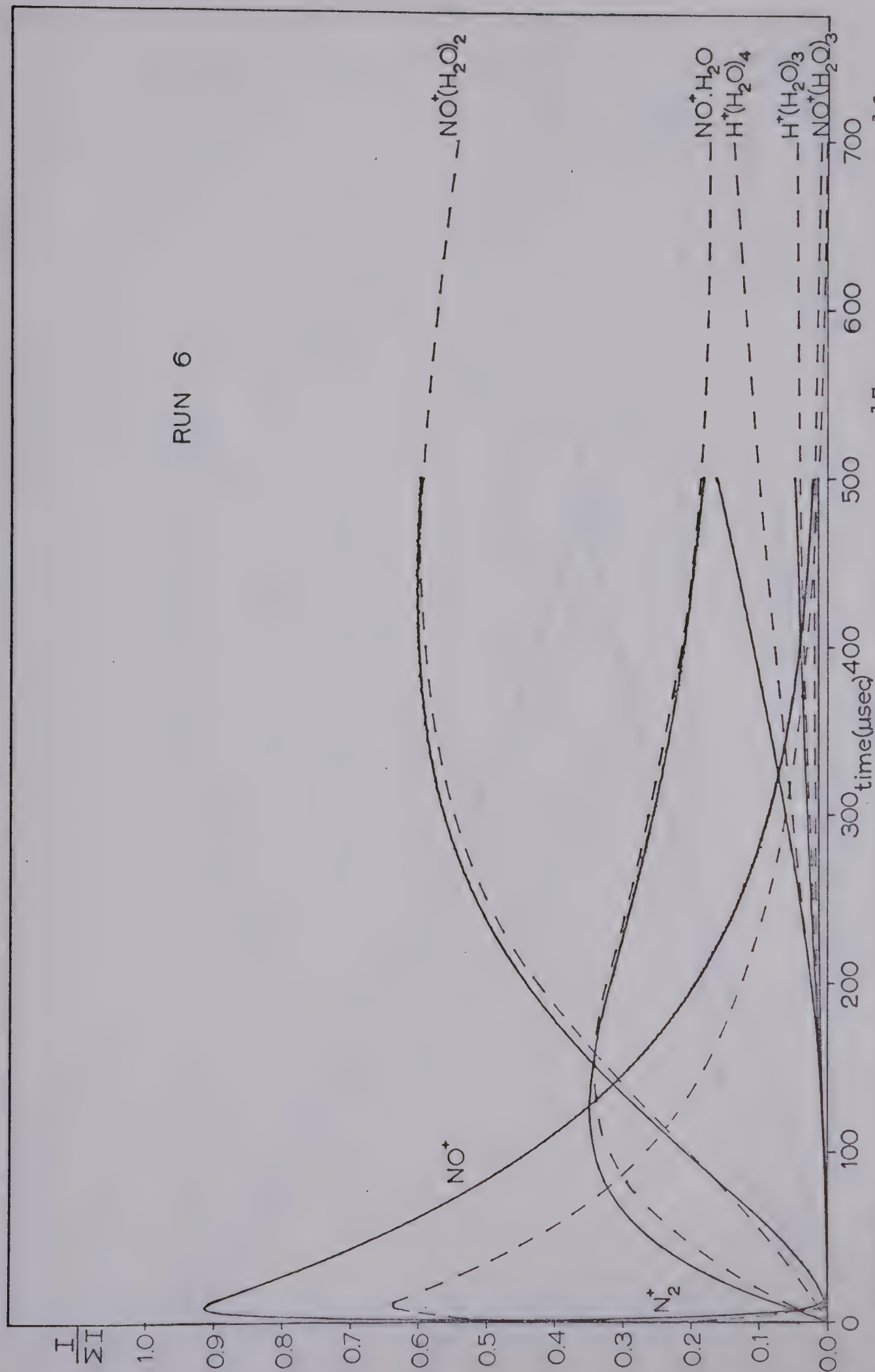


FIGURE 3.7 Normalised ion intensity curves $[\text{N}_2] = 8.4 \times 10^{17}$, $[\text{NO}] = 1.0 \times 10^{16}$, $[\text{H}_2\text{O}] = 1.0 \times 10^{14}$ molecule cc^{-1} .

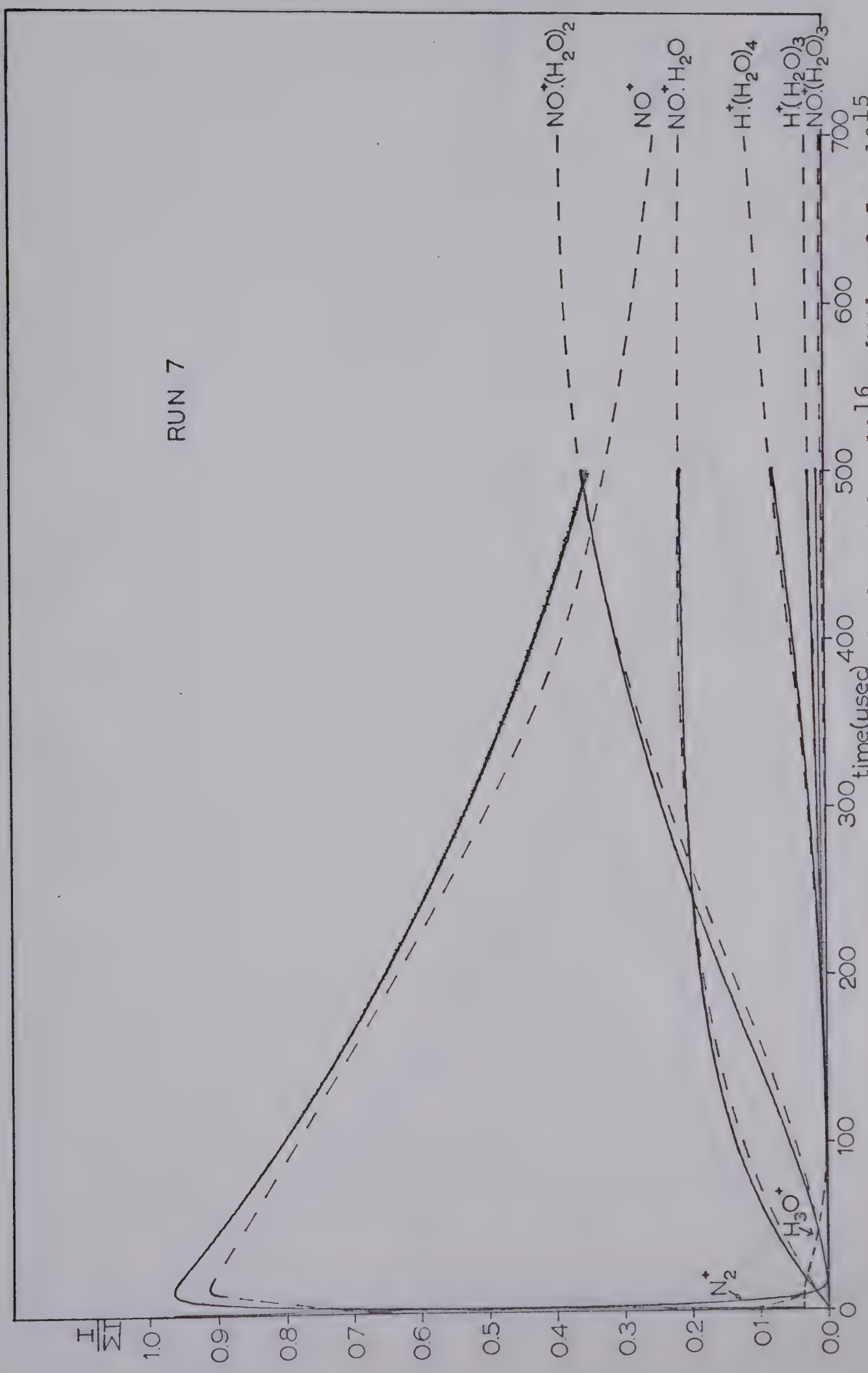


FIGURE 3.8 Normalised ion intensity curves $[N_2] = 5.9 \times 10^{16}$, $[NO] = 2.5 \times 10^{15}$, $[H_2O] = 1.4 \times 10^{14}$ molecule cc^{-1} .

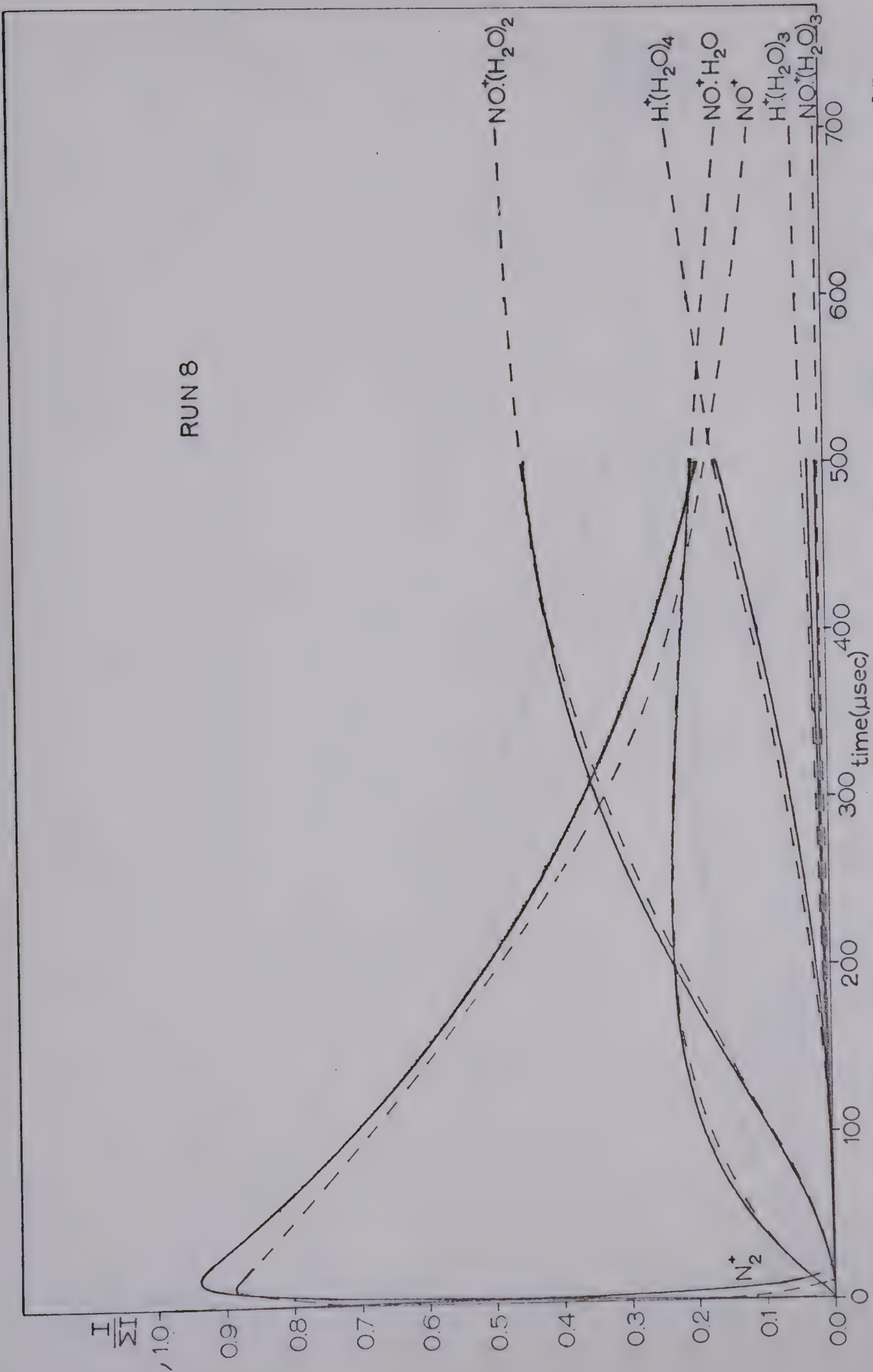


FIGURE 3.9 Normalised ion intensity curves $[N_2] = 6.0 \times 10^{16}$, $[NO] = 2.9 \times 10^{15}$, $[H_2O] = 1.3 \times 10^{14}$ molecule cc^{-1} .

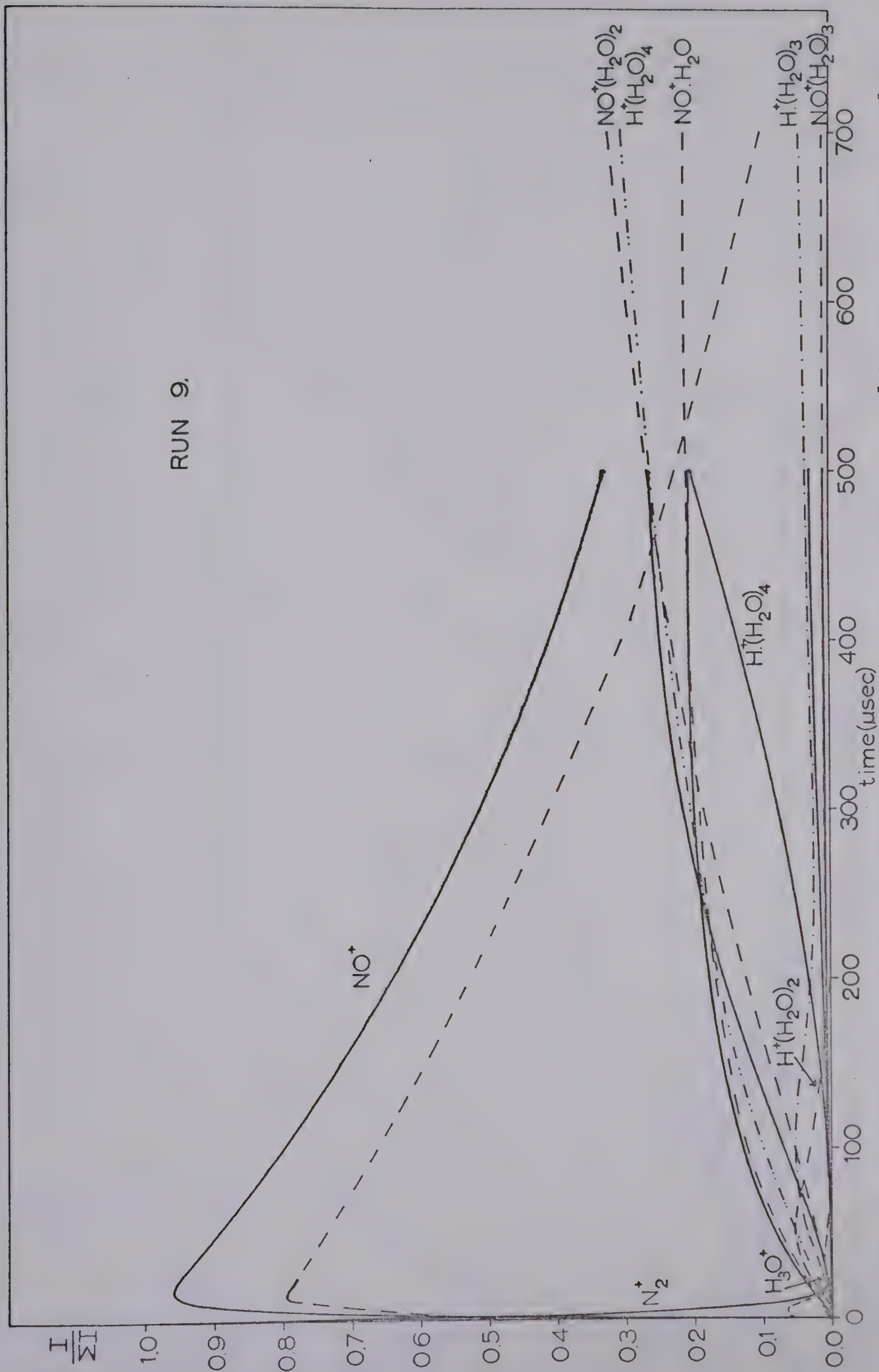
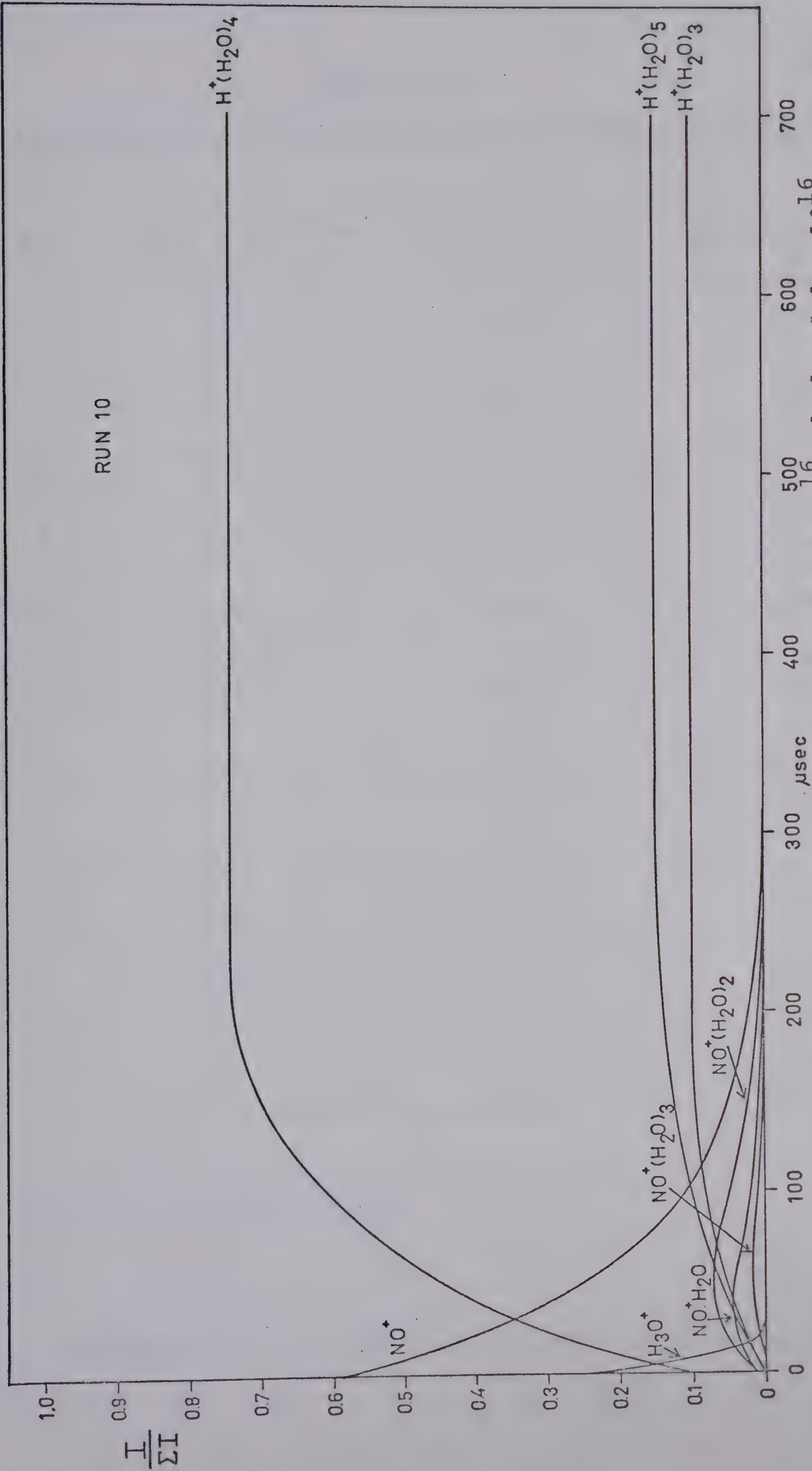


FIGURE 3.10 Normalised ion intensity curves $[N_2] = 6.2 \times 10^{16}$, $[NO] = 1.0 \times 10^{15}$, $[H_2O] = 1.4 \times 10^{14}$ molecule cc^{-1} .



RUN 10

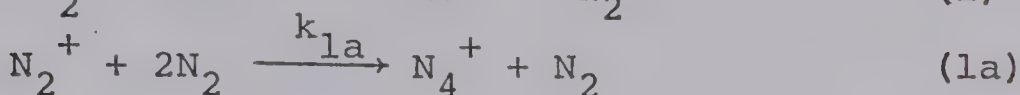
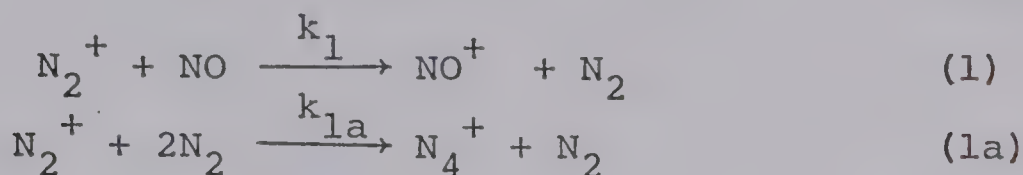
FIGURE 3.11 Normalised Ion Intensity Curves $[\text{N}_2] = 5.5 \times 10^{16}$, $[\text{NO}] = 1.1 \times 10^{16}$, $[\text{H}_2\text{O}] = 2.0 \times 10^{15}$ molecule cc^{-1} .

TABLE (3.1)Concentrations of Reactants in Experiments at 308°K

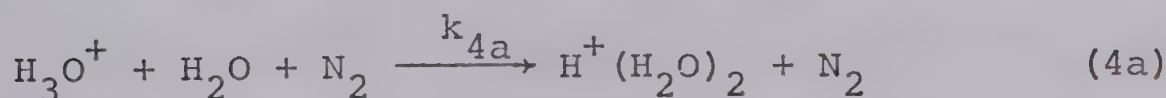
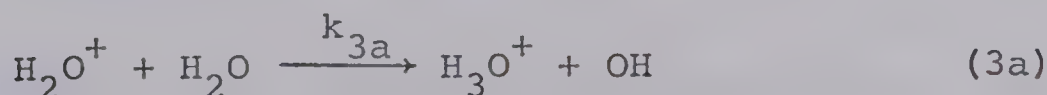
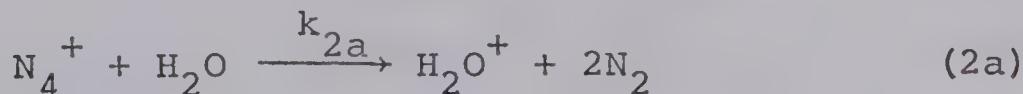
Run	$[N_2] \times 10^{-16} \text{ a}$	$[NO] \times 10^{-15} \text{ a}$	$[H_2O] \times 10^{-14} \text{ a}$
1	7.8	19.2	1.2
2	8.2	12.0	1.0
3	5.2	11.6	0.7
4	3.7	11.6	2.1
5	6.7	12.8	1.2
6	8.4	10.0	1.0
7	5.9	2.5	1.4
8	6.0	2.9	1.3
9	6.2	1.0	1.4
10	5.5	11.3	19.7

(a) Units of molecule cc^{-1} .

N_2^+ was the primary ion whose intensity decayed rapidly. It could either charge exchange with NO, or associate with a molecule of N_2 as in reaction (1a).



The charge transfer to NO is quite rapid and has been measured on two occasions by Ferguson and Fehsenfeld (72,73) to be 5×10^{-10} cc molecule⁻¹ sec⁻¹ and 3.3×10^{-10} cc molecule⁻¹ sec⁻¹ respectively. The formation of N_4^+ initiates the production of proton hydrates by charge exchange with water:



.....



The kinetics of this reaction sequence are well known from previous studies with this instrument (30). The rate constant, k_{1a} is 8.0×10^{-29} cc² molecule⁻² sec⁻¹.

The rate of reaction (1) is given by:

$$R_1 = k_1 [N_2^+] [NO] \quad (3.01)$$

The rate of reaction (1a) is given by:

$$R_{1a} = k_{1a} [N_2^+] [N_2]^2 \quad (3.02)$$

Therefore:

$$\frac{R_1}{R_{1a}} = \frac{k_1 [NO]}{k_{1a} [N_2]^2} \quad (3.03)$$

Under conditions where the NO partial pressure is relatively high e.g. 0.2 torr, the pressure of N_2 is 2.0 torr and assuming that 1 torr of gas at 300°K contains 3×10^{-16} molecules cc^{-1} :

$$\frac{R_1}{R_{1a}} = \frac{5 \times 10^{-10} \times 6 \times 10^{15}}{8 \times 10^{-29} \times (6 \times 10^{16})^2} \approx 10 \quad (3.04)$$

charge transfer to NO is therefore ten times faster than the N_4^+ cluster formation at high NO pressures and reaction (1) occurs preferentially. At lower pressures of NO e.g. 0.02 torr, $R_1 = R_{1a}$ and both reactions (1) and (1a) are observed.

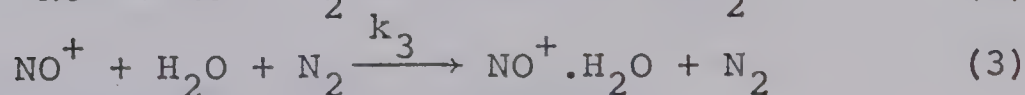
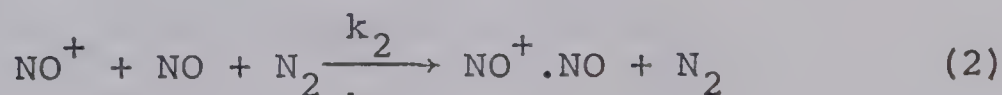
It is possible for N^+ , N_3^+ and N_4^+ to charge exchange with NO also. The rate constants for the charge transfers are quite large e.g.



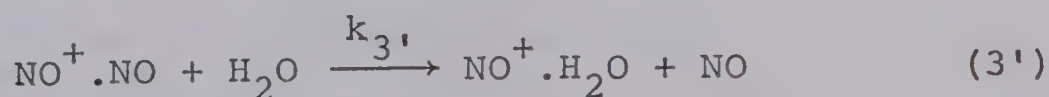
The rate constant for reaction (6a) is 8×10^{-10} cc molecule⁻¹

sec^{-1} (72). The abundances of N^+ , N_3^+ and N_4^+ are very low and these reactions are not normally observed except at very low NO pressures when reaction (1a) is much more favourable than reaction (1).

Inspection of the ion intensity curves, figures (3.2) to (3.11), shows that NO^+ can disappear by two different types of reactions, one is a dimerisation reaction (2) and the other hydration (3) of NO^+ .



Since the kinetics were complicated by the fact that the dimer itself can react with water, reaction (3') to give $\text{NO}^+.\text{H}_2\text{O}$, it was necessary to calculate the conditions which would make one reaction dominate.



The rate constants k_2 and k_3 evaluated by Lineberger and Puckett (49) were used to estimate the optimum conditions to suppress one of the reactions.

Comparing the rates of reactions (2) and (3):

$$\frac{R_2}{R_3} = \frac{k_2[\text{NO}^+][\text{NO}][\text{N}_2]}{k_3[\text{NO}^+][\text{H}_2\text{O}][\text{N}_2]} \quad (3.05)$$

Therefore:

$$\frac{R_2}{R_3} = \frac{5 \times 10^{-30} [\text{NO}]}{1.5 \times 10^{-28} [\text{H}_2\text{O}]} \quad (3.06)$$

when $R_2 = R_3$, equation (3.07) is obtained:

$$[\text{NO}] = 30 [\text{H}_2\text{O}] \quad (3.07)$$

Therefore when $[\text{NO}] \gg 30 [\text{H}_2\text{O}]$, the dimerisation is the dominant reaction and when $[\text{NO}] \ll 30 [\text{H}_2\text{O}]$, hydration of NO^+ is favoured. The choice of the conditions thus enabled the rate constants to be determined directly.

3.3 Pseudo-First-Order Rate Constants, γ

To calculate the rate constant of a reaction, the variation of intensity of the ion with time is studied. If a general reaction (3.08) is observed:



The rate of the reaction may be expressed by:

$$R = k[\text{A}^+][\text{B}]$$

During an ion-molecule reaction the number of neutral species B is very much greater than that of the A^+ ions. Therefore the concentration of the neutral species can be assumed to be constant with time compared to the rapidly changing concentration of the ion. Since [B] is constant a pseudo-first-order rate constant, γ can be defined that

is equal to $k[B]$. Equation (3.08) now becomes:

$$R = \gamma[A^+] \quad (3.09)$$

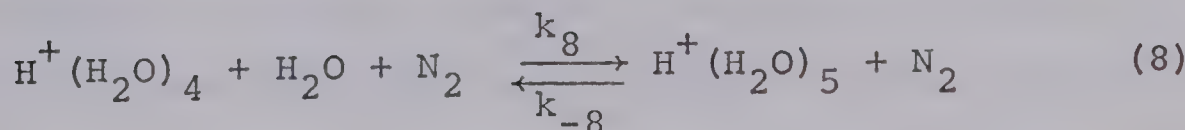
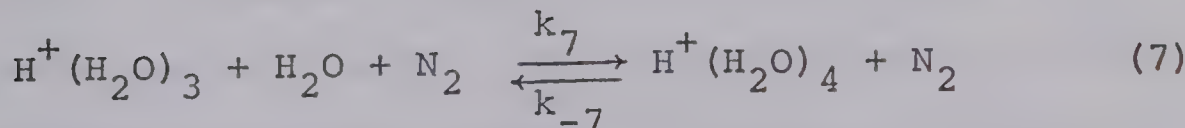
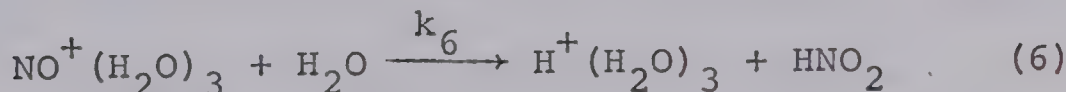
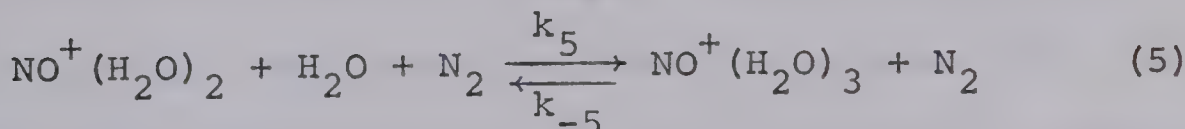
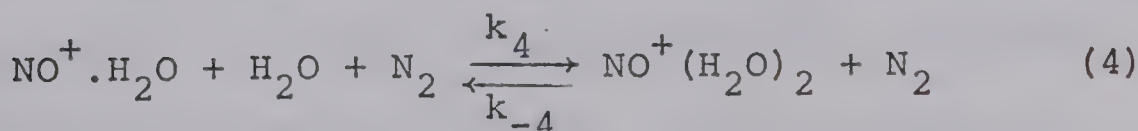
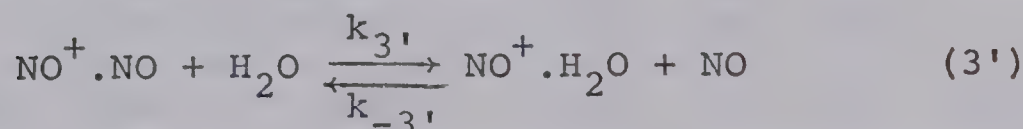
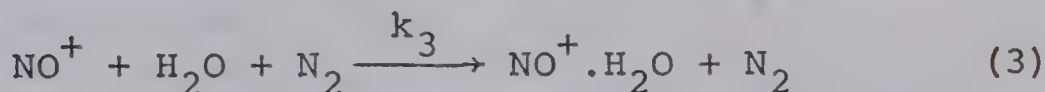
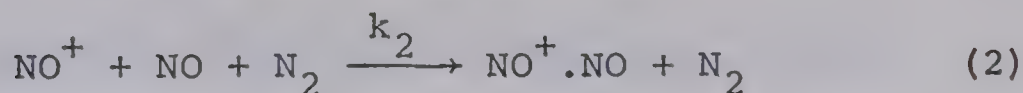
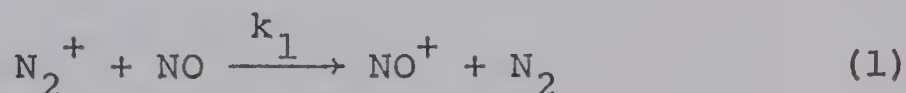
Once the pseudo-first-order rate constant has been evaluated, it can be converted to the rate constant of appropriate order by dividing by the concentration of the neutral species involved in the reaction. The use of pseudo-first-order rate constant in a long sequence of reactions simplifies the mathematical treatment.

3.4 Results at Room Temperature with a Flow of NO, H₂O and N₂.

An inspection of the experimental ion intensity curves (dashed lines) in Figures (3.2) to (3.11) shows that in most experiments the N₂⁺ intensity decays to zero within 25 μsecs. Small amounts of H₃O⁺ and H⁺(H₂O)₂ were observed when the NO partial pressure was small. The intensity of NO⁺ reached a maximum within 10 μsecs. The disappearance of NO⁺ was quite rapid and was followed by the formation of NO⁺.H₂O which approached a constant value at long reaction times. NO⁺(H₂O)₂ followed by NO⁺(H₂O)₃ were also formed which attained approximately constant intensities at long reaction times. These observations implied that NO⁺.H₂O and NO⁺(H₂O)₂ were in equilibrium as were NO⁺(H₂O)₂ and NO⁺(H₂O)₃. H⁺(H₂O)₃ and H⁺(H₂O)₄ became significant at

long reaction times. In experiments with high NO and water pressure $\text{H}^+(\text{H}_2\text{O})_5$ was also observed, as seen in Figure (3.11).

Consideration of the above observations led to the following reaction sequence for the major reactions observed:



Reactions (2) and (3') were included in the reaction mechanism because $\text{NO}^+ \cdot \text{NO}$ was observed to some extent in most reactions.

Rate constants for reactions (2) to (7) were obtained from the experimentally determined ion intensity plots

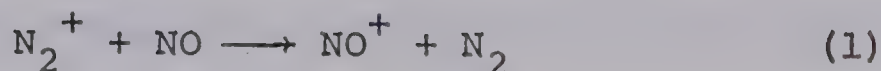
(Figures (3.2) to (3.11) by two different methods. First a set of rate constants was obtained by various graphical plots of the data. A second set of rate constants was then obtained by a computer fitting of the ion intensity curves. The rate constants obtained by graphical methods will be described first.

3.5 Rate Constants Obtained by Graphical Methods

(i) Decay of N_2^+

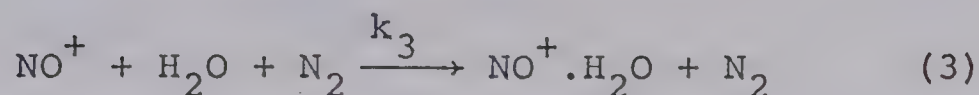
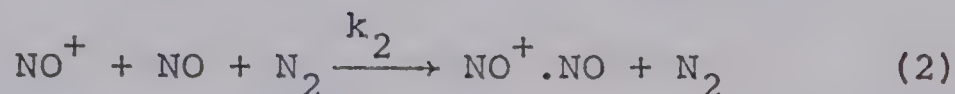
The N_2^+ ion constituted about 10% of the total ionisation at zero time and decayed rapidly. When the electron was pulsed on for 10 μ sec, the ion gate was triggered from the beginning of that pulse. Therefore when the delay time was zero, the ion gate was open for the first 10 μ sec and during that time N_2^+ was decaying by reacting with other molecules but was still being produced by electron impact. The N_2^+ decay could therefore not be described by a simple exponential expression during the first 10 μ sec. Since N_2^+ had decayed to zero intensity by 25 μ sec insufficient measurements could be taken at 5 μ sec intervals to enable the rate constant to be calculated accurately.

Most of the experiments were performed under such conditions that the major reaction of N_2^+ was charge transfer with NO:



(ii) Decay of NO^+

Reactions (2) and (3) could both be involved in the removal of NO^+ .



Therefore the apparent pseudo-first-order rate constant γ_{obs} , describing the decay of NO^+ should be given by:

$$\gamma_{\text{obs}} = \gamma_2 + \gamma_3 \quad (3.10)$$

The variation of the intensity of an ion with time may be described as an exponential decay as in:

$$I = I_0 e^{-\gamma t} \quad (3.11)$$

or:

$$2.303 \log \frac{I}{I_0} = -\gamma t \quad (3.12)$$

where γ is the pseudo-first-order rate constant, I_0 is the normalised intensity of the ion at time zero. Equation (3.12) may only be applied if the intensity of all the precursors of the ion have decayed to zero. Since N_2^+ , which is the precursor of NO^+ , decays to zero intensity within some 20 μsec a plot of $\log I_{\text{NO}^+}$ versus t , for times longer than 20 μsec , should give a straight line with

a slope $-\frac{\gamma_{\text{obs}}}{2.303}$. The logarithmic plots obtained for experiments 1 to 10 are shown in Figure (3.12).

Equation (3.10) can be rewritten:

$$\gamma_{\text{obs}} = k_2[\text{NO}][\text{N}_2] + k_3[\text{H}_2\text{O}][\text{N}_2] \quad (3.13)$$

Dividing both sides of equation (3.13) by $[\text{N}_2][\text{H}_2\text{O}]$:

$$\frac{\gamma_{\text{obs}}}{[\text{N}_2][\text{H}_2\text{O}]} = k_2 \frac{[\text{NO}]}{[\text{H}_2\text{O}]} + k_3 \quad (3.14)$$

If γ_{obs} is determined at different $[\text{NO}]/[\text{H}_2\text{O}]$ ratios, and $\gamma_{\text{obs}}/[\text{N}_2][\text{H}_2\text{O}]$ is plotted against $[\text{NO}]/[\text{H}_2\text{O}]$, the slope of the resulting straight line is equal to k_2 and the intercept is equal to k_3 . A least mean square fit of the points shown in Figure (3.13) led to $k_2 = 8.7 \pm 0.4 \times 10^{-30}$ and $k_3 = 1.8 \pm 0.4 \times 10^{-28} \text{ cc}^2 \text{ molecule}^{-2} \text{ sec}^{-1}$.

(iii) Alternate Determination of Rate Constant k_2
for Reaction $\text{NO}^+ + \text{NO} + \text{N}_2 \rightarrow \text{NO}^+.\text{NO} + \text{N}_2$.

In order to study the formation and reaction of $\text{NO}^+.\text{NO}$ without the complicating effect of the parallel reaction (3), three experiments were performed without water vapour flowing through the system. The whole apparatus was first baked thoroughly to reduce the amount of water as much as possible.

Figures (3.14) to (3.16) show the ion intensity curves (dashed lines) obtained for the experiments with low water concentrations. Under these conditions

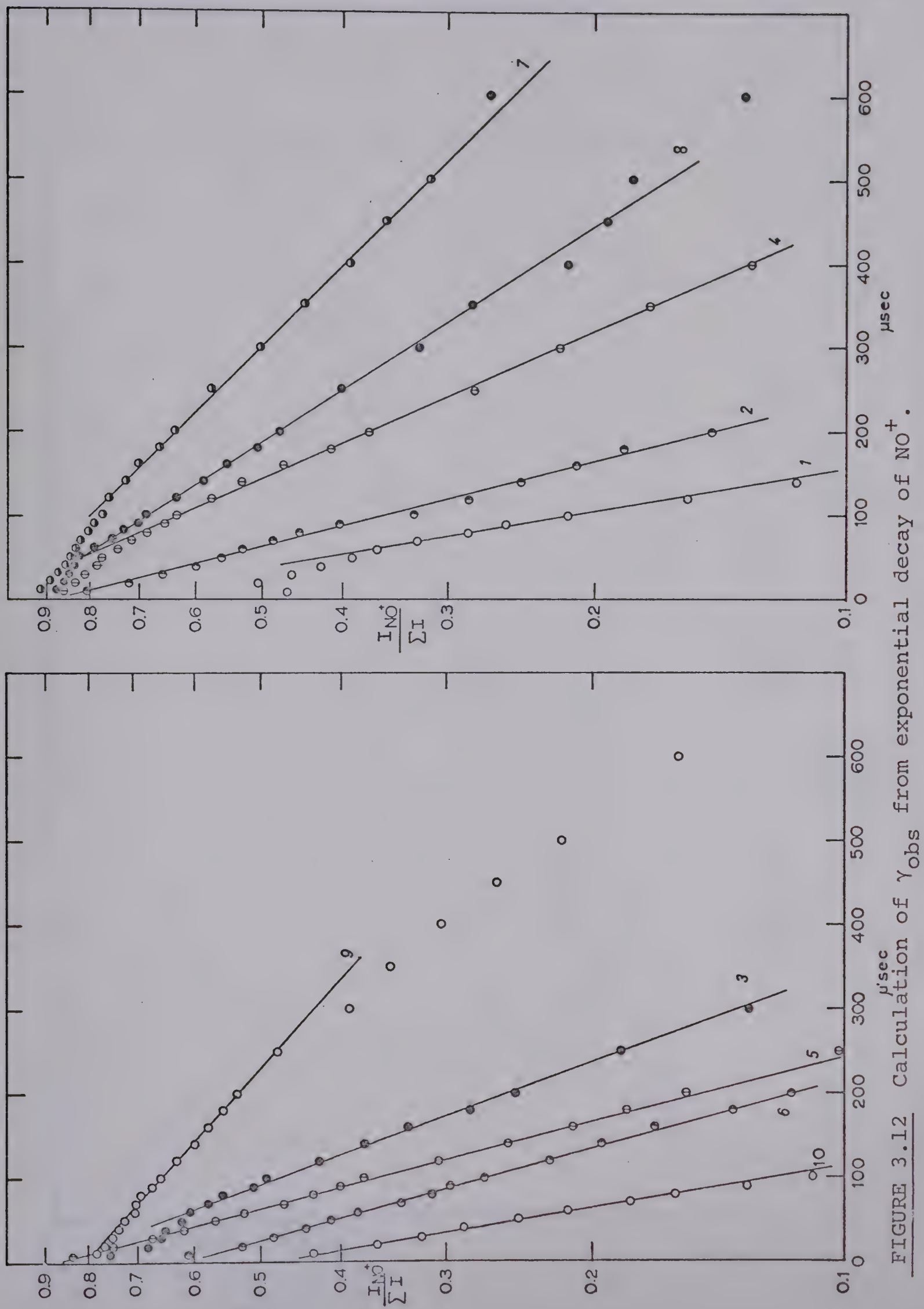


FIGURE 3.12 Calculation of γ_{obs} from exponential decay of NO^+ .

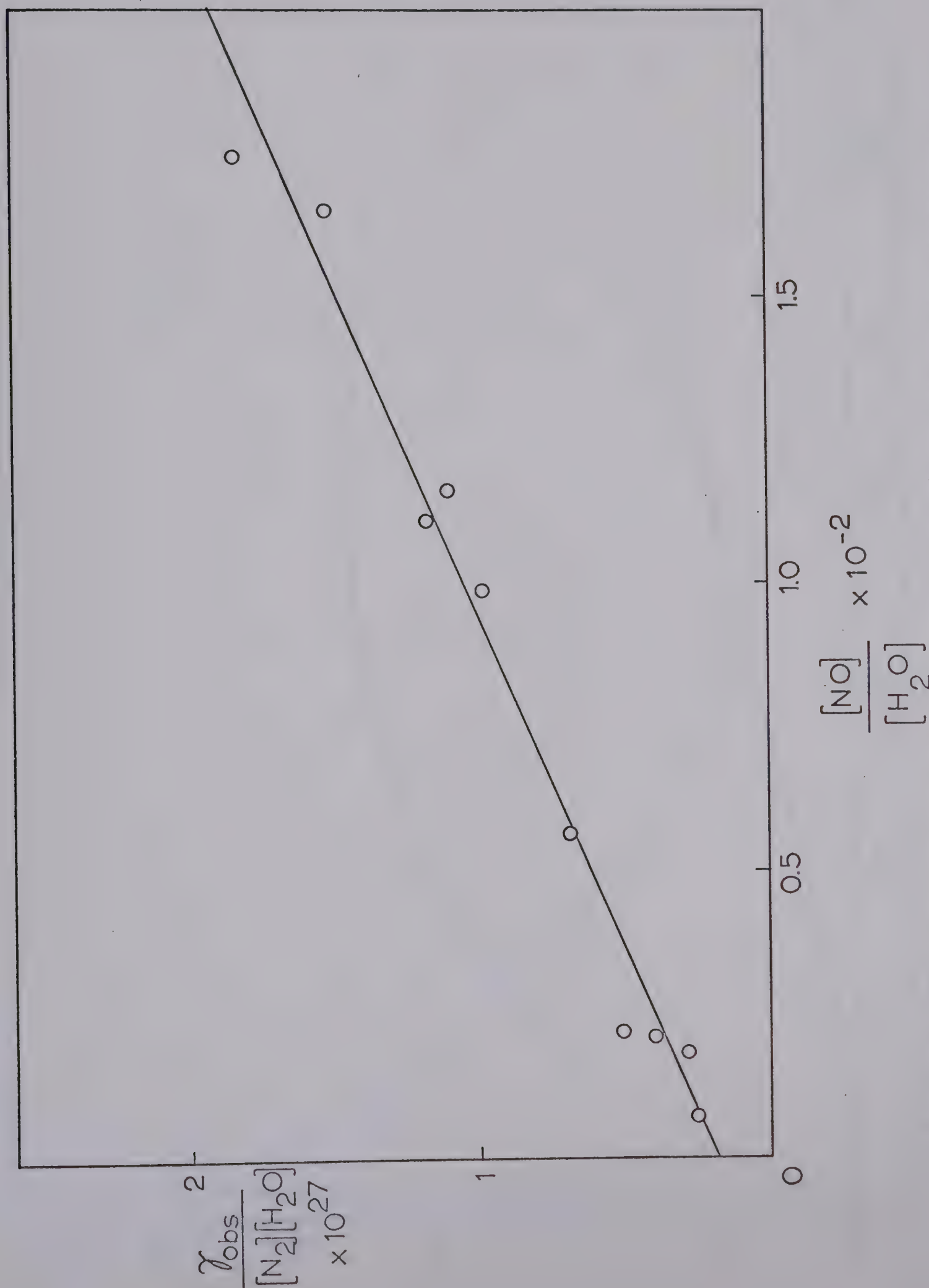


FIGURE 3.13 Determination of k_2 and k_3 from the slope and intercept.

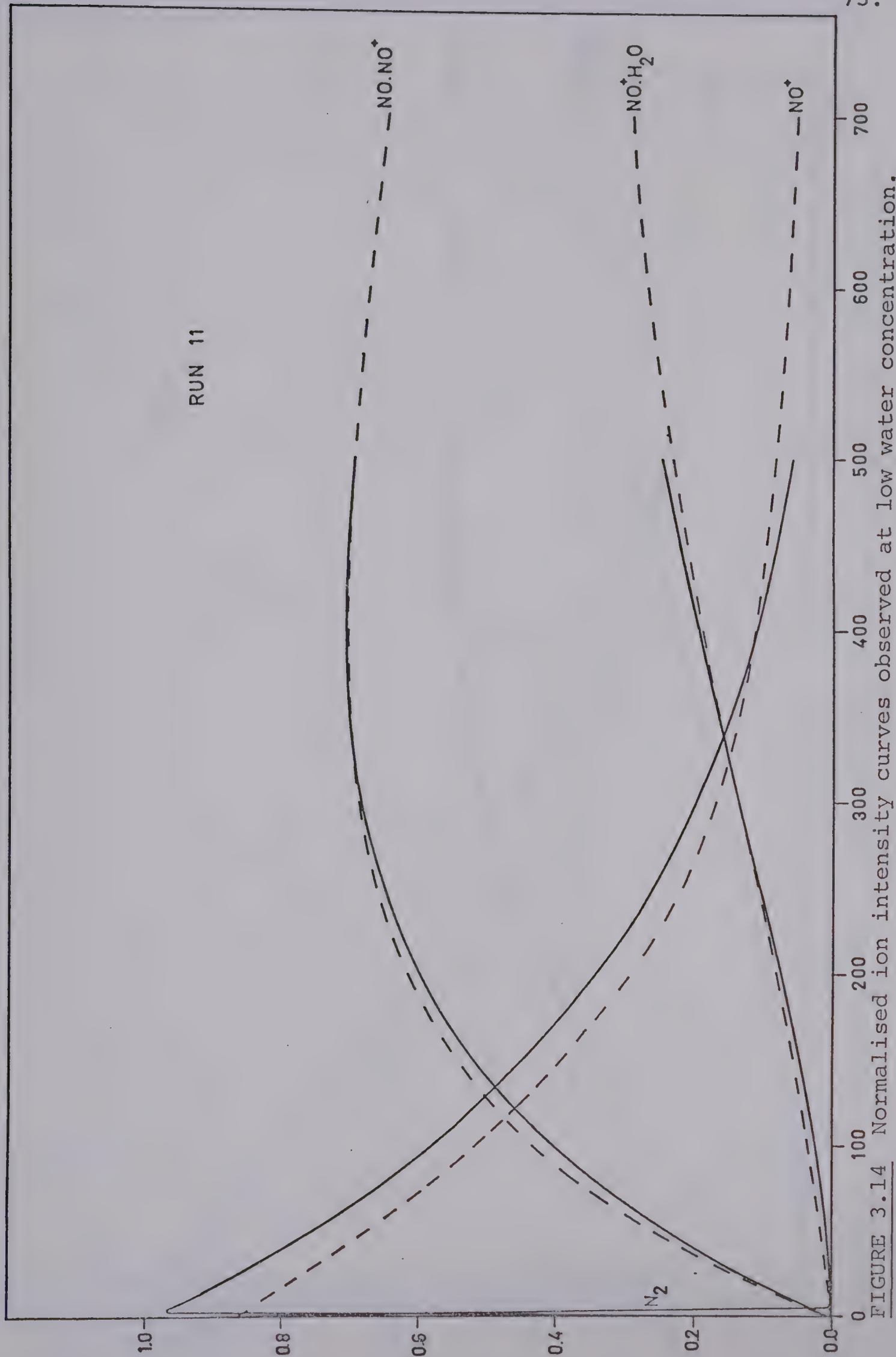


FIGURE 3.14 Normalised ion intensity curves observed at low water concentration.

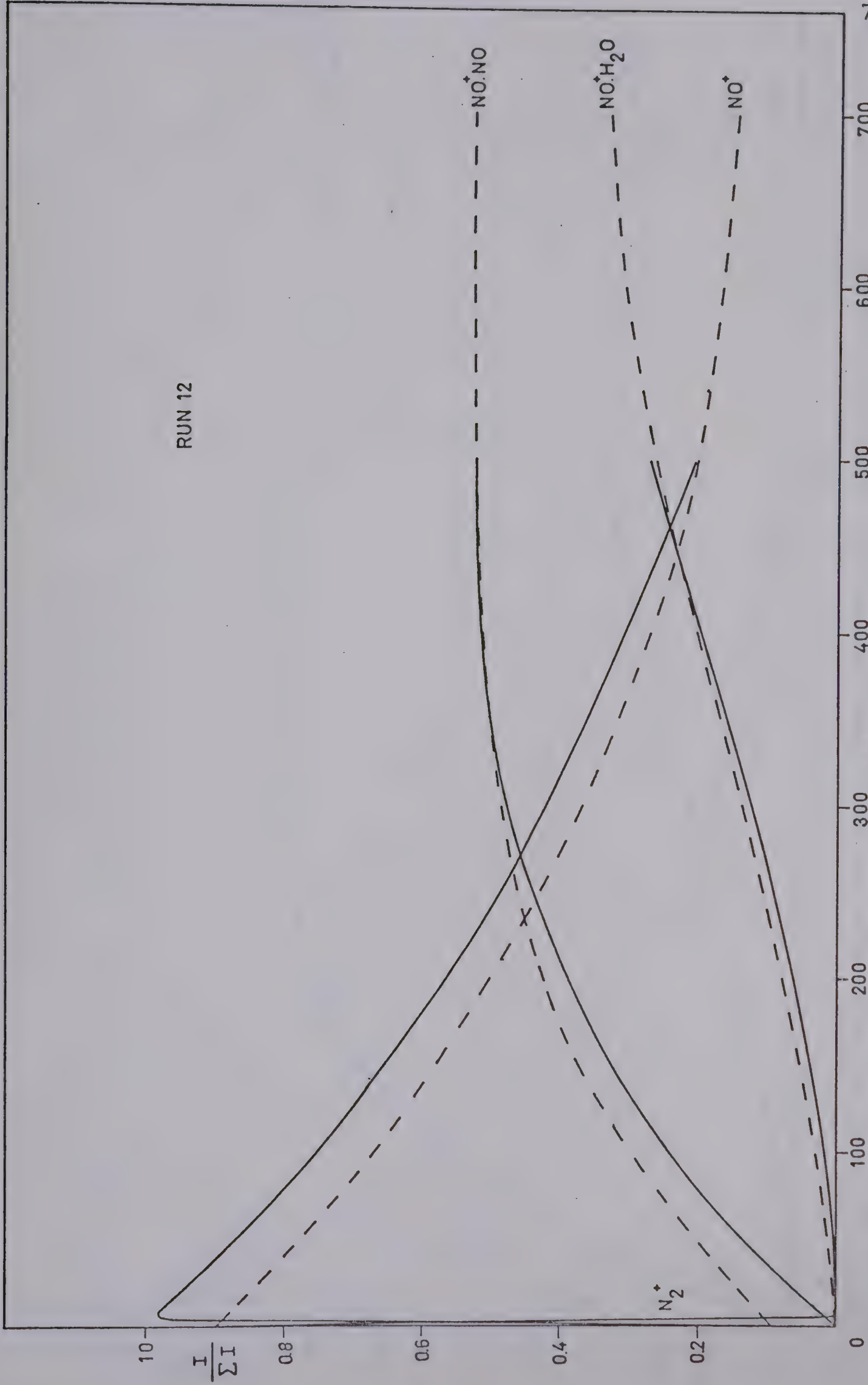


FIGURE 3.15

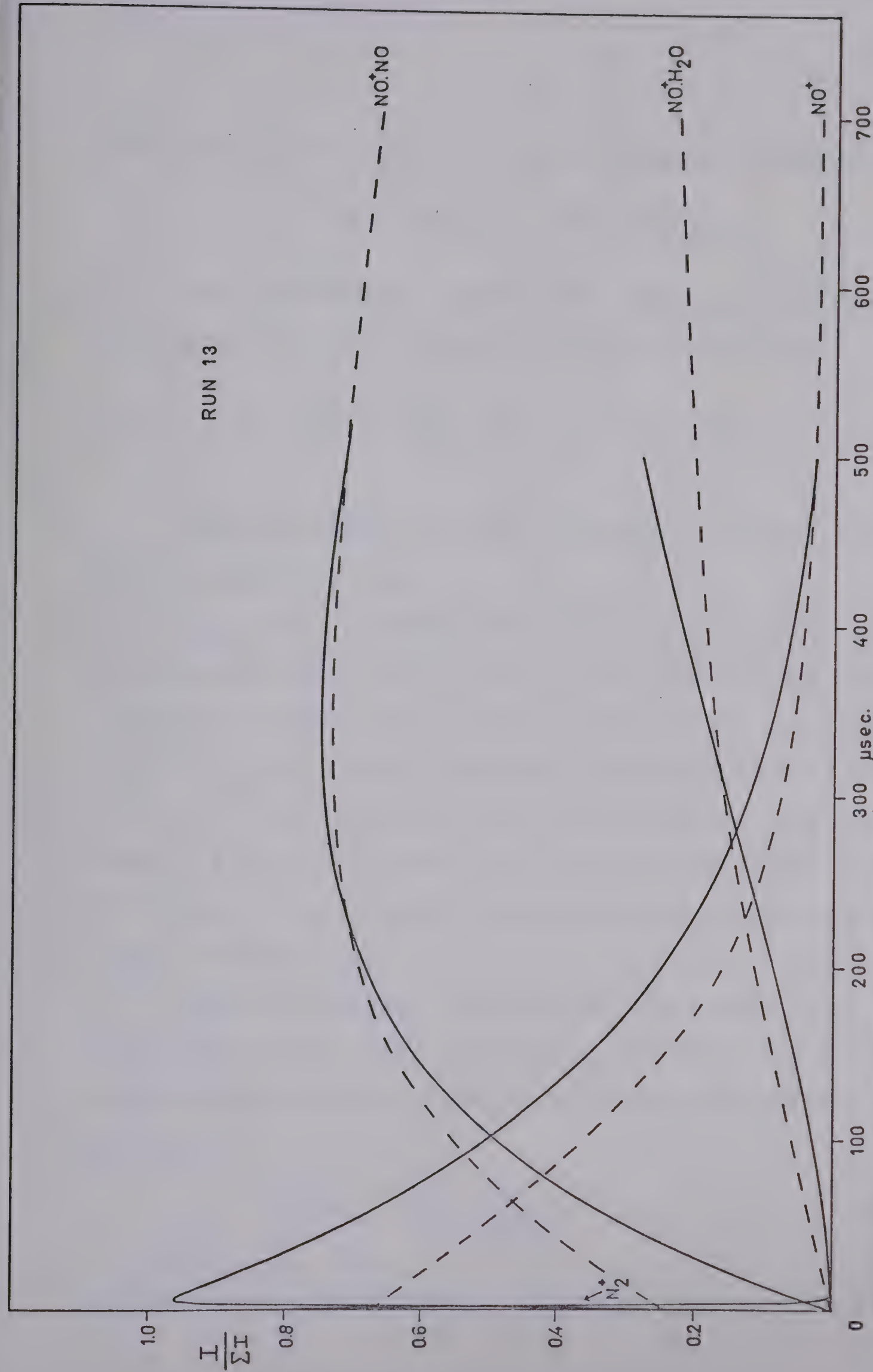
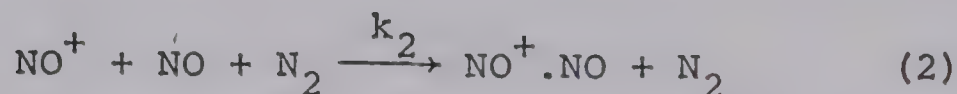
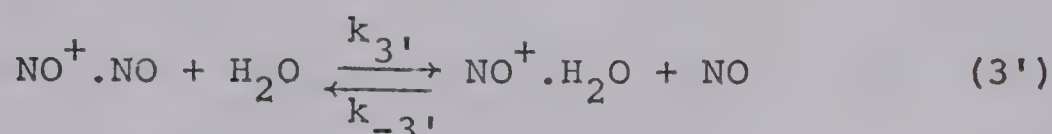


FIGURE 3.16 Normalised ion intensity curves observed at low water concentration.

association of NO with NO^+ is the predominant reaction.



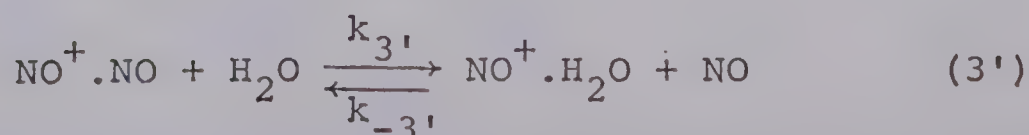
The ion intensity curves show clearly that NO^+ decays to give $\text{NO}^+.\text{NO}$ which in turn gives rise to $\text{NO}^+.\text{H}_2\text{O}$.



The ions $\text{NO}^+.\text{NO}$ and $\text{NO}^+.\text{H}_2\text{O}$ approach equilibrium at approximately 400 μsec .

γ_{obs} was determined from the logarithmic plots of the disappearance of NO^+ , Fig. (3.17). The $\text{NO}^+.\text{H}_2\text{O}$ was assumed to be produced by reaction (3') only. Therefore $\gamma_{\text{obs}} = \gamma_2$. The average value of k_2 obtained from γ_2 was $1.1 \times 10^{-29} \text{ cc}^2 \text{ molecule}^{-2} \text{ sec}^{-1}$, which agrees with the value 0.9×10^{-29} obtained from the slope of Figure (3.13). The values of k_2 obtained from the various experiments are shown in Table (3.2).

The rate constant for reaction (3') could not be calculated as the water concentration could not be determined to any degree of accuracy using the low pressure ion source.



No reactions were observed in these experiments where a

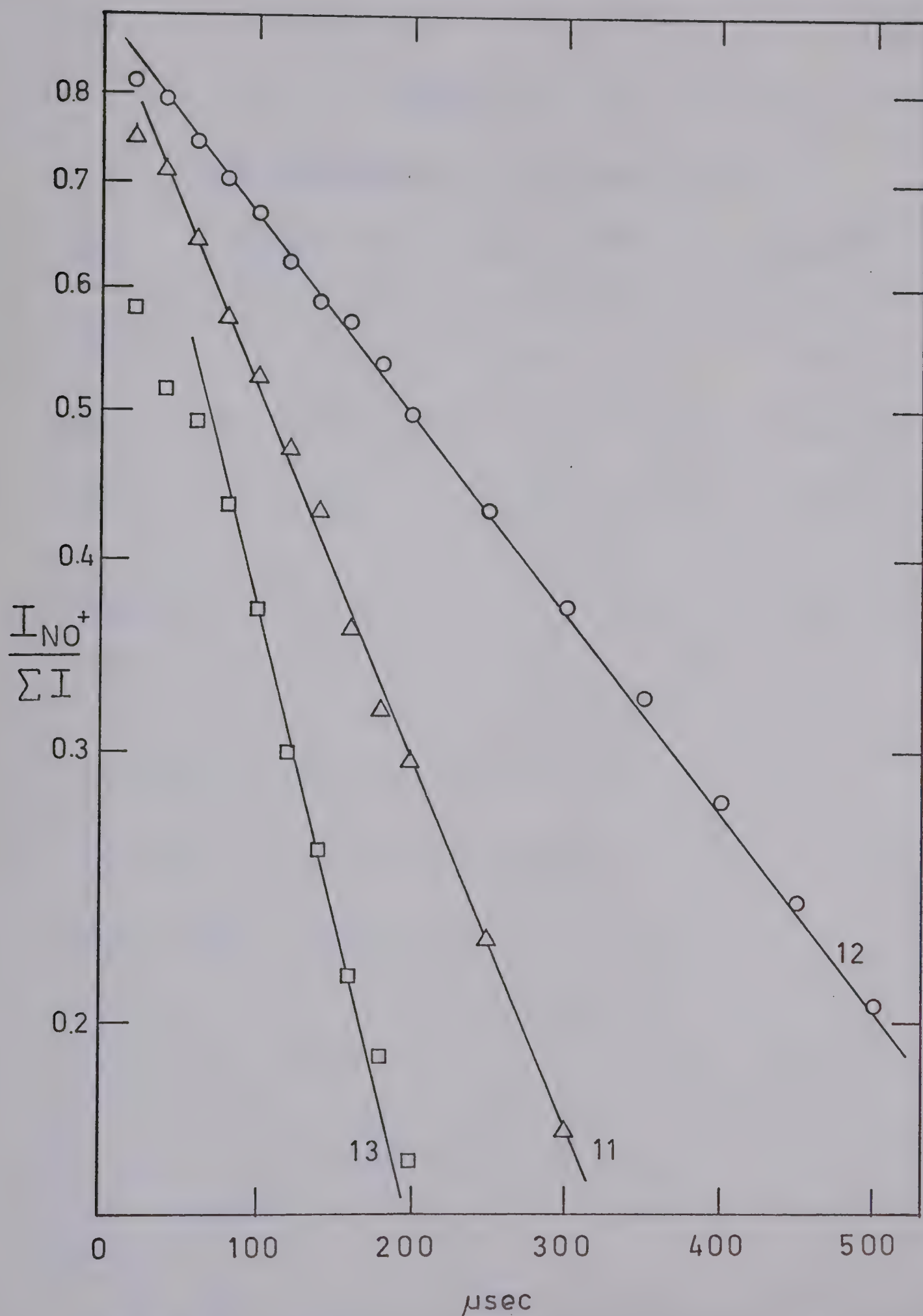


FIGURE 3.17 Logarithmic plots to calculate γ_{obs} . $\gamma_{\text{obs}} = \gamma_2$ under these conditions.

TABLE 3.2Rate Constants for the Decay of NO⁺

Run	<u>[N₂]x10^{-16a}</u>	<u>[NO]x10^{-15a}</u>	<u>k₂=10^{29b}</u>
11	5.4	10.3	1.1
12	5.8	5.0	1.0
13	4.6	17.3	1.2
Average			1.1

(a) Units of molecule cc⁻¹

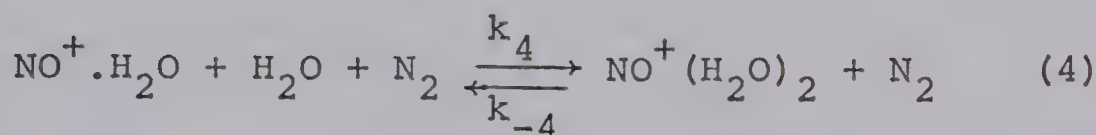
(b) Units of cc² molecule⁻² sec⁻¹

[H₂O] ≈ 10¹³ molecule cc⁻¹

known rate constant could be used to find the water concentration.

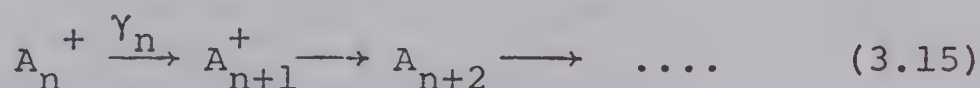
(iv) Reaction of $\text{NO}^+ \cdot \text{H}_2\text{O}$

The dihydrate of NO^+ is produced by reaction (4) from $\text{NO}^+ \cdot \text{H}_2\text{O}$.



Since the precursor of $\text{NO}^+ \cdot \text{H}_2\text{O}$, NO^+ , had not decayed to zero the logarithmic plot method could not be used to calculate γ_4 for reaction (4). The graphical integration method was used to determine γ_4 .

The graphical integration method considers a consecutive first order reaction sequence:



where γ_n is the rate constant of the n^{th} reaction. All of the products formed after the n^{th} reaction, I_{n+1} , I_{n+2} , ... throughout the reaction sequence, must have originated via the n^{th} reaction. Therefore the sum of all the product ions after the n^{th} reaction at a time t must be proportional to the integral of the intensity the ion I_n between time zero and t :

$$\text{I}_{n+1} + \text{I}_{n+2} + \dots = \gamma_n \int_0^t \text{I}_n \cdot dt \quad (3.16)$$

γ_n may be obtained graphically by determining the integral $\int_0^t I_n dt$ for different times t and plotting against $\sum_{m=n+1} I_m$, the sum of the ion intensities of the products after reaction n at time t and measure the slope of the straight line. Applying this method to reaction (4)

$$\begin{aligned} \int_0^t \text{products} &= I_{\text{NO}^+(\text{H}_2\text{O})_2}^t + I_{\text{NO}^+(\text{H}_2\text{O})_3}^t + I_{\text{H}^+(\text{H}_2\text{O})_3}^t + I_{\text{H}^+(\text{H}_2\text{O})_4}^t \\ &= \gamma_4 \int_0^t I_{\text{NO}^+\text{H}_2\text{O}} dt \end{aligned} \quad (3.17)$$

$\int_0^t \text{products}$ was plotted versus $\int_0^t I_{\text{NO}^+\text{H}_2\text{O}} dt$ and γ_4 for each experiment was calculated from the slope in Figure (3.18).

If reaction (4) was second order then $k_4 = \gamma_4/[\text{H}_2\text{O}]$ but if the reaction involved a third body then $k_4 = \gamma_4/[\text{H}_2\text{O}][\text{N}_2]$. The third-order dependence of k_4 was demonstrated by plotting $\gamma_4/[\text{N}_2][\text{H}_2\text{O}]$ and $\gamma_4/[\text{H}_2\text{O}]$ versus the nitrogen pressure. Figure (3.19) shows that the apparent second order rate constant varies with nitrogen pressure whereas $\gamma_4/[\text{N}_2][\text{H}_2\text{O}]$ versus nitrogen pressure has a zero gradient. The average value of k_4 was $1.0 \times 10^{-27} \text{ cc}^2 \text{ molecule}^{-2} \text{ sec}^{-1}$.

The equilibrium constant K_4 for reaction (4) may be calculated from equation (3.18). This equation is valid only if the ions involved have reached equilibrium

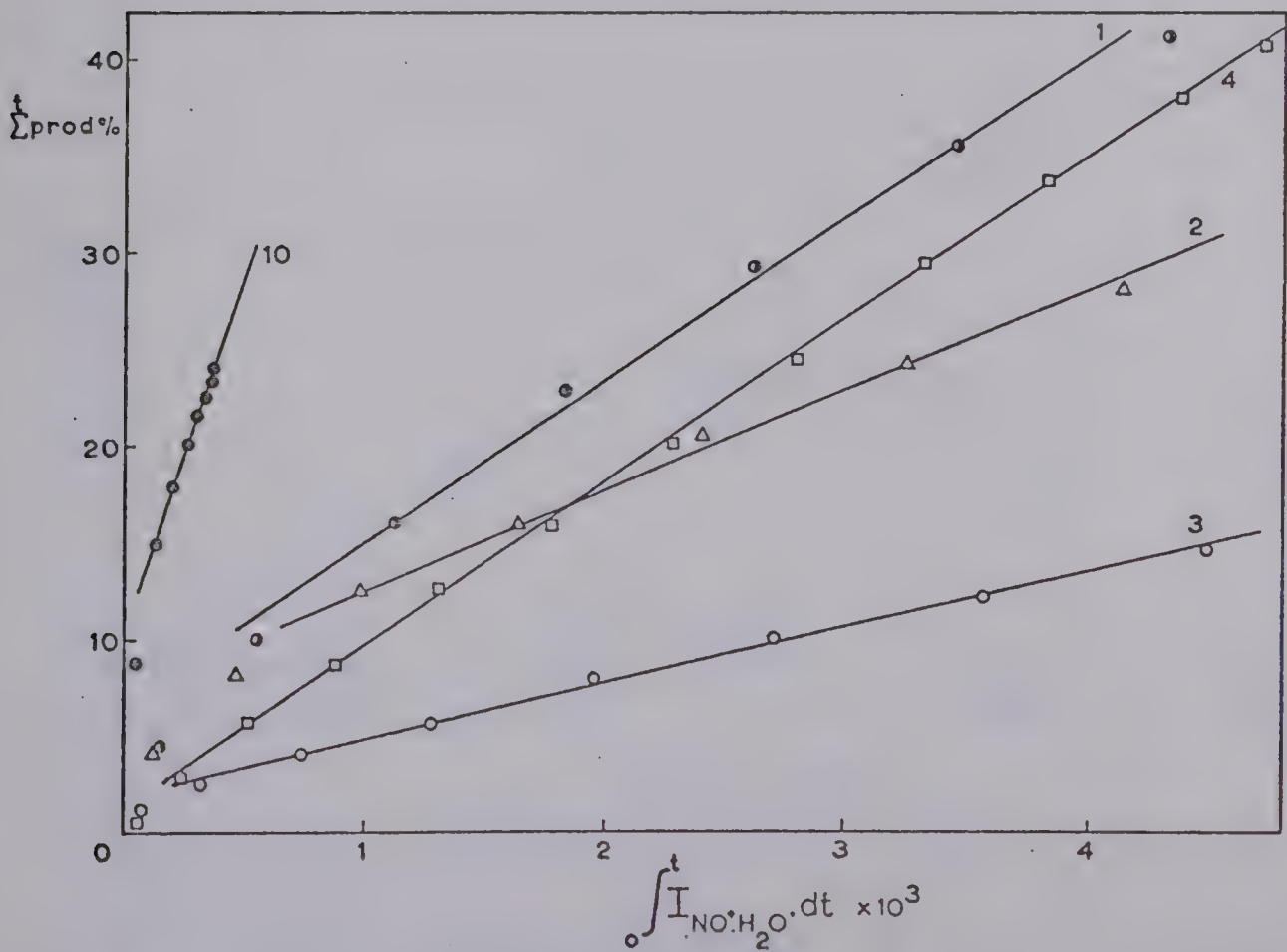
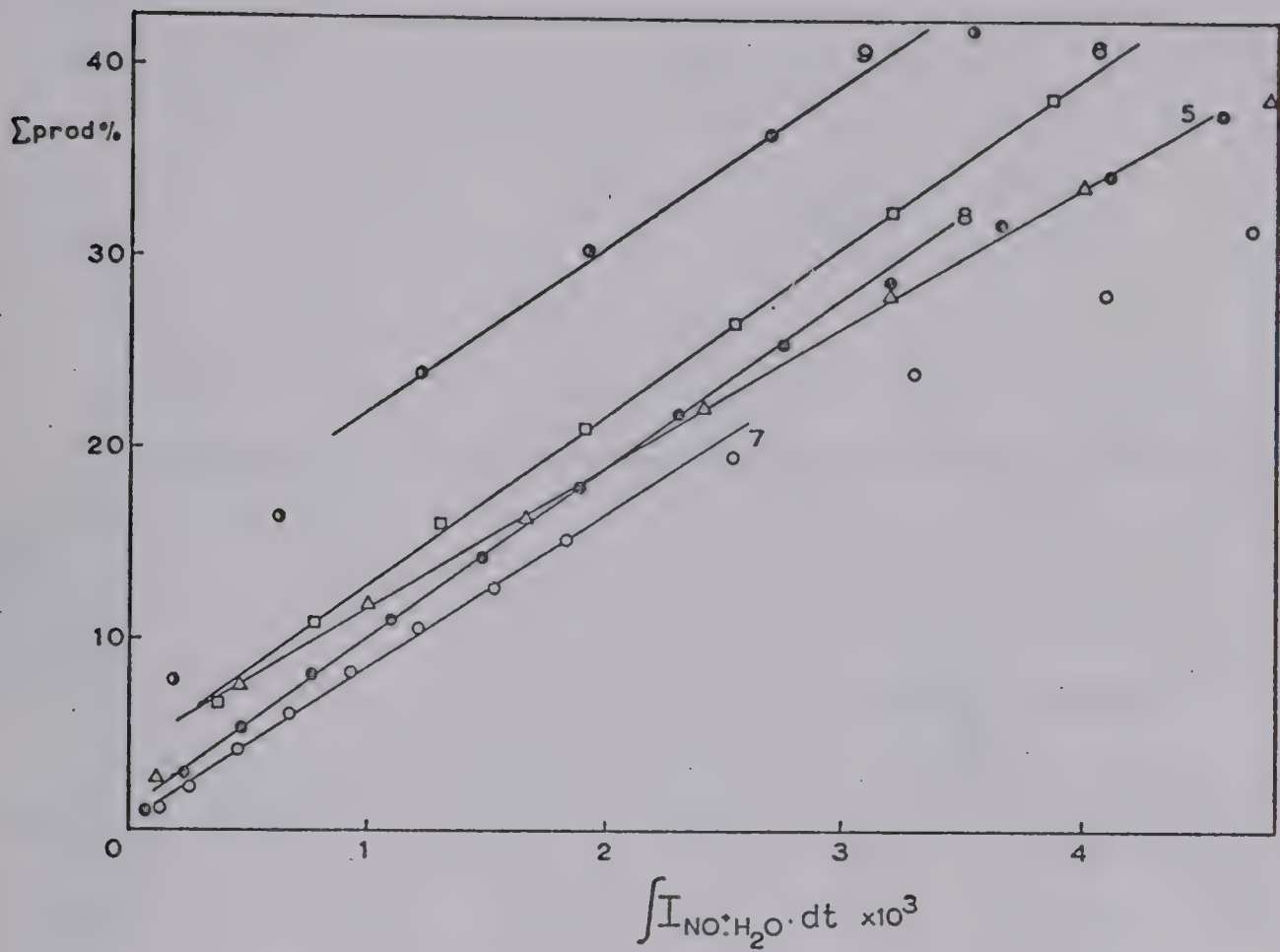


FIGURE 3.18 Calculation of γ_4 by the graphical integration method.

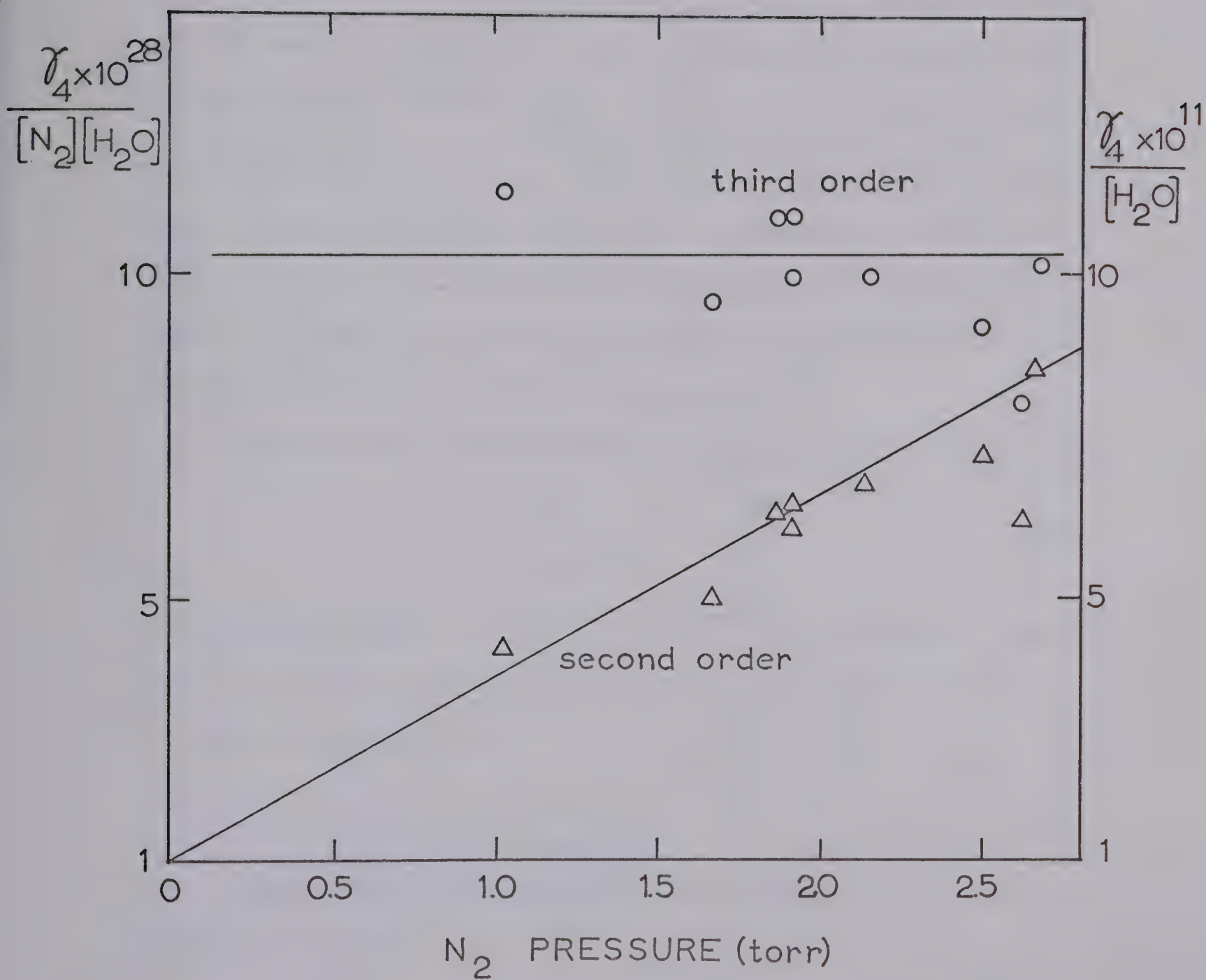


FIGURE 3.19 Determination of second or third-order dependence of k_4 .

$$K_4 = \frac{I_{\text{NO}^+(\text{H}_2\text{O})_2}}{I_{\text{NO}^+\text{H}_2\text{O} \cdot [\text{H}_2\text{O}]}} \quad (3.18)$$

It can be seen from the ion intensity curves (Figures 3.2 to 3.11) that the intensities of $\text{NO}^+\text{H}_2\text{O}$ and $\text{NO}^+(\text{H}_2\text{O})_2$ did not reach a constant value. However, an estimate of the equilibrium ratio $I_{\text{NO}^+(\text{H}_2\text{O})_2} / I_{\text{NO}^+\text{H}_2\text{O}}$ may be obtained by measuring the ratio at various times between 400 and 1000 μsec . Since the ratio was found to approach a constant value at long reaction times, this value was used in equation (3.18). The average value of K_4 obtained in this manner was $2 \times 10^{-14} \text{ cc molecule}^{-1}$.

The reverse rate constant k_{-4} may be calculated from:

$$K_4 = \frac{k_4}{k_{-4}} \quad (3.19)$$

The average value of k_{-4} was $5 \times 10^{-14} \text{ cc molecule}^{-1} \text{ sec}^{-1}$. Table 3.3 shows the values of k_4 , K_4 and k_{-4} for the different experiments.

(v) Reaction of $\text{NO}^+(\text{H}_2\text{O})_2$

The $\text{NO}^+(\text{H}_2\text{O})_2$ ion reacted with water to give the trihydrate of NO^+ by:

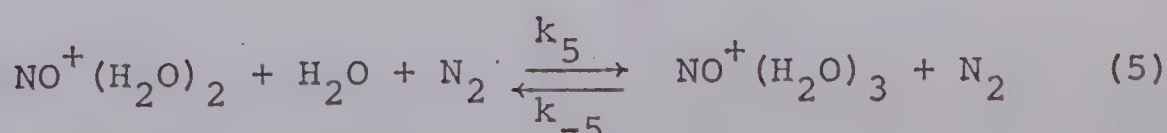


TABLE (3.3)

Rate and Equilibrium Constants for Reaction (4) $\text{NO}^+ \cdot \text{H}_2\text{O} + \text{H}_2\text{O} + \text{N}_2 \rightleftharpoons \text{NO}^+(\text{H}_2\text{O})_2 + \text{N}_2$

Run	$[\text{N}_2] \times 10^{-16}\text{a}$	$[\text{NO}] \times 10^{-15}\text{a}$	$[\text{H}_2\text{O}] \times 10^{-14}\text{a}$	$k_4 \times 10^{27}\text{b}$	$K_4 \times 10^{14}\text{c}$	$k_{-4} \times 10^{14}\text{d}$
1	7.8	19.2	1.2	0.9	1.8	5.1
2	8.2	12.0	1.0	0.6	2.0	3.0
3	5.2	11.6	0.7	0.9	1.7	5.1
4	3.7	11.6	2.1	1.1	1.7	6.6
5	6.7	12.8	1.2	1.0	3.2	3.2
6	8.5	10.0	1.0	1.0	3.1	3.3
7	5.9	2.5	1.4	1.1	1.4	7.8
8	6.0	2.9	1.3	1.1	2.7	4.0
9	6.2	1.0	1.4	1.0	1.1	9.4
10	5.5	11.3	19.7	1.1	-	-
Average				1.0	2.1	4.8

- (a) Units of molecule cc^{-1}
- (b) Units of $\text{cc}^2 \text{ molecule}^{-2} \text{ sec}^{-1}$
- (c) Units of cc molecule^{-1}
- (d) Units of $\text{molecule}^{-1} \text{ sec}^{-1}$

The pseudo-first-order rate constant γ_5 for reaction (5) was calculated by the graphical integration method. γ_5 for each experiment was obtained from the slope of the plot of $\int_0^t I_{\text{NO}^+(\text{H}_2\text{O})_2} dt$ versus \sum products as shown in Figure (3.20). A disadvantage of the graphical integration method is evident in Figure (3.20). When the reaction was reversible, the straight line became a curve because more of the reacting ion, $\text{NO}^+(\text{H}_2\text{O})_2$ was formed than if the reaction were simply unidirectional. The integral was therefore larger than expected and the total product intensity was smaller, giving the graph the curved appearance. In these instances the slope should be measured at reaction times before the contribution of the reverse reaction is significant. In reaction (5) the reverse reaction was fast and affected the slope at early reaction times so that the values obtained for k_5 may be taken only as a guide to the magnitude of the forward rate constant.

A plot of $\gamma_5/[\text{N}_2][\text{H}_2\text{O}]$ and $\gamma_5/[\text{H}_2\text{O}]$ against nitrogen pressure indicated that k_5 is third-order dependent (Figure (3.21)). The average value obtained for k_5 was $2.3 \times 10^{-28} \text{ cc}^2 \text{ molecule}^{-2} \text{ sec}^{-1}$.

The equilibrium constant, K_5 for reaction (5) was calculated from the constant value of the ratio of

$I_{\text{NO}^+(\text{H}_2\text{O})_3}$ to $I_{\text{NO}^+(\text{H}_2\text{O})_2}$ in:

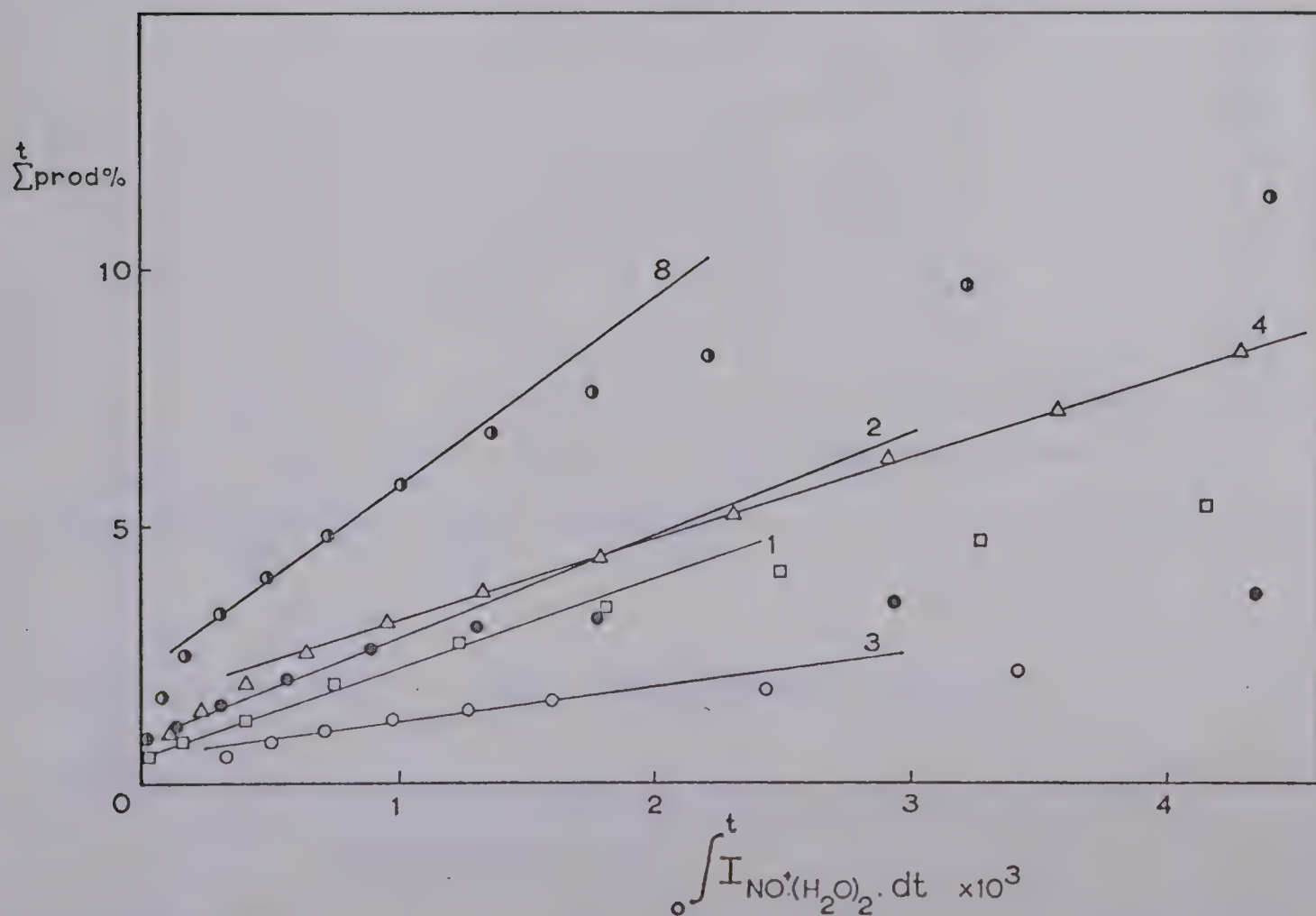
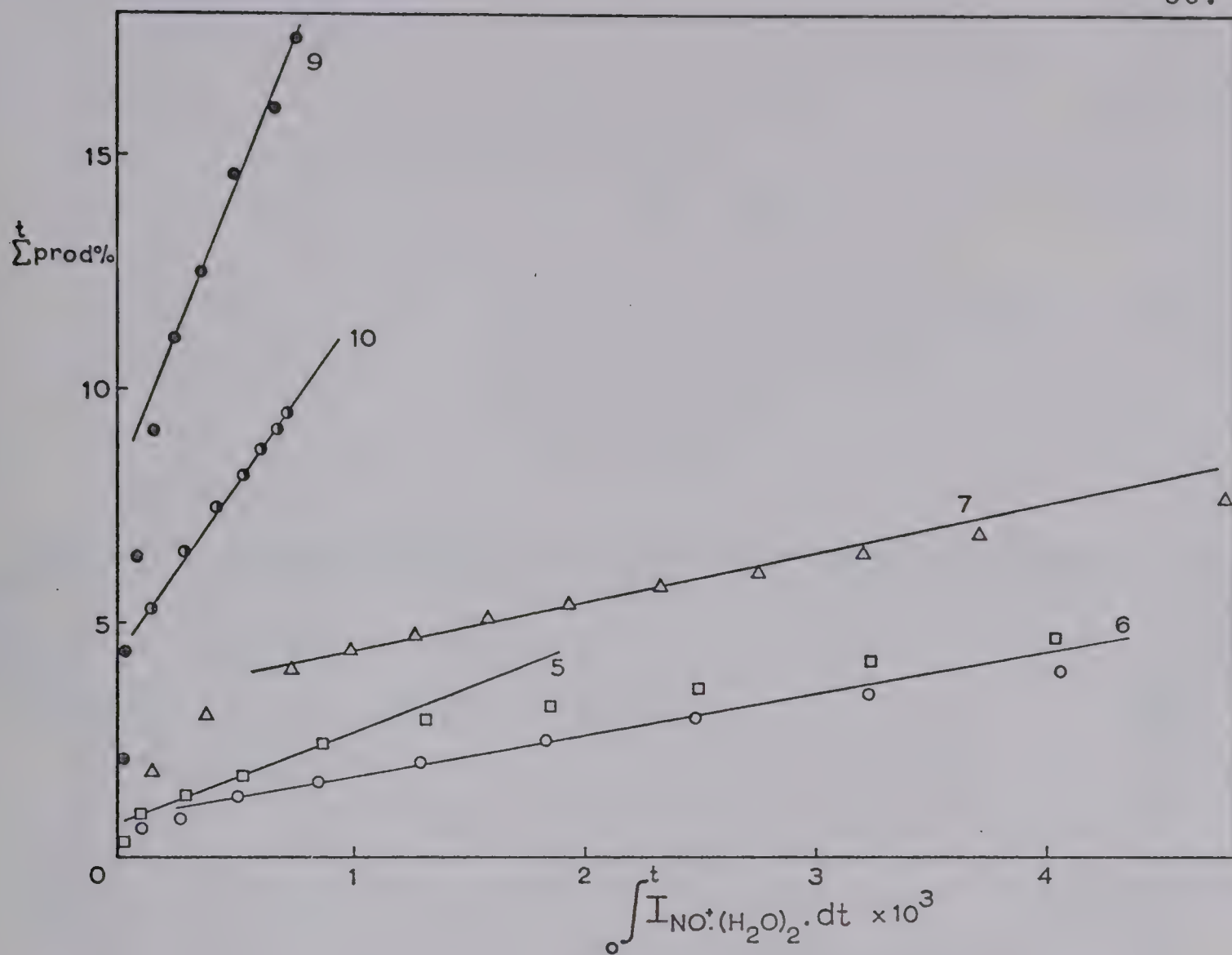


FIGURE 3.20 Calculation of γ_5 by the graphical integration method.

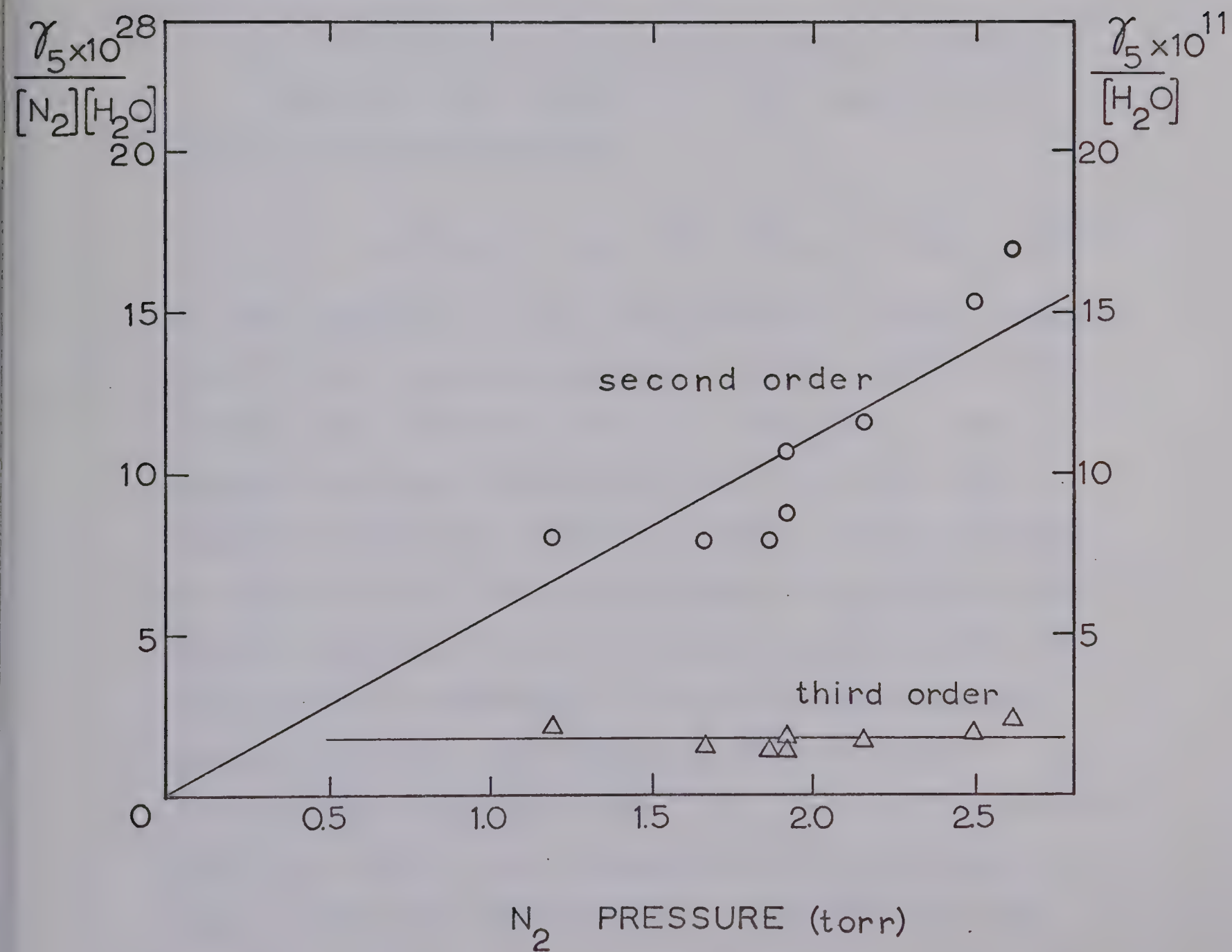


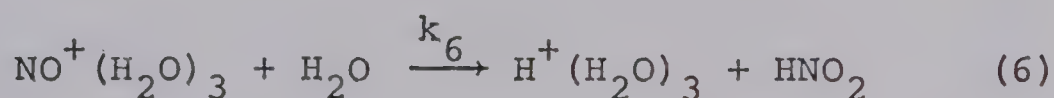
FIGURE 3.21 Determination of second or third order dependence of k_5 .

$$K_5 = \frac{I_{\text{NO}^+(\text{H}_2\text{O})_3}}{I_{\text{NO}^+(\text{H}_2\text{O})_2[\text{H}_2\text{O}]}} \quad (3.21)$$

The average value of K_5 was 3.1×10^{-16} cc molecule⁻¹ and that of k_{-5} from k_5/K_5 was 7×10^{-13} cc molecule⁻¹ sec⁻¹. Table (3.4) shows the reaction parameters obtained for each experiment.

(vi) Kinetics of the Proton Hydrate Formation

$\text{NO}^+(\text{H}_2\text{O})_3$ was removed by a fast reaction with water which yielded $\text{H}^+(\text{H}_2\text{O})_3$



The rate constant, k_6 for the cross-over reaction between the NO^+ water clustering sequence and the proton hydrate sequence was calculated from γ_6 . Values of γ_6 were obtained from the slopes of Figure (3.22) using the graphical integration method. Reaction (6) was shown to be second-order by the zero gradient of $\gamma_6/[\text{H}_2\text{O}]$ plotted versus nitrogen pressure in Figure (3.23), whereas the third order rate constant $\gamma_6/[\text{N}_2][\text{H}_2\text{O}]$ decreases with nitrogen pressure. The average value of k_6 was 1.3×10^{-10} cc molecule⁻¹ sec⁻¹. k_6 could not be measured for runs 7 and 8 as the intensity of $\text{NO}^+(\text{H}_2\text{O})_3$ was very small. Table (3.5) shows the rate constants for runs 1 to 10.

The equilibrium constants K_7 and K_8 were calculated

TABLE (3.4)

Rate and Equilibrium Constants for the Reaction $\text{NO}^+ (\text{H}_2\text{O})_2 + \text{H}_2\text{O} + \text{N}_2 \xrightleftharpoons[k_{-5}]{k_5} \text{NO}^+ (\text{H}_2\text{O})_3 + \text{N}_2$

Run	$[\text{N}_2] \times 10^{-16}\text{a}$	$[\text{NO}] \times 10^{-15}\text{a}$	$[\text{H}_2\text{O}] \times 10^{-14}\text{a}$	$k_5 \times 10^{28}\text{b}$	$k_{-5} \times 10^{12}\text{c}$	$K_5 \times 10^{16}\text{d}$
1	7.8	19.2	1.2	2.0	0.4	4.6
2	8.2	12.0	1.0	3.4	1.0	3.3
3	5.2	11.6	0.7	1.9	0.5	4.2
4	3.7	11.6	2.1	2.5	0.7	3.5
5	6.7	12.8	1.2	1.7	0.5	3.4
6	8.4	10.0	1.0	1.0	0.2	4.6
7	5.9	2.5	1.4	1.4	1.6	0.9
8	6.0	2.9	1.3	1.0	0.8	1.3
9	6.2	1.0	1.4	1.9	0.9	2.1
10	5.5	11.3	19.7	6.4	-	-
Average				2.3	0.7	3.1

- (a) Units of molecule cc^{-1}
- (b) Units of $\text{cc}^2 \text{ molecule}^{-2} \text{ sec}^{-1}$
- (c) Units of $\text{cc molecule}^{-1} \text{ sec}^{-1}$
- (d) Units of cc molecule^{-1}

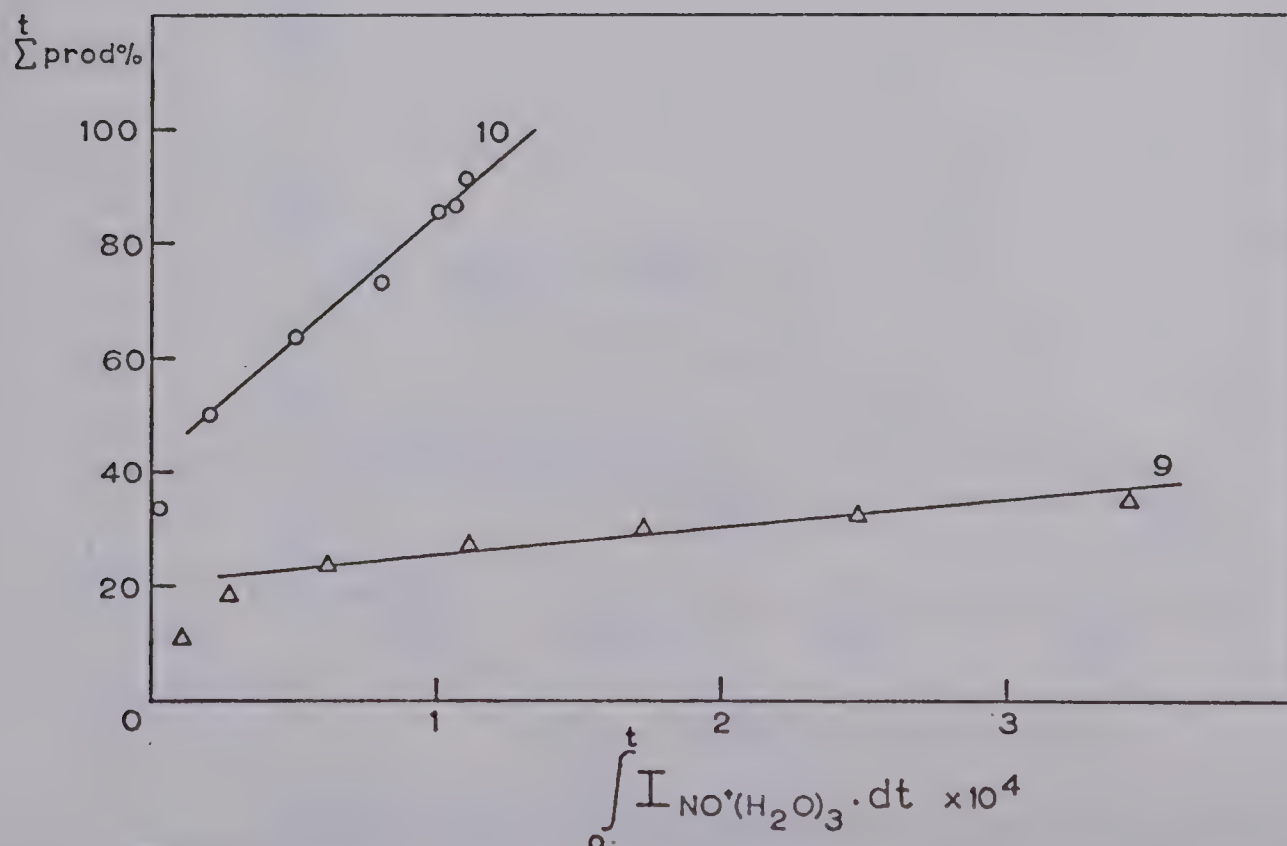
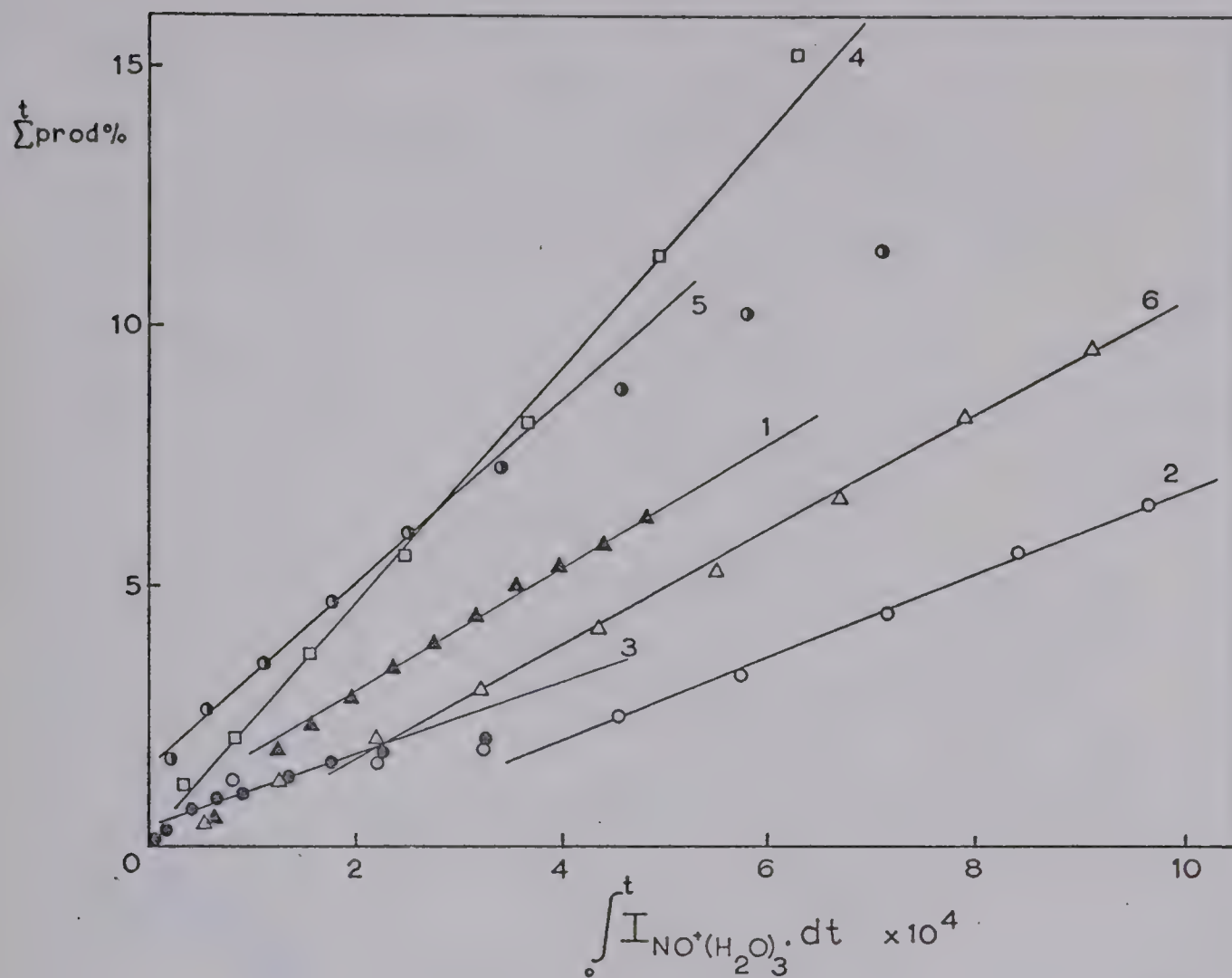


FIGURE 3.22 Calculation of γ_6 by the graphical integration method.

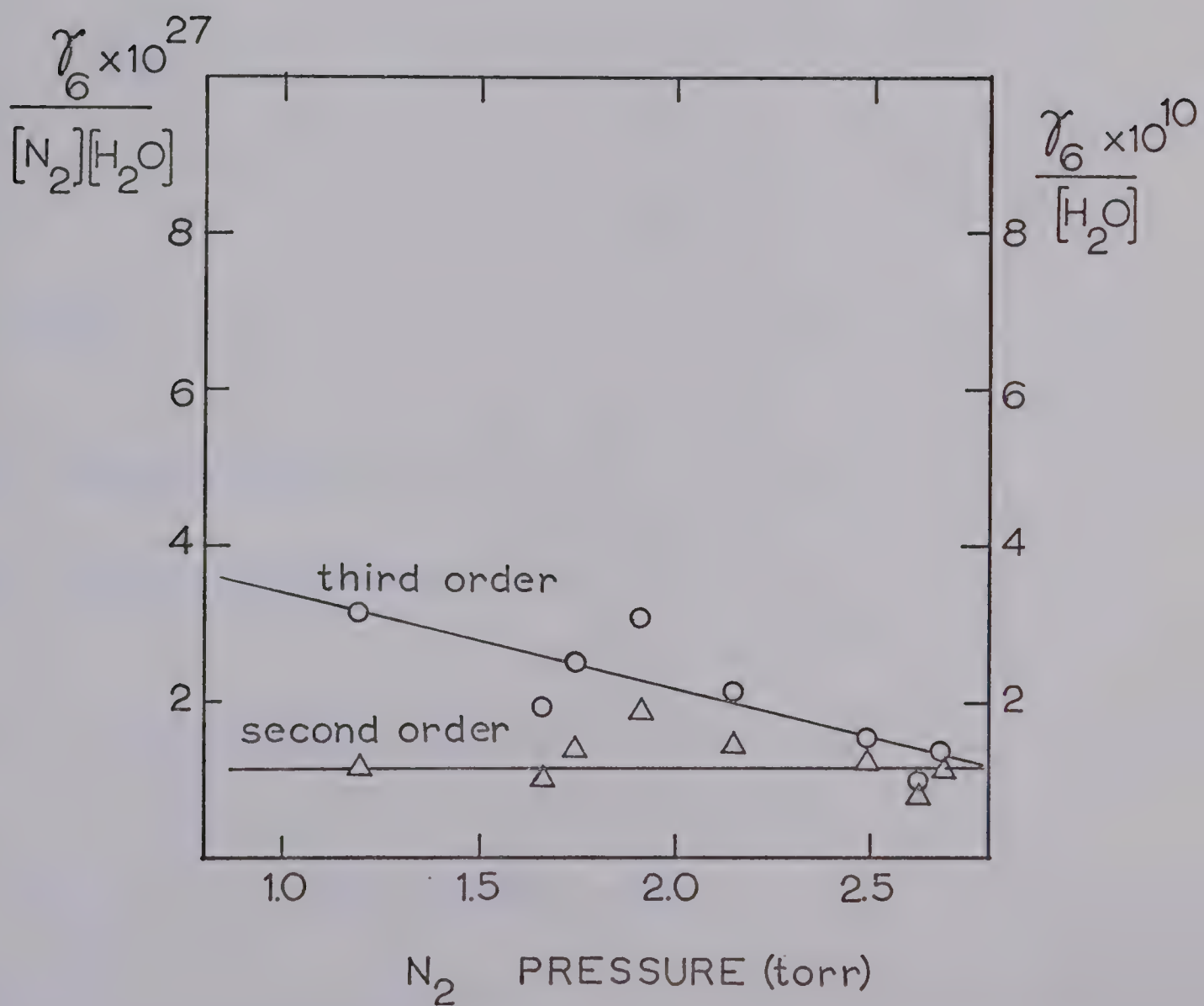
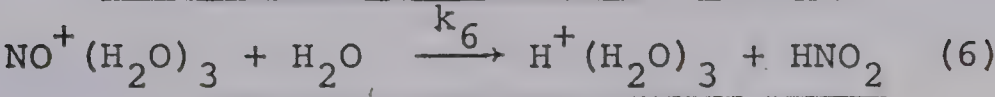


FIGURE 3.23 Determination of second or third-order dependence of k_6 .

TABLE (3.5)

Rate Constants for the Reaction



Run	$[\text{N}_2] \times 10^{-16a}$	$[\text{NO}] \times 10^{-15a}$	$[\text{H}_2\text{O}] \times 10^{-14a}$	$k_6 \times 10^{10b}$
1	7.8	19.2	1.2	1.2
2	8.2	12.0	1.0	0.8
3	5.2	11.6	0.7	1.0
4	3.7	11.6	2.1	1.2
5	6.7	12.8	1.2	1.4
6	8.4	10.0	1.0	1.2
7	5.9	2.5	1.4	-
8	6.0	2.9	1.3	-
9	6.2	1.0	1.4	1.9
10	5.5	11.3	19.7	2.0
Average				1.3

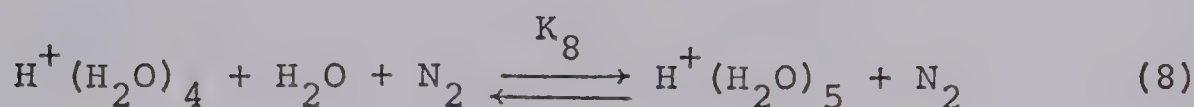
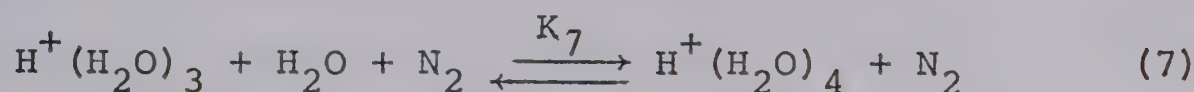
(a) Units of molecule cc^{-1}

(b) Units of $\text{cc molecule}^{-1} \text{ sec}^{-1}$

where possible at times where the ratio $I_{H^+(H_2O)_n} / I_{H^+(H_2O)_{n-1}}$ was constant.

$$K = \frac{I_{H^+(H_2O)_n}}{I_{H^+(H_2O)_{n-1}} [H_2O]} \quad (3.22)$$

Table (3.6) gives a summary of the values obtained for the equilibrium constants K_7 and K_8 .



The average value of K_7 was 4.3×10^{-14} cc molecule⁻¹ which can be compared to measurements previously obtained on this instrument (30) of 6×10^{-14} cc molecule⁻¹. K_8 was calculated to be 2.7×10^{-16} cc molecule⁻¹ compared to earlier measurements of 1×10^{-16} cc molecule⁻¹.

3.6 Computer Fitting of Ion Intensity Curves

Once the rate constants had been evaluated, their validity was estimated by fitting the experimental results with theoretical curves using a computer. A set of differential equations can be written for reactions (1) to (7). The rate of formation of an ion of intensity I at time t

TABLE (3.6)

Equilibrium Constants for Hydrate Clustering $H^+(H_2O)_3 + H_2O + N_2 \xrightarrow{K_7} H^+(H_2O)_4 + N_2$ (7)
 $H^+(H_2O)_4 + H_2O + N_2 \xrightarrow{K_8} H^+(H_2O)_5 + N_2$ (8)

Run	$[N_2] \times 10^{-16a}$	$[NO] \times 10^{-15a}$	$[H_2O] \times 10^{-14a}$	$K_7 \times 10^{14b}$	$K_8 \times 10^{16b}$
1	7.8	19.2	1.2	4.8	2.5
2	8.2	12.0	1.0	3.8	3.3
3	5.2	11.6	0.7	-	-
4	3.7	11.6	2.1	3.5	2.4
5	6.7	12.8	1.2	4.4	-
6	8.4	10.0	1.0	5.2	-
7	5.9	2.5	1.4	3.6	-
8	6.0	2.9	1.3	4.5	-
9	6.2	1.0	1.4	4.8	-
10	5.5	11.3	19.7	-	-
Average				4.3	2.7

(a) Units of molecule cc^{-1}

(b) Units of cc molecule $^{-1}$

in terms of a pseudo-first-order rate constant γ_n is:

$$\frac{dI_{N_2^+}}{dt} = -\gamma_1 I_{N_2^+} \quad (3.23)$$

$$\frac{dI_{NO^+}}{dt} = \gamma_1 I_{N_2^+} - \gamma_{obs} I_{NO^+} \quad (3.24)$$

$$\frac{dI_{NO^+H_2O}}{dt} = \gamma_{obs} I_{NO^+} - \gamma_4 I_{NO^+H_2O} + \gamma_{-4} I_{NO^+(H_2O)_2} \quad (3.25)$$

$$\frac{dI_{NO^+(H_2O)_2}}{dt} = \gamma_4 I_{NO^+H_2O} - (\gamma_{-4} + \gamma_5) I_{NO^+(H_2O)_2} + \gamma_{-5} I_{NO^+(H_2O)_3} \quad (3.26)$$

$$\frac{dI_{NO^+(H_2O)_3}}{dt} = \gamma_5 I_{NO^+(H_2O)_2} - (\gamma_{-5} + \gamma_6) I_{NO^+(H_2O)_3} \quad (3.27)$$

$$\frac{dI_{H^+(H_2O)_3}}{dt} = \gamma_6 I_{NO^+(H_2O)_3} - \gamma_7 I_{H^+(H_2O)_3} + \gamma_{-7} I_{H^+(H_2O)_4} \quad (3.28)$$

$$\frac{dI_{H^+(H_2O)_4}}{dt} = \gamma_7 I_{H^+(H_2O)_3} - \gamma_{-7} I_{H^+(H_2O)_4} \quad (3.29)$$

Initially the integrated forms (74) of equations

(3.23) to (3.29) were used to calculate the theoretical intensity using a digital computer (IBM 360/67). However, an analog computer was found to be more suitable for this task. A difference between analog and digital computing is that the former is continuous, while the latter is discrete. An analog computer may be used to construct an electrical analog of the set of differential equations (3.23) to (3.29) which were chosen to approximate the behaviour of the system. Insufficient integrator modules were available in the analog computer (YEW Model 3302) to program all of the reactions studied, consequently reaction (3') was neglected. Besides being more suitable for the type of problem involved the analog computer was available in an on-line configuration allowing the manipulation of parameters during program operation.

The analog program describing the set of differential equations (3.23) to (3.29) is shown in Figure (3.24). The calculated ion intensity curves were superimposed upon the experimental ion intensity curves and the rate constants adjusted by means of a set of potentiometers until all the theoretical ion intensities fitted the observed ion intensities as closely as possible. The fitted theoretical curves are shown as solid lines in Figures (3.2) to (3.11).

A comparison of the rate constant that gave the

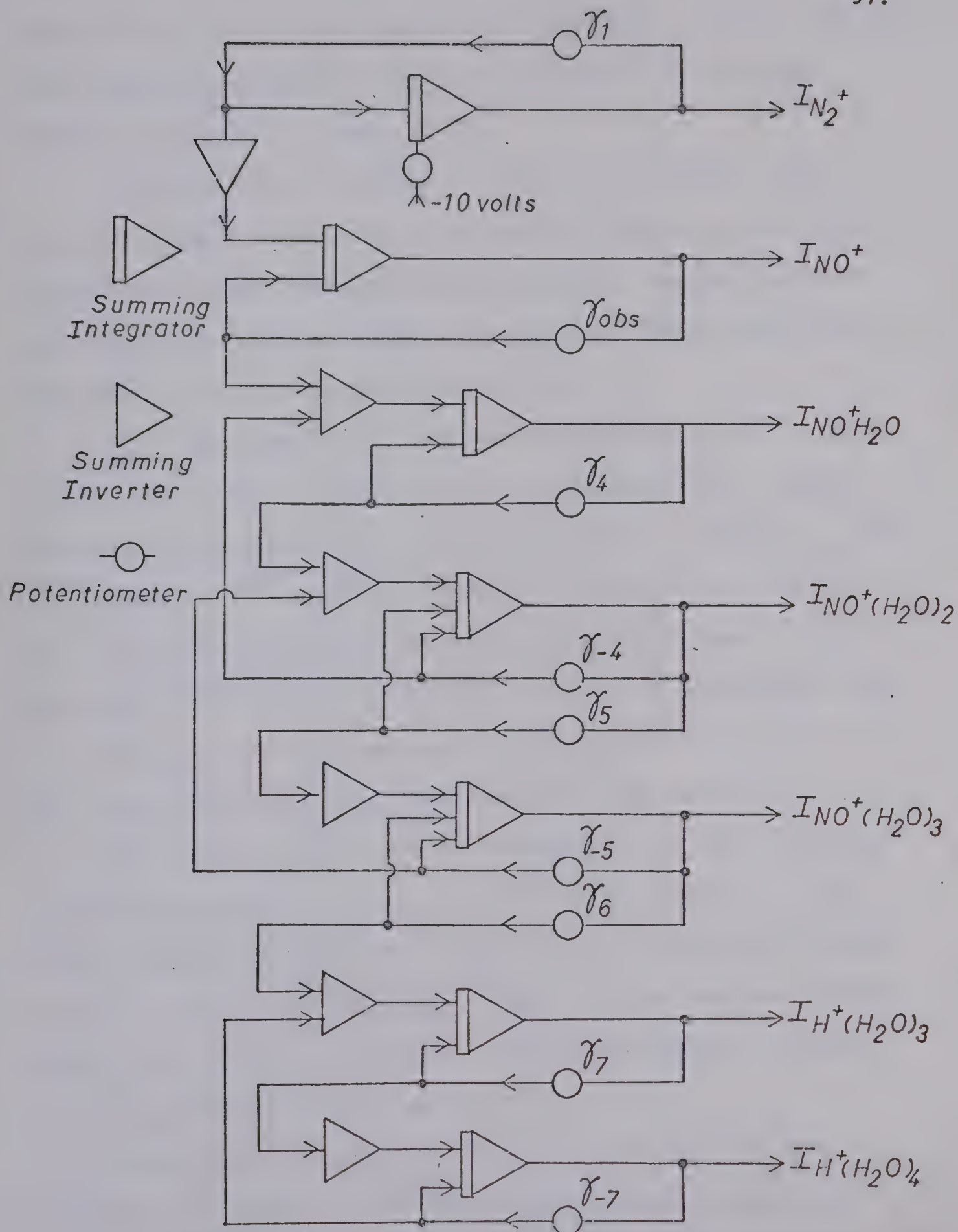


Figure 3.24 Analog Program simulating reactions (1) to (7)

best fit for each individual run with that obtained from the logarithmic plot or by the graphical integration method is shown in Table (3.7).

As explained in section (3.3i), the decay of N_2^+ was not simply exponential and so the apparent rate constant which gave the best fit using the analog computer was approximately an order of magnitude lower than that measured by Ferguson and Fehsenfeld (72).

γ_{obs} was used to calculate the decay of NO^+ . Table (3.8) shows that in general the calculated γ_{obs} values described the behaviour of NO^+ very well. Using γ_{obs} for the decay of NO^+ had the effect of making the formation of $NO^+.H_2O$ faster than was actually observed since the production of $NO^+.NO$ was neglected. The ion intensity curve for $NO^+.H_2O$ could therefore not be fitted too closely up to the point where maximum intensity was achieved.

The average value of k_4 determined by the graphical integration method was $1.0 \times 10^{-28} \text{ cc}^2 \text{ molecule}^{-2} \text{ sec}^{-1}$ which agreed closely with the average theoretical value of $1.2 \times 10^{-28} \text{ cc}^2 \text{ molecule}^{-2} \text{ sec}^{-1}$. The average values of k_{-4} and k_4 were found to compare favourably between the two methods of evaluation.

The average value of the rate constant for the addition of water to $NO^+(H_2O)_2$ giving the trihydrate

TABLE 3.7

Comparison of Calculated and Computer Fitted Rate Constants

Run	$[N_2]^a$ $\times 10^{-16}$	$[NO]^a$ $\times 10^{-15}$	$[H_2O]^a$ $\times 10^{-14}$	k_1 $\times 10^{11b}$		γ_{obs} $\times 10^{-3}$		k_4 $\times 10^{27d}$		k_{-4} $\times 10^{14b}$		k_5 $\times 10^{27d}$		k_{-5} $\times 10^{12b}$		k_6 $\times 10^{10b}$		k_7 $\times 10^{14e}$		k_8
				B	A	B	A	B	A	B	A	B	A	B	A	B	A	B	A	
1	7.8	19.2	1.2	5.2	13.9	12.7	0.9	1.0	5.1	4.5	0.20	0.9	0.4	3.2	1.2	2.0	4.8	6.0	2.5	
2	8.2	12.0	1.0	8.3	9.4	9.4	0.6	0.8	3.0	3.0	0.34	0.7	1.0	2.4	0.8	2.6	3.8	6.0	3.3	
3	5.2	11.6	0.7	3.4	6.4	7.0	0.9	1.1	5.1	5.2	0.19	1.0	0.5	3.4	1.0	6.9	-	7.0	-	
4	3.7	11.6	2.1	4.8	5.2	4.9	1.1	1.3	6.6	4.9	0.25	1.3	0.7	5.8	1.2	2.2	3.5	4.0	2.4	
5	6.7	12.8	1.2	8.2	9.1	9.5	1.0	1.2	3.2	3.3	0.17	1.2	0.5	3.3	1.4	1.6	4.4	4.0	-	
6	8.4	10.0	1.0	3.9	8.5	8.5	1.0	1.3	3.3	3.0	0.10	1.1	0.2	3.5	1.2	3.6	5.2	4.0	-	
7	5.9	2.5	1.4	14.0	2.4	2.3	1.1	1.1	7.8	5.1	0.14	1.1	1.6	3.8	-	2.2	3.6	4.0	-	
8	6.0	2.9	1.3	8.8	3.6	3.6	1.1	1.2	4.0	4.0	0.43	1.0	0.8	3.6	-	3.4	4.5	4.0	-	
9	6.2	1.0	1.4	2.9	2.2	2.5	1.0	1.5	9.4	11.4	0.19	1.2	2.1	2.3	1.9	5.5	4.8	4.2	-	
Average				6.6	-	-	1.0	1.2	4.8	4.9	0.23	1.1	0.7	3.4	1.3	3.3	4.3	4.8	2.7	

A. Calculated by Graphical Methods.

B. Best Computer Fit.

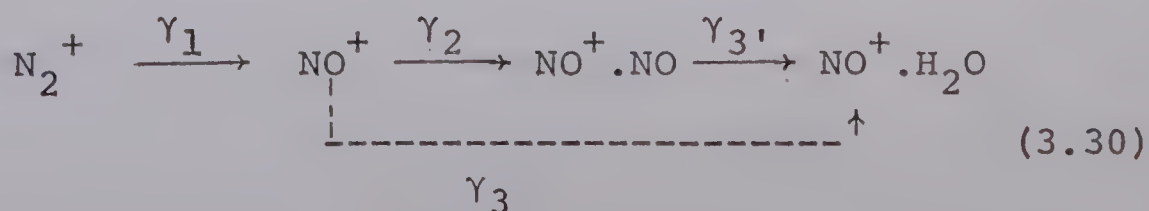
- (a) Units of molecule cc^{-1}
- (b) Units of $cc\ molecule^{-1}\ sec^{-1}$
- (c) Units of sec^{-1}
- (d) Units of $cc^2\ molecule^{-2}\ sec^{-1}$
- (e) Units of $cc\ molecule^{-1}$

was found to be $2.3 \times 10^{-28} \text{ cc}^2 \text{ molecule}^{-2} \text{ sec}^{-1}$ from the graphical integration plots (Figure 3.20) and $1.1 \times 10^{-27} \text{ cc}^2 \text{ molecule}^{-2} \text{ sec}^{-1}$ from the best analog fit. Because of the difficulty of measuring the slopes from Figure (3.17) the value of k_5 was not too reliable. The value of k_5 obtained theoretically was thought to be more accurate. The reverse rate constant was correspondingly larger in the analog fit.

The rate constant for reaction (6) was found to be $1.2 \times 10^{-10} \text{ cc molecule}^{-1} \text{ sec}^{-1}$ from the graphical integration method (Figure 3.22) and $3.3 \times 10^{-10} \text{ cc molecule}^{-1} \text{ sec}^{-1}$ from the best analog fit. The relative intensity of $\text{NO}^+(\text{H}_2\text{O})_3$ was very small and the estimation of $\int I_{\text{NO}^+(\text{H}_2\text{O})_3}$ may have been inaccurate. The theoretical value of k_6 is probably more accurate.

The values of k_7 and k_{-7} determined by the best analog fit were in good agreement with values for proton hydration with N_2 as a third body obtained previously using this instrument (30).

Theoretical curves were also obtained for the experiments where reaction (2) and (3') were studied (11,12,13). The analog program describing the reaction scheme is shown in Figure (3.25).



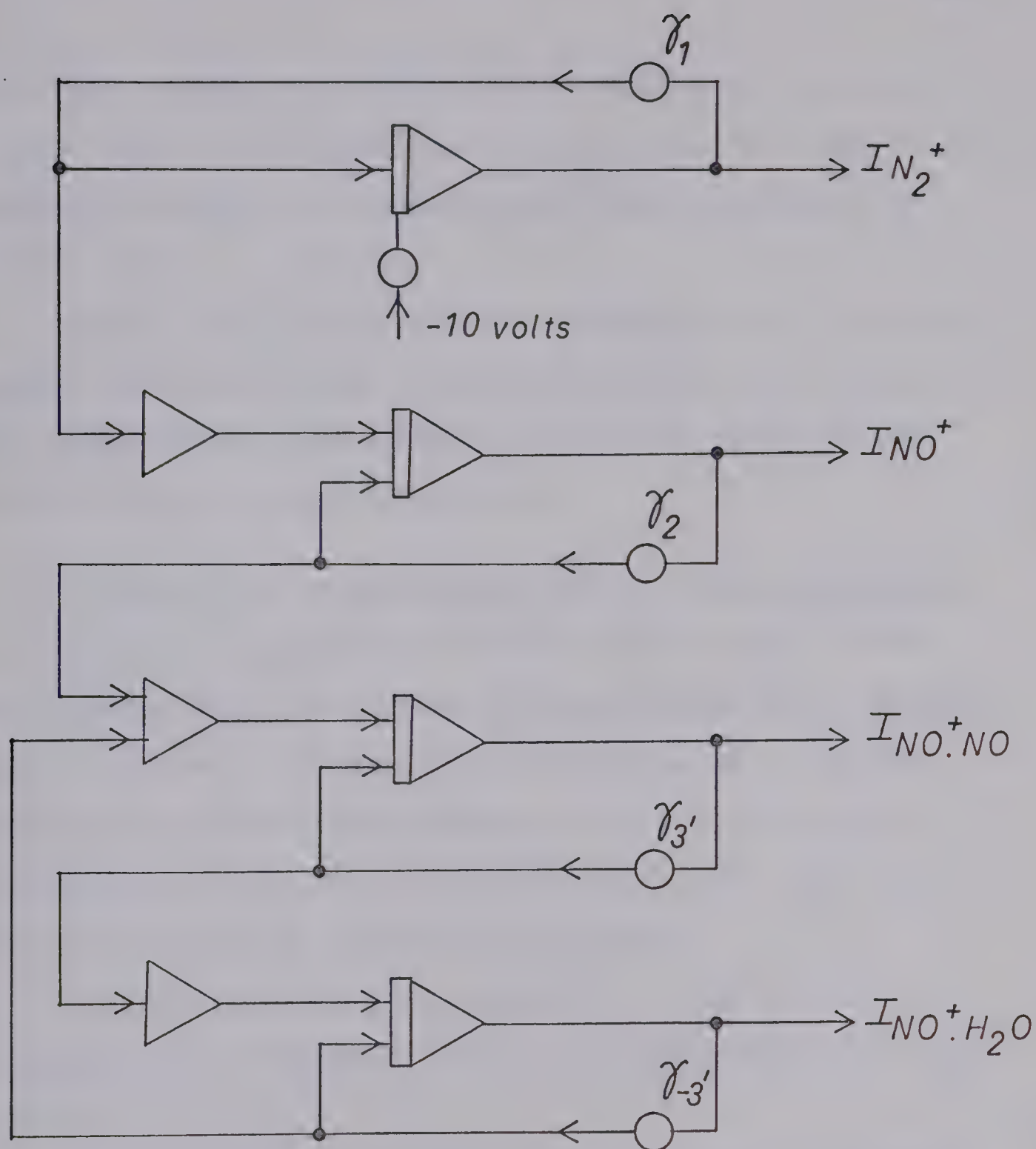


FIGURE 3.25 Analog Program simulating reactions (1), (2) and (3').

The best analog fits are shown as solid lines in Figures (3.21) to (3.23). The rate constants from the best theoretical fit are compared with those calculated in Table (3.8).

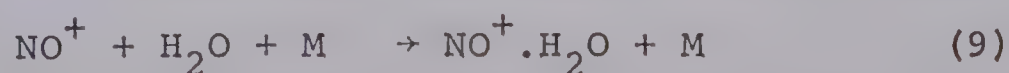
Table (3.8) shows that the agreement for k_2 is very good. The best analog fit led to a value for γ_3 , but k_3 , could not be calculated as the water concentration could not be measured accurately.

3.7 Discussion of Results Obtained at Room Temperature

After the completion of the present work, Puckett and Teague (75) and Kaufman (76) published their results on the hydration of NO. Table 3.9 shows the reaction mechanism and the final values of the rate constants determined in this study and for comparison, rate constants obtained by other research groups.

The small value of k_1 compared to that measured by Ferguson and Fehsenfeld (72,73) was explained in section (3.5).

The studies of reaction (9) have been quite extensive. Both Kaufman et al (76) and Fehsenfeld and Ferguson (79) have studied the hydration of NO^+ with different third bodies such as helium, argon, nitrogen and oxygen. The values that they obtained for k_9 with



nitrogen as a third body (reaction (3)) are shown in

TABLE 3.8

Comparison of Calculated and Computer Fitted Rate Constants
 for the Reaction $\text{NO}^+ + \text{NO} + \text{N}_2 \xrightarrow{k_2} \text{NO}^+ \cdot \text{NO} + \text{N}_2$ (2)

Run	$[\text{N}_2]^a$	$[\text{NO}]^a$	$[\text{H}_2\text{O}]^a$	$k_2 \times 10^{29b}$	
	$\times 10^{-16}$	$\times 10^{-15}$	$\times 10^{-13}$	calculated	computer fit
11	5.4	10.3	5.6	1.1	1.1
12	5.8	5.0	4.7	1.0	1.2
13	4.6	17.3	5.0	1.2	1.2
Average				1.1	1.2

(a) Units of molecule cc^{-1}

(b) Units of $\text{cc}^2 \text{ molecule}^{-2} \text{ sec}^{-1}$

TABLE 3.9

Determined Rate Constants for Reactions (1) to (8)

Reaction	Determined Rate Constants (this work)	Determined Rate Constants (other workers)	Third Bodies
(1) $N_2^+ + NO \xrightarrow{k_1} NO^+ + N_2$	$k_1 > 6 \times 10^{-11}$	5×10^{-10a} 3.3×10^{-10a}	- -
(2) $NO^+ + NO + N_2 \xrightarrow{k_2} NO^+ \cdot NO + N_2$	$k_2 = 8.7 \times 10^{-30}$	5.0×10^{-30b} 5.0×10^{-30c} $\sim 30 \times 10^{-30d}$ $\sim 33 \times 10^{-30e}$	NO NO NO NO
(3) $NO^+ + H_2O + N_2 \xrightarrow{k_3} NO^+ \cdot H_2O + N_2$	$k_3 = 1.8 \times 10^{-28}$	1.5×10^{-28f} 1.6×10^{-28c} 1.4×10^{-28g} 1.6×10^{-28h}	NO NO N_2 N_2
(3') $NO^+ \cdot NO + H_2O \xrightleftharpoons[k_{-3}']{k_3'} NO^+ \cdot H_2O + NO$	$k_3' =$ $k_{-3}' =$	1.4×10^{-9c} 9×10^{-14c}	- -
(4) $NO^+ \cdot H_2O + H_2O + N_2 \xrightleftharpoons[k_{-4}]{k_4} NO^+ (H_2O)_2 + N_2$	$k_4 = 1.0 \times 10^{-27}$ $k_{-4} = 5.0 \times 10^{-14}$	1.1×10^{-27c} 1.4×10^{-14c}	NO -
(5) $NO^+ (H_2O)_2 + H_2O + N_2 \xrightleftharpoons[k_{-5}]{k_5} NO^+ (H_2O)_3 + N_2$	$k_5 = 1.1 \times 10^{-27}$ $k_{-5} = 3.4 \times 10^{-12}$	1.9×10^{-27c} 1.9×10^{-12c}	NO -

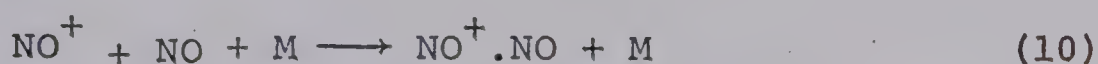
TABLE 3.9 (continued)

(6)	$\text{NO}^+(\text{H}_2\text{O})_3 + \text{H}_2\text{O} \xrightarrow{k_6} \text{H}^+(\text{H}_2\text{O})_3 + \text{HNO}_2$	$k_6 = 3.3 \times 10^{-10}$	$7 \times 10^{-11\text{c}}$	NO
(7)	$\text{H}^+(\text{H}_2\text{O})_3 + \text{H}_2\text{O} + \text{N}_2 \xrightleftharpoons[k_{-7}]{k_7} \text{H}^+(\text{H}_2\text{O})_4 + \text{N}_2$	$\frac{k_7}{k_{-7}} = 4.3 \times 10^{-14}$	$2 \times 10^{-13\text{c}}$ $6 \times 10^{-14\text{i}}$	NO
(8)	$\text{H}^+(\text{H}_2\text{O})_4 + \text{H}_2\text{O} + \text{N}_2 \xrightleftharpoons[k_{-8}]{k_8} \text{H}^+(\text{H}_2\text{O})_5 + \text{N}_2$	$\frac{k_8}{k_{-8}} = 2.7 \times 10^{-16}$	$3.7 \times 10^{-16\text{c}}$ $1 \times 10^{-16\text{i}}$	NO N ₂

- (a) Ferguson and Fehsenfeld, Ref. (72,73).
- (b) Lineburger and Puckett, Ref. (54).
- (c) Puckett and Teague, Ref. (75).
- (d) Searles and Sieck, Ref. (77).
- (e) Strausz, Duholke and Gunning, Ref. (78).
- (f) Lineburger and Puckett, Ref. (49).
- (g) Howard, Rundle and Kaufman, Ref. (76).
- (h) Fehsenfeld and Ferguson, Ref. (79).
- (i) Good, Durden and Kebarle, Ref. (30).

Table (3.10) and agree very closely with the values obtained in the present work. Lineburger and Puckett (49), Puckett and Teague (75) determined the rate constant k_9 for the case where $M = \text{NO}$. Both NO and N_2 are efficient third bodies and lead to a similar rate constant for reaction (9).

The dimerisation of NO has also been studied by several workers with different third bodies.



Experiments done by Searles and Sieck (77) and Duholke and Strausz (78) led to a rate constant a factor of six higher than that measured by Lineberger and Puckett (54) and Puckett and Teague (75) when $M = \text{NO}$. Duholke and Strausz found that k_{10} was 1.8×10^{-28} when $M = \text{He}$. The value of k_{10} ($=k_2$ for $M = \text{N}_2$) for the present work was midway between the two sets of data.

The agreement between k_4 and k_5 was quite reasonable.

In general the third order rate constants agree very well with previous measurements, but the second order rate constants e.g. k_{-4} , k_{-5} , k_6 are approximately a factor of 2 larger in the present work than those reported by Puckett and Teague (75).

Puckett and Teague conducted their experiments at 296°K , whereas the present studies were carried out at 308°K . Since third-order rate constants do not vary much

with temperature but second-order rate constants involving dissociation i.e. k_{-4} , k_{-5} can, the appreciable difference in the two set of values may be due to a temperature effect.

If a reaction has rate constants k_1 and k_2 at temperatures T_1 and T_2 respectively then the Arrhenius equation may be written:

$$2.303 \log \frac{k_1}{k_2} = \frac{-\Delta H}{R} \frac{T_1 - T_2}{T_1 T_2} \quad (3.31)$$

Assuming that for a second-order ion-molecule reaction the exothermicity is approximately +10 kcal/mole then:

$$\log \frac{k_1}{k_2} = \frac{-10,000 \times 12}{2 \times 2.303 \times 308 \times 296} = -0.28 \quad (3.32)$$

$$\frac{k_1}{k_2} \approx .5 \quad (3.33)$$

Thus k_2 is expected to be approximately twice k_1 , which was the effect observed experimentally. Therefore the rate constants determined by Puckett and Teague can be said to be in reasonable agreement when the effect of the difference of temperature is taken into account.

3.8 Reactions Observed at Higher Temperatures

Several experiments were carried out at temperatures between 35°C and 130°C. The total pressure was maintained

at 2 torr. The NO pressure was approximately 0.03 torr in runs 15, 16, and 17 and 0.3 torr in run 14. The water vapour pressure was about 5 mtorr.

Figure (3.26) shows the ions observed at different temperatures when the electron beam is not pulsed. The intensity of each ion is expressed as a percentage of the largest peak, NO^+ . Two trends are observed, the intensity of $\text{NO}^+(\text{H}_2\text{O})_3$ became smaller as the temperature increased and eventually disappeared. The intensities of $\text{NO}^+\text{H}_2\text{O}$ and $\text{NO}^+(\text{H}_2\text{O})_2$ also gradually decreased with increasing temperature. There was also a tendency for the H_3O^+ , $\text{H}^+(\text{H}_2\text{O})_2$ and $\text{H}^+(\text{H}_2\text{O})_3$ intensities to increase and $\text{H}^+(\text{H}_2\text{O})_4$ to decrease and finally disappear as the temperature rose.

The ion intensity curves for the experiments performed above room temperature are shown in Figures (3.27) to (3.30). The NO concentration was low to prevent the dimerisation of NO occurring by reaction (2). In all runs the amount of NO^+NO observed was either zero or too small to measure the delay curve for that ion. It was assumed that the NO^+ reacted to give $\text{NO}^+\text{H}_2\text{O}$ only so γ_3 could be evaluated from the logarithmic plot (Figure (3.31)). The values of k_3 obtained are shown in Table 3.10.

The Arrhenius equation (3.34) may be used to find the activation energy of reaction (3).

$$k = Ae^{-\frac{E_a}{RT}} \quad (3.34)$$

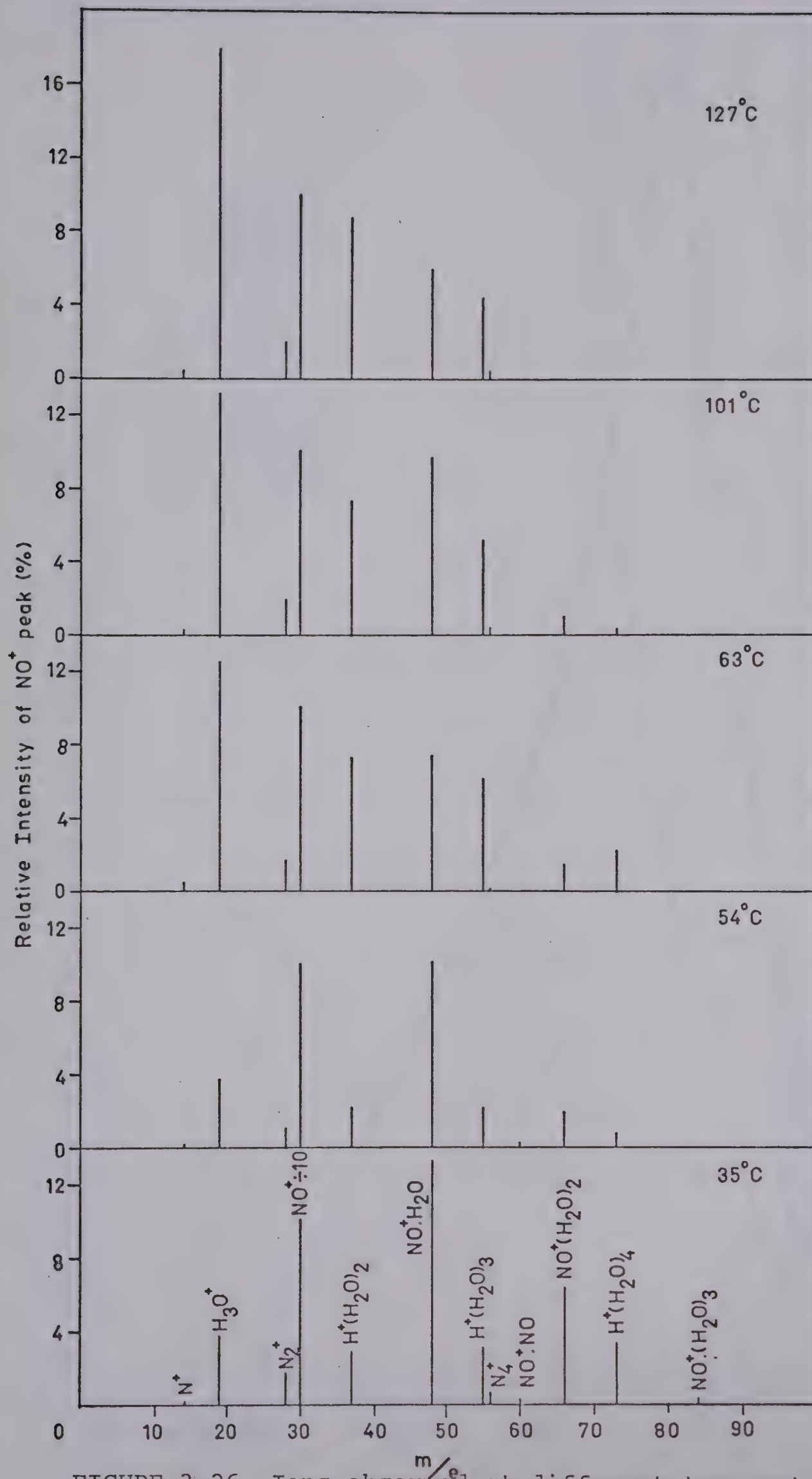


FIGURE 3.26 Ions observed at different temperatures.

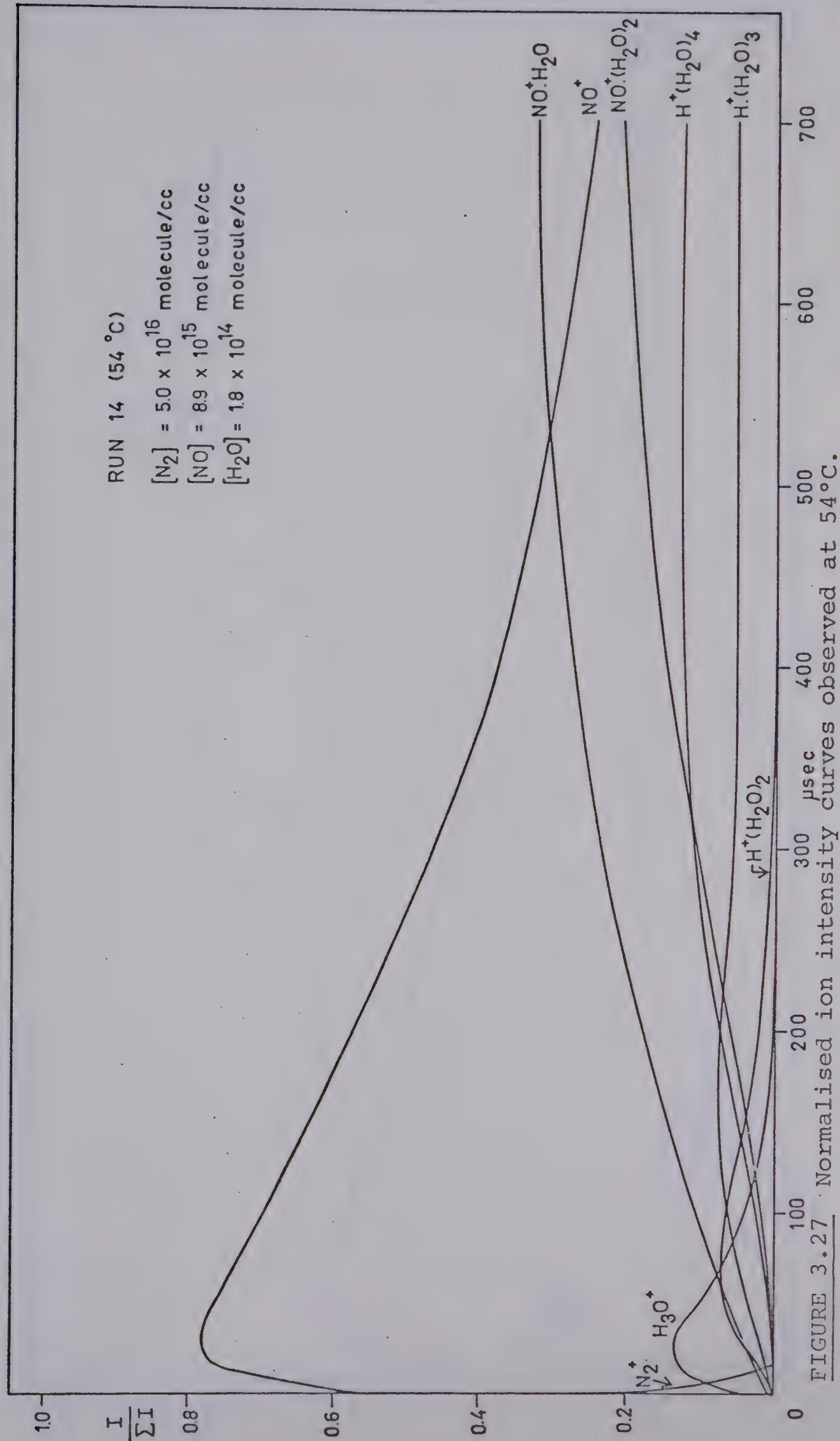


FIGURE 3.27 Normalised ion intensity curves observed at 54°C.

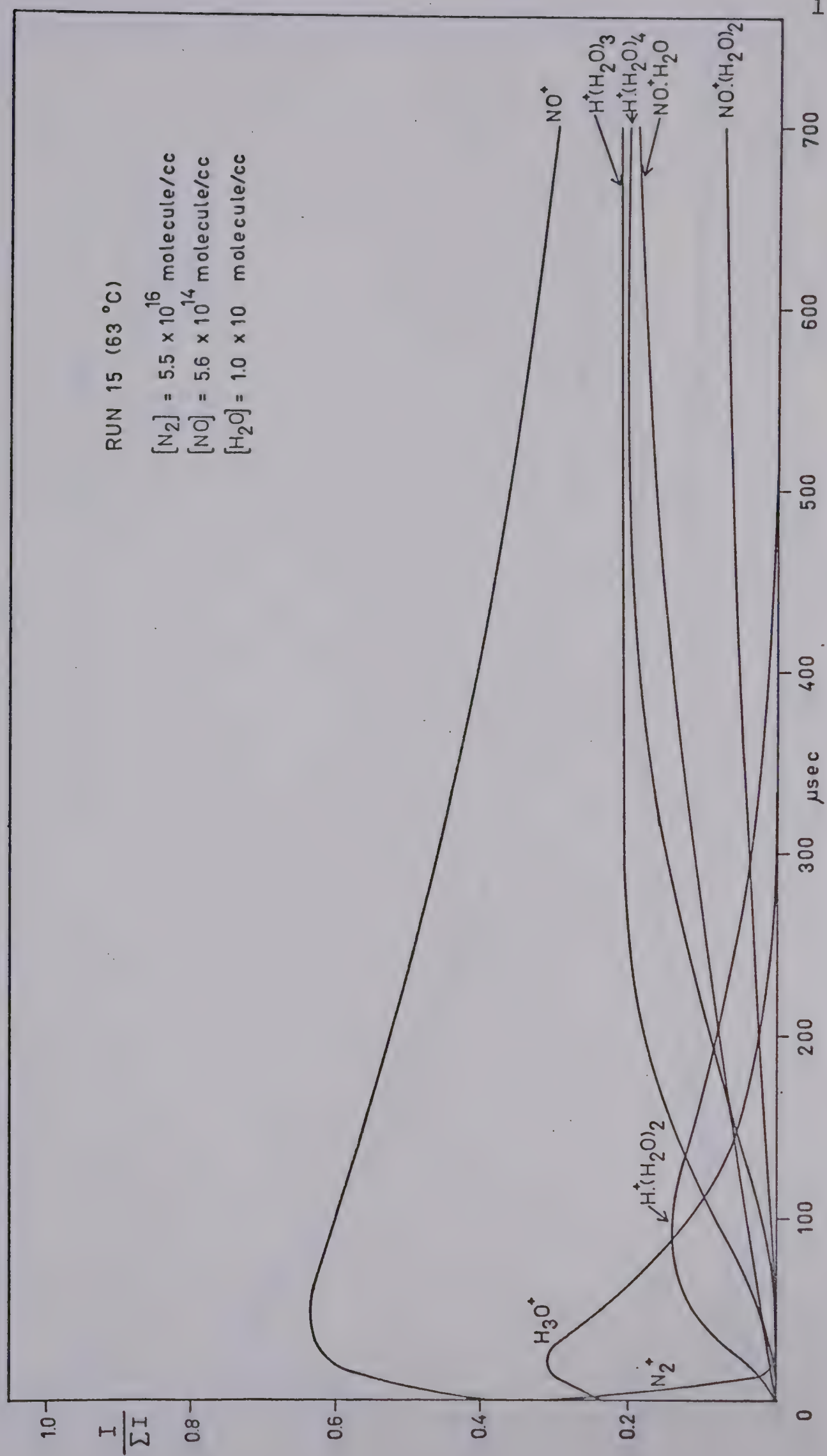


FIGURE 3.28 Normalised ion intensity curves observed at 63°C.

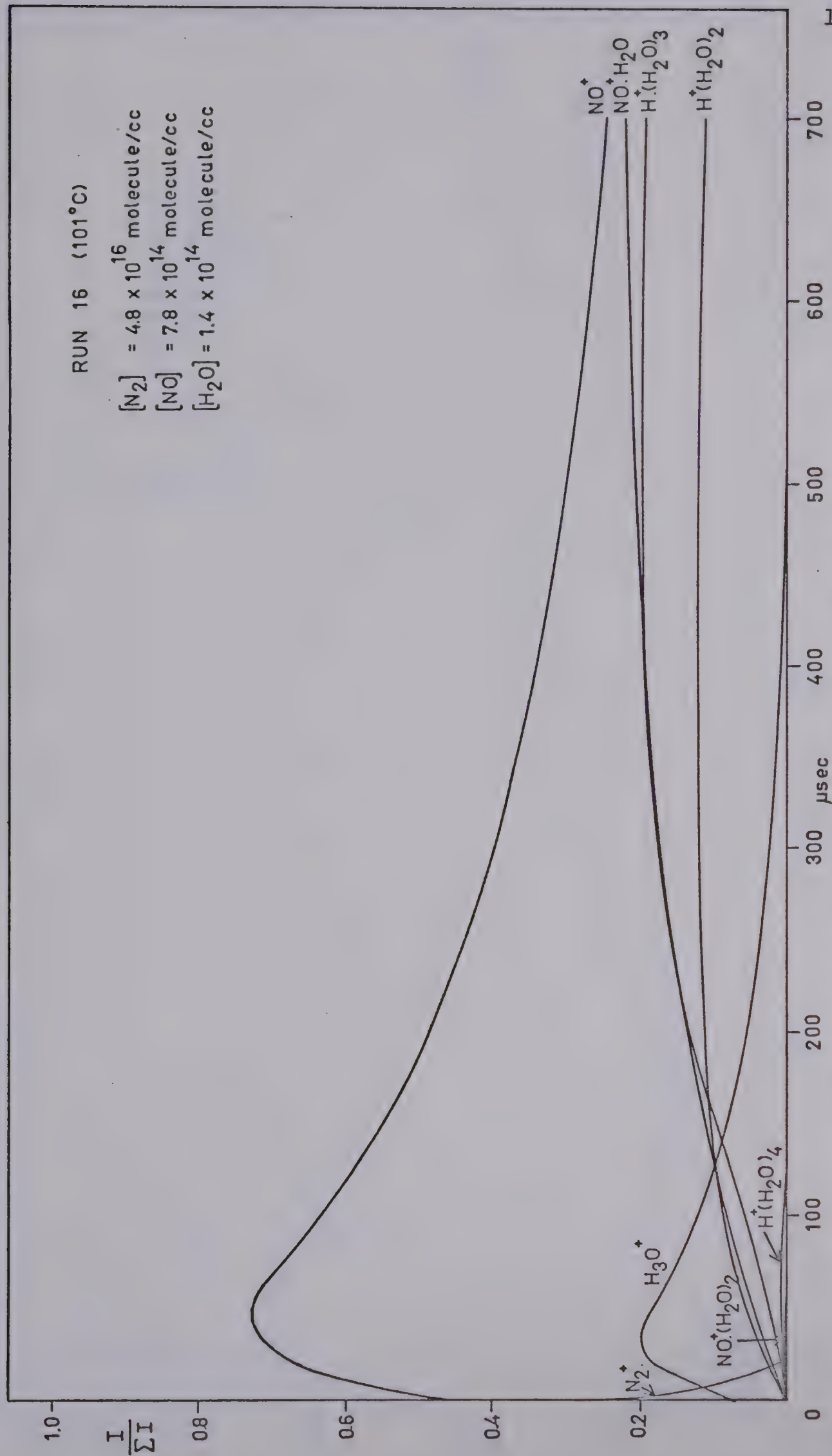


FIGURE 3.29 Normalised ion intensity curves observed at 101°C.

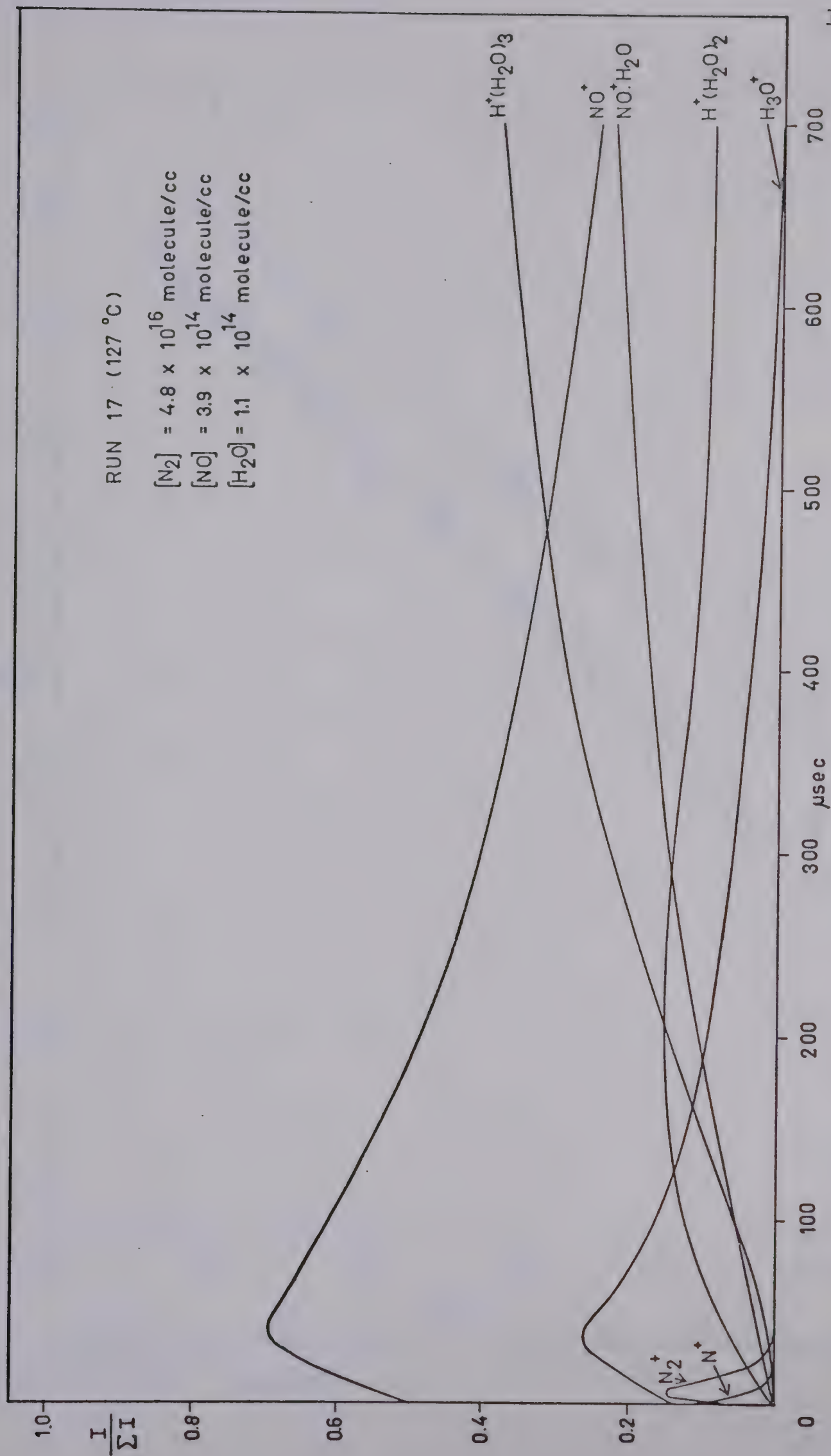


FIGURE 3.30 Normalised ion intensity curves observed at 127°C.

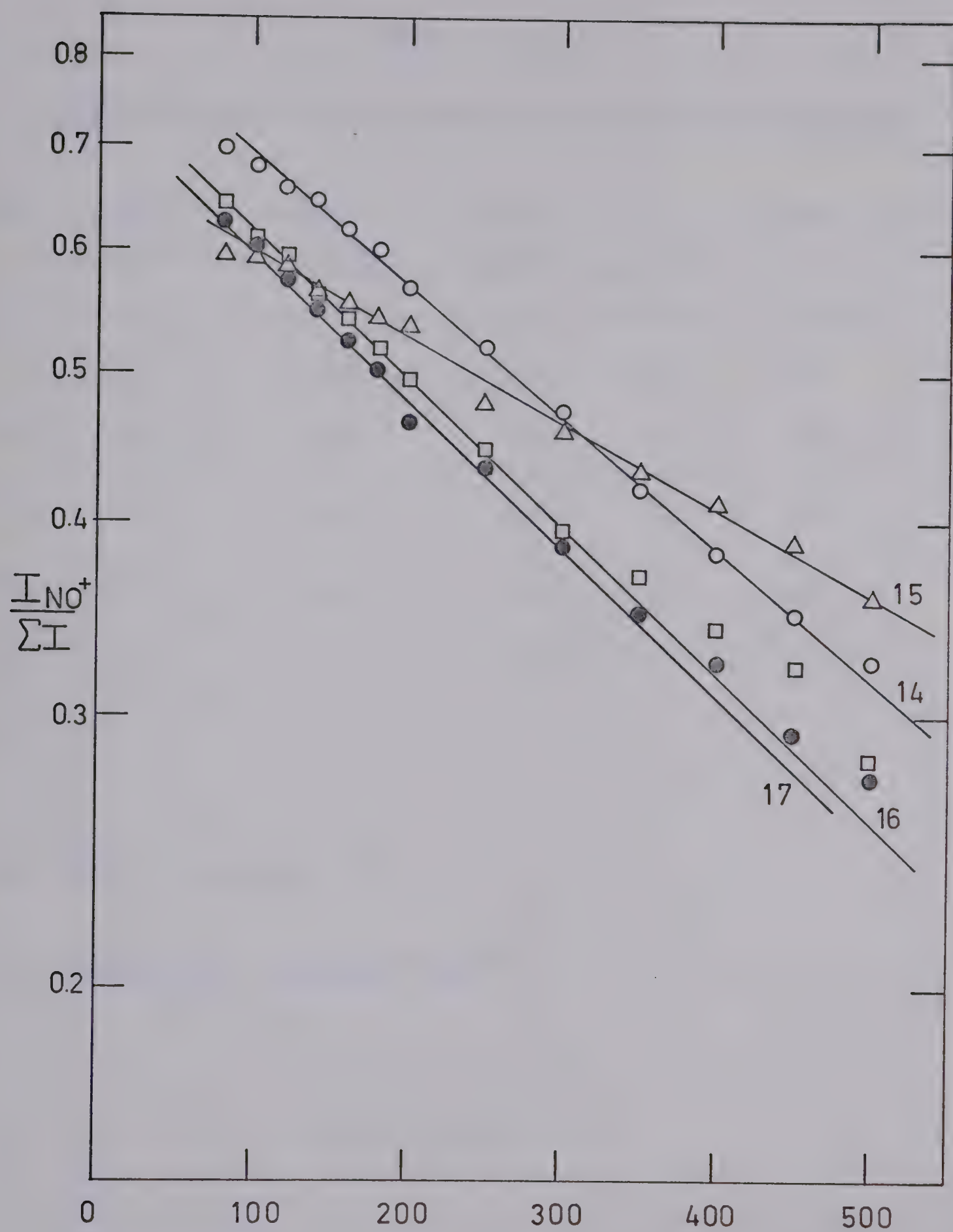


FIGURE 3.31 Calculation of γ_3 from exponential decay of NO^+ .

TABLE 3.10

Rate Constants for Reaction (3) at Various Temperatures

Run	$[\text{N}_2]^a$ $\times 10^{-16}$	$[\text{NO}]^a$ $\times 10^{-14}$	$[\text{H}_2\text{O}]^a$ $\times 10^{-14}$	k_3^b $\times 10^{28}$	T°C
9	6.2	9.7	1.4	1.8	35
14	5.0	88.6	1.8	2.2	54
15	5.5	5.6	1.0	2.3	63
16	4.8	7.8	1.4	3.9	101
17	4.8	3.9	1.1	4.0	127

(a) Units of molecule cc^{-1}

(b) Units of $\text{cc}^2 \text{ molecule}^{-2} \text{ sec}^{-1}$

A plot of $\ln k_3$ versus $1/T^\circ\text{K}$ is shown in Figure (3.32). The straight line obtained gave the activation energy as +2 kcal/mole for reaction (3).

The rate constants for reaction (4) at the different temperatures were determined by the graphical integration method (Figure (3.33)), assuming the following reaction path:

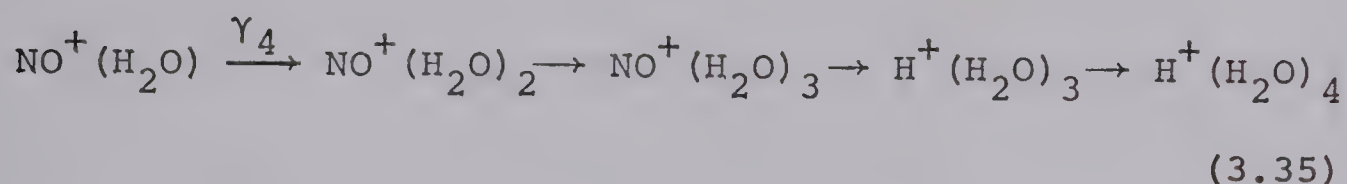


Table (3.11) shows the rate constants obtained from the graphical integration method. On inspection, the values of k_4 obtained in runs 9, 14 and 16 appear to be reasonable but k_4 values determined for runs 15 and 17 are approximately a factor of 10 higher than those expected from interpolation of the results at other temperatures.

Runs 15 and 17 had the lowest water and nitric oxide concentration. Using the graphical integration method γ_4 is calculated from:

$$\gamma_4 = \frac{\int_0^t I_{\text{NO}^+ \cdot \text{H}_2\text{O}}}{\sum \text{products}} \quad (3.36)$$

If \sum products did not actually contain all of the products i.e. some branching reaction was not included then the expression for γ_4 will be larger than if the branch was considered.

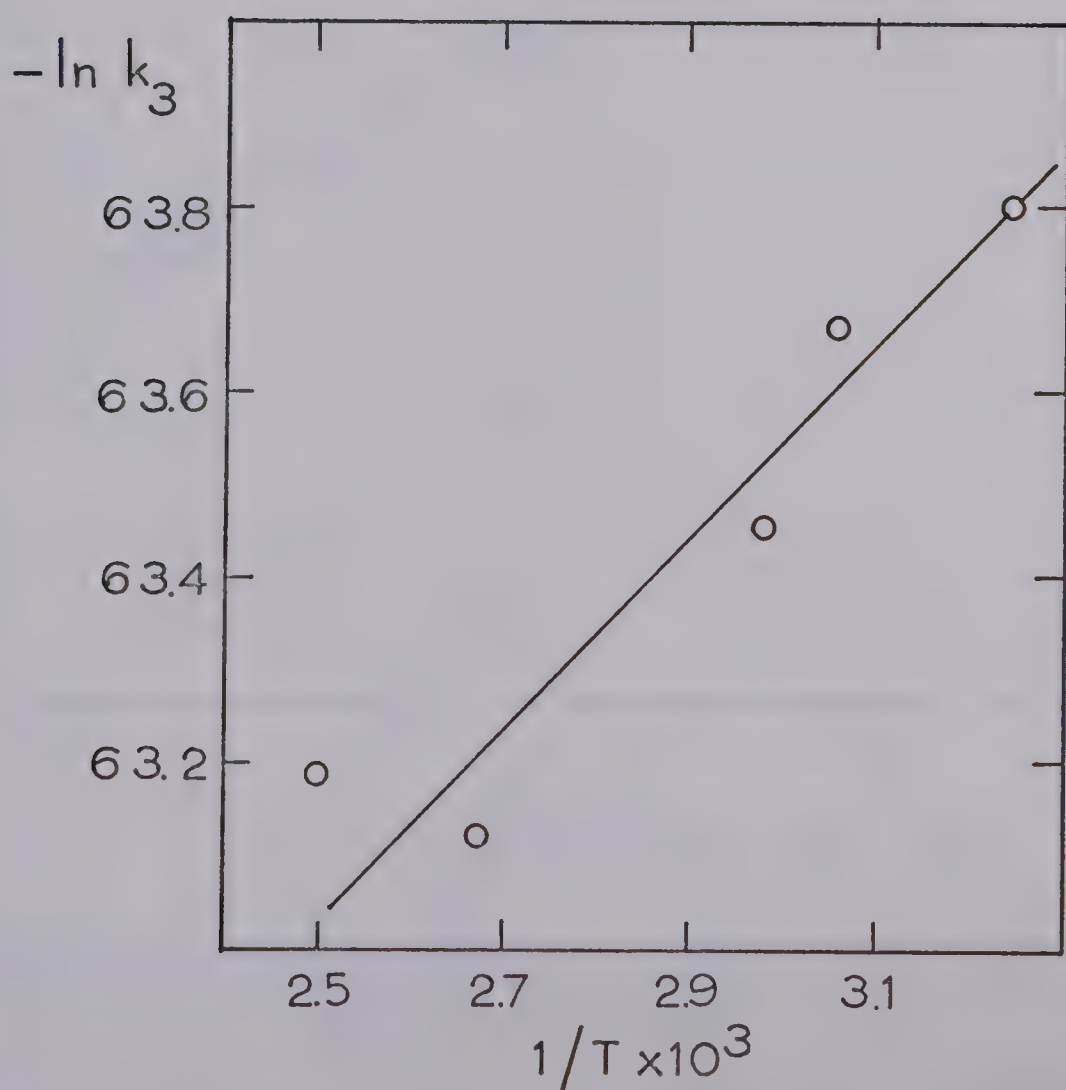


FIGURE 3.32 Arrhenius plot to determine E_a for reaction (3).

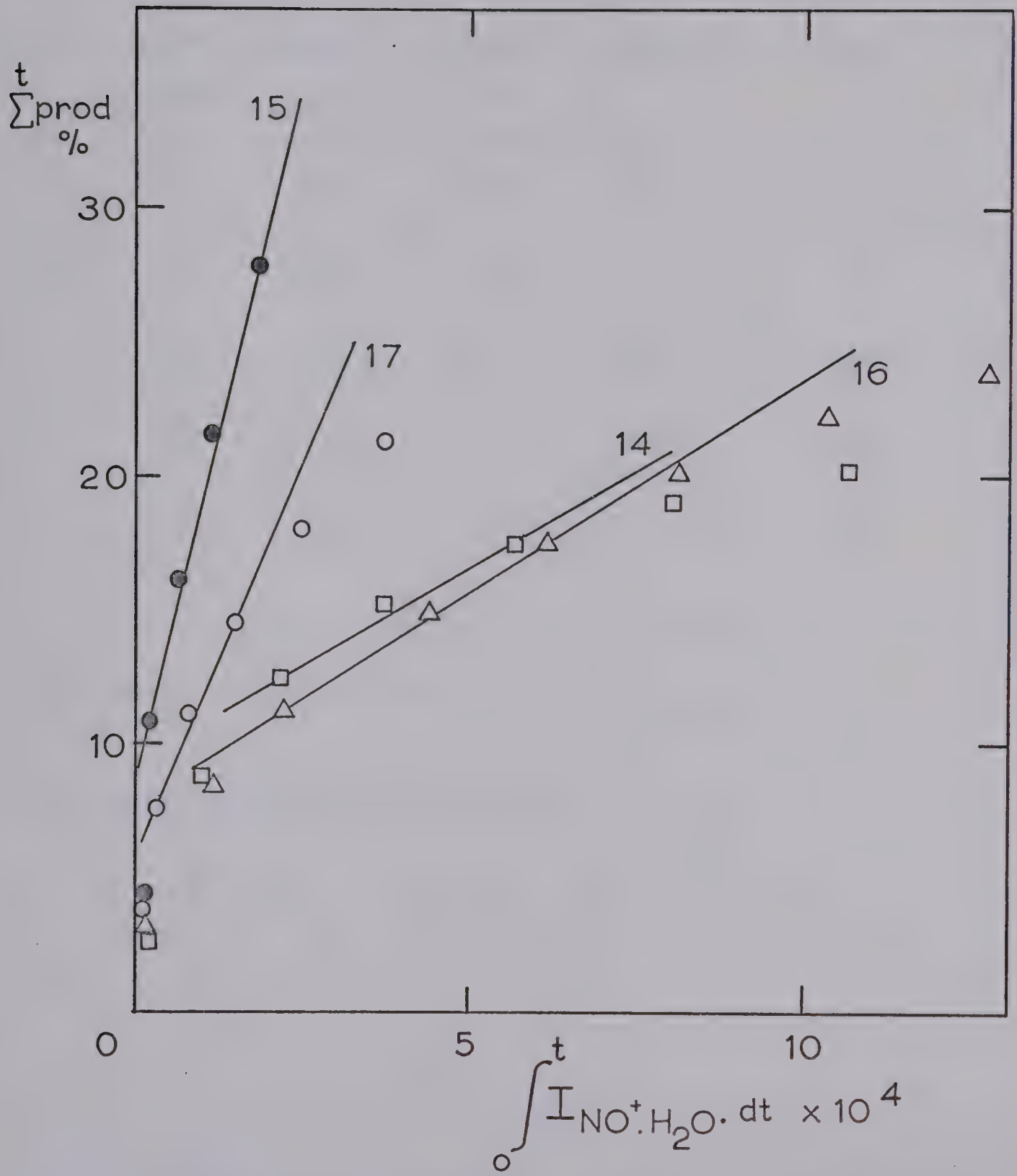


FIGURE 3.33 Calculation of γ_4 by the graphical integration method.

TABLE (3.11)Rate Constants for Reaction (4) at Various Temperatures

Run	$[\text{N}_2]^a$ $\times 10^{-16}$	$[\text{NO}]^a$ $\times 10^{-14}$	$[\text{H}_2\text{O}]^a$ $\times 10^{-14}$	$k_4 \times 10^{27b}$	$T^\circ\text{C}$
9	6.2	9.7	1.4	1.1	35
14	5.0	88.6	1.8	1.7	54
15	5.5	5.6	1.0	20.0	63
16	4.8	7.8	1.4	2.5	101
17	4.8	3.9	1.1	11.0	127

(a) Units of molecule cc^{-1} (b) Units of $\text{cc}^2 \text{ molecule}^{-2} \text{ sec}^{-1}$

Ferguson and Fehsenfeld (50) have suggested that the cross-over reaction (11) may occur for $n=3$ at room temperature because the reaction is exothermic or slightly endothermic and endothermic when $n=1$ or 2 and therefore not observed.

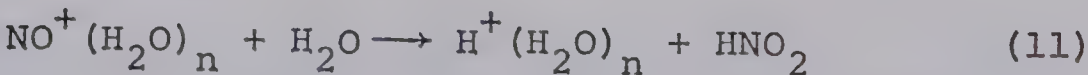
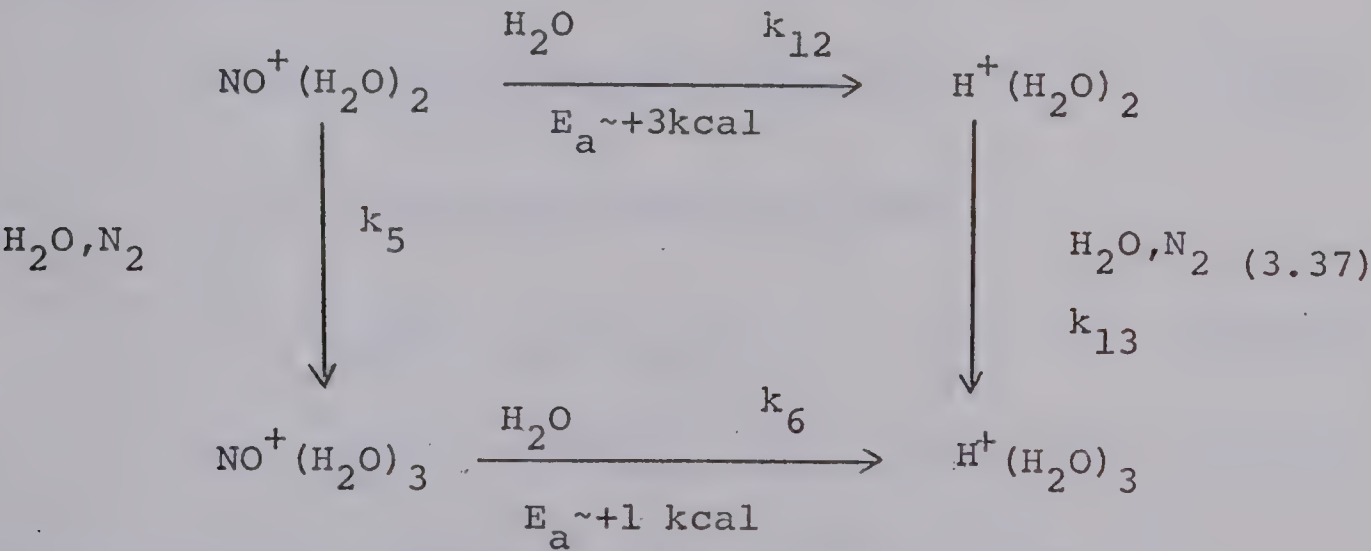


Figure (3.26) and the results obtained for k_4 suggest that as the temperature is raised the cluster of NO^+ may cross-over to the proton hydrate clusters for $n=2$.

If $\text{NO}^+(\text{H}_2\text{O})_2$ crosses over to $\text{H}^+(\text{H}_2\text{O})_2$ then there is competition between reactions (5) and (12).



The cross-over rate constants k_6 and k_{10} may be found by equation (3.38) and (3.39). It is assumed that the activation energy for reaction (6) is very small, about +1 kcal/mole and the activation energy for reaction (12)

is more positive, about +3 kcal/mole. A is assumed to be approximately 1×10^{-9} and the temperature 300°K

$$k_{12} = 10^{-9} e^{-3/RT} \approx 10^{-12} \quad (3.38)$$

$$k_6 = 10^{-9} e^{-1/RT} \approx 10^{-10} \quad (3.39)$$

Reaction (12) is therefore 100 times slower than reaction (6), and (6) will occur preferentially.

The rate of reaction (12) is given by:

$$R_{12} = k_{12} [\text{NO}^+ (\text{H}_2\text{O})_2] [\text{H}_2\text{O}] \quad (3.40)$$

The rate of reaction (5) is given by:

$$R_5 = k_5 [\text{NO}^+ (\text{H}_2\text{O})_2] [\text{H}_2\text{O}] [\text{N}_2] \quad (3.41)$$

k_5 is 1×10^{-27} . When the rates are equal

$$10^{-12} = 10^{-27} [\text{N}_2] \quad (3.42)$$

$$[\text{N}_2] = 10^{-15} \text{ molecule cc}^{-1} \quad (3.43)$$

If $P_{\text{N}_2} = 2$ torr, then $[\text{N}_2] = 6 \times 10^{16} \text{ molecules cc}^{-1}$.

$$R_{12} = 10^{-12} \quad (3.44)$$

$$R_5 = 6 \times 10^{-11} \quad (3.45)$$

Therefore at 300°K the clustering of NO is more favourable than the cross-over reaction. As the temperature is increased k_5 will not change very much as it is third-order

dependent but k_{12} is second-order and will increase with temperature. At a certain point R_{12} will become greater than R_5 and $H^+(H_2O)_2$ will be observed.

Burke (80) has suggested an alternative mechanism for the production of proton hydrates in the ionosphere from hydrates of NO^+ . He proposed that the hydrogen atom, whose concentration is quite significant in the D region, is involved:



Reaction (14) is exothermic and Burke derived $D(NO^+ - 3H_2O) \leq 55 \text{ kcal mole}^{-1}$ or $D(NO^+ - H_2O) \ll 55 \text{ kcal mole}^{-1}$. However, in the present work the amount of hydrogen atoms present would be very small and reaction (14) would not be observed.

3.9 Conclusions

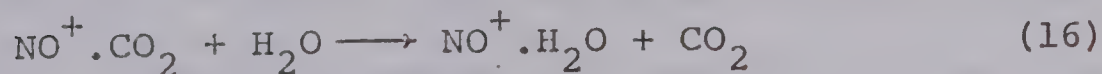
The rate constants evaluated for reactions (2) to (6) are reproducible within a factor of 2. The measured rate constants are also in good agreement with those reported for similar systems (Table 3.9).

The reaction parameters evaluated in the nitric oxide, water system are quite large and the rates of the reactions are fast when the pressures of the neutral reactants are in the torr range. The concentration of water in the ionosphere is approximately 10^{-7} torr at 80 km which is much lower than that used in these experiments.

In order to form $\text{H}^+(\text{H}_2\text{O})_3$ from NO^+ , three successive third-body hydration reactions, (3)-(5), must occur. Since the water concentration is low in the ionosphere the rates of the hydration reactions must be very slow. It is unlikely therefore that the conversion of NO^+ to $\text{H}^+(\text{H}_2\text{O})_n$ is the major process for the production of proton hydrates.

Mechanisms of the reactions of NO^+ with other molecules present in the ionosphere have been investigated recently which may produce proton hydrates.

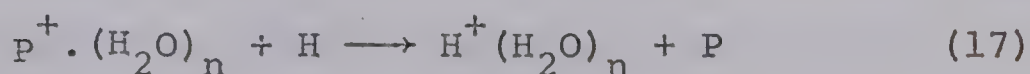
Recent studies of the association of NO^+ with O_2 , N_2 , CO_2 and NH_3 (81,82) have shown that the rate constants for the attachment of O_2 and N_2 are very small, of the order of $10^{-33} \text{ cc}^2 \text{ molecule}^{-2} \text{ sec}^{-1}$. The association of NO^+ with CO_2 was found to be $4 \times 10^{-30} \text{ cc}^2 \text{ molecule}^{-2} \text{ sec}^{-1}$ at 290°K . $\text{NO}^+.\text{CO}_2$ could then react with water to give $\text{NO}^+.\text{H}_2\text{O}$.



Dunkin et al (81) calculated that due to the large $[\text{CO}_2]/[\text{H}_2\text{O}]$ ratio in the ionosphere, about 10^2 , NO^+ is converted to the hydrate via reactions (15) and (16) rather than direct hydration (3). They suggested that association of NO^+ with CO_2 could explain the previously calculated low NO^+ loss rates compared to the known pro-

duction rates for NO^+ noticed by Reid (56).

The alternative mechanism for the formation of proton hydrates proposed by Burke involves a hydrogen atom.



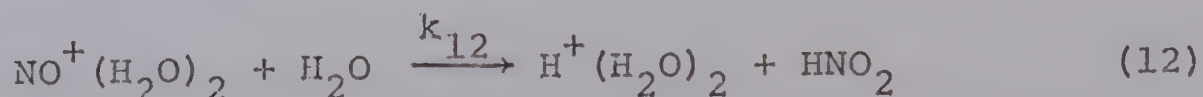
Burke suggests that P may be O_2^+ , NO^+ and possibly Fe^+ and Mg^+ .

Calculations by Hunt (83) have implied that NO^+ rather than O_2^+ is the major precursor of proton hydrates but this depends entirely on the occurrence of reaction (14). If reaction (14) does not occur in the ionosphere then O_2^+ is the major precursor of the proton hydrates (84).

3.10 Suggestions for Further Experiments

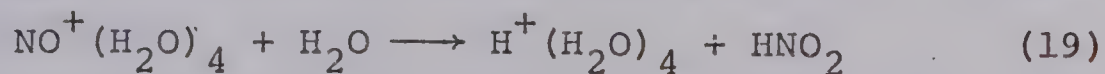
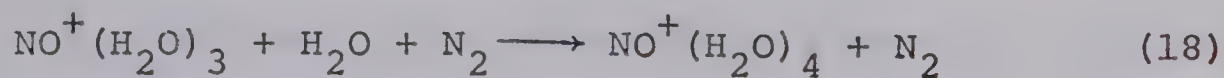
The materials used in the construction of the present ion source prevent the temperature being raised above 150°C . A new ion source has been constructed that can withstand temperatures over 400°C .

The experiments carried out in this work at temperatures between 35°C and 130°C used very low pressures of NO and H_3O^+ and $\text{H}^+ (\text{H}_2\text{O})_2$ were observed by reactions (1a) to (4a) (section 3.2). It was therefore difficult to see how much $\text{H}^+ (\text{H}_2\text{O})_2$ was being formed by:



Implementation of the new ion source will enable higher temperatures to be achieved. Higher pressures of NO, about 0.3 torr and about 5 mtorr of water will suppress the formation of H_3O^+ and $\text{H}^+(\text{H}_2\text{O})_2$ from N_2^+ and N_4^+ . The increase of $\text{H}^+(\text{H}_2\text{O})_2$ intensity should be observed as the temperature is raised due to the tendency of $\text{NO}^+(\text{H}_2\text{O})_2$ to disappear by reaction (12) instead of reaction (5).

The new ion source also contains a cooling coil in order to study reactions at temperatures below 300°K. It is possible that reactions (18) and (19) may occur at lower temperatures



In fact an ion with m/e 102 has been observed to a very small extent occasionally in this work.

R E F E R E N C E S

1. J. J. Thompson, Phil. Mag., 24, 241 (1912).
2. A. J. Dempster, Phil. Mag., 31, 438 (1916).
3. H. D. Smyth, Phys. Rev., 25, 452 (1925).
4. T. P. Hogness and E. G. Lunn, Phys. Rev., 26, 44 (1925).
5. V. L. Tal'rose, A. K. Lyubimova, Doklady Akad. Nauk. SSSR, 86, 909 (1952), per Chem. Abstracts, 47, 2590 (1953).
6. D. P. Stevenson and D. O. Schissler, J. Chem. Phys., 23, 1353 (1955).
7. D. O. Schissler and D. P. Stevenson, J. Chem. Phys., 24, 926 (1956).
8. H. Gutbier, Z. Naturforsch., A12, 499 (1957).
9. H. Friedman, Proc. Inst. Radio Engineers, 47, 272 (1959).
10. R. S. Narcisi and A. D. Bailey, J. Geophys. Res., 70, 3687 (1965).
11. C. Y. Johnson, E. B. Meadows and J. C. Holmes, J. Geophys. Res., 63, 443 (1958).
12. A. Galli, A. Giardini-Guidoni and G.G. Volpi, J. Chem., Phys., 39, 518 (1963).
13. E. E. Ferguson, F. C. Fehsenfeld, P. D. Goldan and A. L. Schmeltekopf, J. Geophys. Res., 70, 4323 (1965).
14. W. Swider Jr., J. Geophys. Res., 70, 4859 (1965).
15. P. F. Knewstubb, "Mass Spectrometry and Ion-Molecule Reactions", Cambridge University Press, London, (1969), Chap. 1.

16. P. Langevin, Annales de Chimie et Physique, 5, 245 (1905).
17. E. W. McDaniel, "Collision Phenomena in Ionised Gases", Wiley and Sons Ltd., New York, (1964), pp.701-726.
18. G. Giomousis and D. P. Stevenson, J. Chem. Phys., 29, 294 (1958).
19. J. V. Dugan and J. L. Magee, J. Chem. Phys., 47, 3103 (1967).
20. D. K. Bohme, J. B. Hasted and P. P. Ong, Chem. Phys. Letters, 1, 259 (1967).
21. E. W. McDaniel, V. Cermak, A. Dalgarno, E. E. Ferguson and L. Friedman "Ion-Molecule Reaction" Wiley & Sons Inc., 1970 p.159.
22. D. R. Bates, "Atomic and Molecular Processes", Academic Press, New York, (1962), pp.601,708.
23. E. Lindholm, I. Szabo and P. Wilnemiuss, Arkiv Fysik, 25, 417 (1963).
24. H. von Koch, Arkiv Fysik, 28, 529 (1965).
25. F. H. Field and F. W. Lampe, J. Amer. Chem. Soc., 80, 5583 (1958).
26. G. R. Freeman, "Radiation Chemistry", University of Alberta, Edmonton, 1966, p.193.
27. F. H. Field and F. W. Lampe, J. Amer. Chem. Soc., 81, 3238 (1959).
28. I. Dzidic and P. Kebarle, J. Phys. Chem., 74, 1466 (1970).

29. J. H. Yang and D. C. Conway, J. Chem. Phys., 40, 1729 (1964).
30. A. Good, D. A. Durden and P. Kebarle, J. Chem. Phys., 52, 212 (1970).
31. R. N. Varney, Phys. Rev., 174, 165 (1968).
32. D. K. Bohme, D. B. Dunkin, F. C. Fehsenfeld and E. E. Ferguson, J. Chem. Phys., 51, 863 (1969).
33. F. H. Field, J. Amer. Chem. Soc., 83, 1523 (1961).
34. F. H. Field, J. L. Franklin and M. S. B. Munson, J. Amer. Chem. Soc., 85, 3575 (1963).
35. F. H. Field and M. S. B. Munson, J. Amer. Chem. Soc., 87, 3289 (1965).
36. M. S. B. Munson and F. H. Field, J. Amer. Chem. Soc., 87, 3294 (1965).
37. P. Kebarle and E. W. Godbole, J. Chem. Phys., 39, 1131 (1963).
38. P. Kebarle and A. M. Hogg, J. Chem. Phys., 42, 668 (1965).
39. P. Kebarle, R. M. Haynes and S. Searles, "Advances in Chemistry", Series No. 58, Amer. Chem. Soc., Washington, D. C. (1966) p.210.
40. P. Kebarle and A. M. Hogg, J. Chem. Phys., 42, 798 (1965).
41. V. L. Tal'rose and E. L. Frankevitch, Russ. J. Phys. Chem., 34, 1275 (1960).
42. V. L. Tal'rose, Pure. Appl. Chem. 5, 455 (1962).
43. W. L. Fite, J. A. Rutherford, W. R. Snow and V. A. J. van Lint, Disc. Faraday Soc., 33, 264 (1962).

44. J. Sayers and D. Smith, Disc. Faraday Soc., 37, 167 (1964).
45. F. C. Fehsenfeld, A. L. Schmeltekopf and E. E. Ferguson, J. Chem. Phys., 44, 4087 (1966).
46. A. L. Schmeltekopf, F. C. Fehsenfeld, G. I. Gilman and E. E. Ferguson, Plan. Space Sci., 15, 401 (1967).
47. Chemical and Engineering News, 44, No.13, 1966.
48. R. S. Narcisi and W. Roth, "Advances in Electronics and Electron Physics", Vol. 29, Academic Press Inc., New York, 1970.
49. W. C. Lineburger and L. J. Puckett, BRL Report No. 1443, Bull. Am. Phys. Soc., 14, 261 (1969).
50. F. C. Fehsenfeld and E. E. Ferguson, J. Geophys. Res., 74, 2217 (1969).
51. A. Good, D. A. Durden and P. Kebarle, J. Chem. Phys., 52, 222 (1970).
52. E. E. Ferguson and F. C. Fehsenfeld, J. Geophys. Res., 74, 5743 (1969).
53. M. M. Shahin, J. Chem. Phys., 45, 2600 (1965).
54. W. C. Lineburger and L. J. Puckett, BRL Report No. 1438, Phys. Rev., 186, 116 (1969).
55. E. A. Mechtly and L. G. Smith, J. Atmos. Terr. Phys., 30, 1555 (1968).
56. G. C. Reid, J. Geophys. Res., 75, 2551 (1970).
57. R. C. Gunton, T. M. Shaw, Phys. Rev., 140A, 756 (1965).

58. M. A. Biondi, Can. J. Chem., 47, 1711 (1969).
59. M. Nicolet, J. Geophys. Res., 70, 679 (1965).
60. M. Nicolet, J. Geophys. Res., 70, 691 (1965).
61. D.A. Durden, Ph.D. Thesis, University of Alberta, 1969, Chap. 2.
62. D. A. Durden, P. Kebarle and A. Good, J. Chem. Phys., 50, 805 (1969).
63. W. Paul and H. Steinwedel, Z. Naturforsch, 8A, 448 (1963).
64. W. Paul and M. Raether, Z. Physik, 140, 262 (1955).
65. W. Paul, H. P. Reinhard and U. von Zahn, Z. Physik, 152, 143 (1958).
66. U. von Zahn, S. Gebauer and W. Paul, 10th Annual Meeting of the ASTM Committee E-14 on Mass Spectrometry, New Orleans, La., June 1962, p.232.
67. C. Brunée, L. Delgmann and K. Kronenberger, 11th Annual Meeting of the ASTM Committee E-14 on Mass Spectrometry, San Francisco, California, May 1963.
68. P. Kebarle and E. W. Godbole, J. Chem. Phys., 36, 302 (1962).
69. J. H. Beynon "Mass Spectrometry and its Application to Organic Chemistry", Elsevier, New York, 1960 P.214.
70. H. E. Stanton, W. A. Chupka and M. G. Inghram, Rev. Sci. Instr., 27, 109 (1956).
71. F. W. Lampe, J. L. Franklin and F. H. Field, J. J. Amer. Chem. Soc., 79, 6129 (1957).
72. P. D. Goldan, A. L. Schmeltekopf, F.C. Fehsenfeld, H. I. Schiff and E. E. Ferguson, J. Chem. Phys., 44,

4095 (1966).

73. F. C. Fehsenfeld, D. B. Dunkin and E. E. Ferguson, *Plan. Space Sci.*, 18, 1267 (1970).
74. N. M. Rodriguin and E. N. Rodriguina, Ed. R. F. Schneider, D. Van Nostrand Co. Inc., New Jersey, 1963.
75. L. J. Puckett and M. W. Teague, *J. Chem. Phys.*, 54, 2564 (1971).
76. C. J. Howard, H. W. Rundle and F. Kaufman, *Bull. Am. Phys. Soc.*, 16, 213 (1971).
77. S. K. Searles and L. W. Sieck, *J. Chem. Phys.*, 53, 794 (1970).
78. O. P. Strausz, W. K. Duholke and H. E. Gunning, *J. Amer. Chem. Soc.*, 92, 4128 (1970).
79. F. C. Fehsenfeld and E. E. Ferguson, *Bull. Am. Phys. Soc.*, 16, 213 (1971).
80. R. R. Burke, *J. Geophys. Res.*, 75, 1345 (1970).
81. D. B. Dunkin, F. C. Fehsenfeld, A. L. Schmeltekopf and E. E. Ferguson, *J. Chem. Phys.*, 54, 3817 (1971).
82. F. C. Fehsenfeld and E. E. Ferguson, *J. Chem. Phys.*, 54, 439 (1971).
83. B. G. Hunt, *J. Atm. Terr. Phys.*, 33, 929 (1971).
84. L. Thomas, *J. Atm. Terr. Phys.*, 33, 157 (1971).

B29991